DESIGN AND PERFORMANCE ANALYSIS OF A VARIABLE PITCH AXIAL FLOW FAN FOR ANKARA WIND TUNNEL

A THESIS SUBMITTED TO
THE GRADUATE SCHOOL OF NATURAL AND APPLIED SCIENCES
OF
MIDDLE EAST TECHNICAL UNIVERSITY

BY

LEVENT YALÇİN

IN PARTIAL FULFILLMENT OF THE REQUIREMENTS
FOR
THE DEGREE OF MASTER OF SCIENCE
IN
AEROSPACE ENGINEERING

JANUARY 2006

Approval of the Graduate School of Natural and Applied Sciences.

Prof. Dr. Canan ÖZGEN
Director

I certify that this thesis satisfies all the requirements as a thesis for the degree of Master of Science.

Prof. Dr. Nafiz ALEMDAROĞLU
Head of Department

This is to certify that we have read this thesis and that in our opinion it is fully adequate, in scope and quality, as a thesis for the degree of Master of Science.

Prof. Dr. İ. Sinan AKMANDOR
Supervisor

Examining Committee Members

Emeritus Prof. Dr. Cahit ÇIRAY (ODTU-AEE)

Prof. Dr. İ. Sinan AKMANDOR (ODTU-AEE)

Prof. Dr. M. Haluk AKSEL (ODTU-ME)

Prof. Dr. Cevdet ÇELENLİGİL (ODTU-AEE)

Dr. Oğuz UZOL (ODTU-AEE)

I hereby declare that all information in this document has been obtained and presented in accordance with academic rules and ethical conduct. I also declare that, as required by these rules and conduct, I have fully cited and referenced all material and results that are not original to this work.

Levent YALÇİN

ABSTRACT

DESIGN AND PERFORMANCE ANALYSIS OF A VARIABLE PITCH AXIAL FLOW FAN FOR ANKARA WIND TUNNEL

Yalçin, Levent

M.S., Department of Aerospace Engineering

Supervisor: Prof. Dr. İ. Sinan Akmandor

January 2006, 136 pages.

In this study, a variable pitch axial flow fan is designed and analyzed for Ankara Wind Tunnel (AWT). In order to determine the loss characteristics of AWT, an algorithm is developed and the results are validated. Also some pressure and velocity measurements are made at the fan section to find the losses experimentally. After completion of the fan design, analyses are made at different volumetric flow rates and blade angles including the design point and the performance characteristics of the fan are obtained and thereafter the operating range of the tunnel is determined.

Keywords: Ankara Wind Tunnel, tunnel losses, variable pitch axial flow fan design and analysis, performance characteristics of fan.

ÖZ

ANKARA RÜZGAR TÜNELİ İÇİN PALA AÇISI DEĞİŞTİRİLEBİLEN EKSENEL BİR FAN TASARIMI VE PERFORMANS ANALİZİ

Yalçin, Levent

Yüksek Lisans, Havacılık ve Uzay Mühendisliği Bölümü

Tez Yöneticisi: Prof. Dr. İ. Sinan Akmandor

Ocak 2006, 136 sayfa.

Bu çalışmada, Ankara Rüzgar Tüneli (ART) için pala açısı değiştirilebilen eksenel bir fan tasarlandı ve analizi yapıldı. ART'nin basınç kayıp karakteristiğini belirlemek için bir algoritma geliştirildi ve sonuçlar doğrulandı. Aynı zamanda kayıpları deneysel olarak bulmak için fan bölgesinde bazı basınç ve hız ölçümleri yapıldı. Fan tasarımının ardından, tasarım noktasınıda içeren farklı debi ve pala açılarında analizler yapıldı ve fan performans karakteristikleri elde edildi ve daha sonra tünelin çalışma hız aralığı belirlendi.

Anahtar Kelimeler: Ankara Rüzgar Tüneli, tünel kayıpları, pala açısı değiştirilebilen eksenel fan tasarımı ve analizi, fan performans karakteristiği.

To My Primary School Teacher…

ACKNOWLEDGMENTS

I would like to express my sincere gratitude to my thesis supervisor, Prof. Dr. İ. Sinan AKMANDOR, for his support, guidance and encouragement throughout this study.

I would like to thank Dr. Gökmen MAHMUTYAZICIOĞLU, Head of Design Engineering Department, and Koray DAYANÇ, my group coordinator in TÜBİTAK-SAGE, for their valuable advices and useful suggestions.

My sincere thanks go to my colleagues in Aerodynamics Division, especially Emel MAHMUTYAZICIOĞLU and Süleyman KURUN for their support and encouragement throughout this study. I am immensely indebted to Argün KATIRCI and Salih KAYABAŞI for their cooperation during the velocity and pressure measurements in Ankara Wind Tunnel.

I would like to thank Murat ILGAZ for listening me patiently and for his valuable comments during several steps of this study.

I would like to thank Raci GENÇ for drawings of the fan. Finally, I can hardly express my gratitude to my parents and my sister for their understanding and endless support.

This work has been supported in part by TÜBİTAK-SAGE, The Scientific and Technological Research Council of Turkey-Defense Industries Research and Development Institute.

TABLE OF CONTENTS

LIST OF TABLES

TABLES

LIST OF FIGURES

FIGURES

LIST OF SYMBOLS

ROMAN SYMBOLS

a speed of sound

A cross-sectional area

A_{FLOW} cross-sectional area of local flow

c blade chord of rotor or stator

C_L lift coefficient with respect to mean velocity V_m

C_{L_i} isolated airfoil lift coefficient

C_D drag coefficient with respect to mean velocity V_m

ER energy ratio (ratio of energy of flow at the test section to the output energy of the fan)

k total pressure coefficient

K total pressure loss coefficient of section

K_0 section total pressure loss coefficient referred to test section conditions

K_{EXP} diffuser loss coefficient due to expansion

K_{MESH} mesh screen type loss parameter

K_{Re} mesh screen Reynolds number sensitivity factor

$K_{TV_{90}}$ turning vane loss parameter for given vanes at a 90° turn

L centerline length of section

M Mach number

n number of rotor or stator blades

N revolutions per second

P_{input} drive power required to be input to flow by the fan

$P_{required}$ total fan motor output power required to drive wind tunnel at specified speed

p static pressure

p_T total (stagnation) pressure

q dynamic pressure

Q volumetric flowrate

r radius of elementary annulus

r_b boss radius

R radius of duct (approximately rotor tip radius)

R gas constant

Re Reynolds number

Re_{REF} reference Reynolds number at which turning vane 90° loss parameter, $K_{TV_{90}}$, was determined

s circumferential spacing of adjecent rotor or stator blades

T temperature

V velocity

V_a axial velocity component

V_θ tangential velocity component

V_m mean velocity relative to rotor or stator blade

x radius ratio (r/R)

x_b boss ratio (r_b/R)

GREEK SYMBOLS

α incidence angle, the angle between β_m and the airfoil chord line

α_N no-lift angle, the angle between ξ and β_N

β_1 angle that V_1 makes with fan axis

β_2 angle that V_2 makes with fan axis

β_3 angle that V_m makes with fan axis

β_N value of β_m for no-lift condition

$\beta_1 - \beta_2$ flow turning angle

β_N value of β_m for no-lift condition

δ flow deviation angle, the angle between β_2 and trailing edge tangent

ε_p swirl coefficient upstream of rotor

ε_s blade solidity, c/s

ϕ angle between the airfoil chord line and the plane of rotation

ϕ corner flow turning angle

γ specific heat ratio of gas

γ lift/drag ratio

η aerodynamic efficiency

η_T total efficiency of the fan

λ friction coefficient for smooth pipes

λ flow coefficient

Λ tip flow coefficient

μ_{STD} standard-day value of viscosity

μ_T reference viscosity at a known temperature

ρ density

2θ diffuser equivalent cone angle: $2\tan^{-1}\left(\dfrac{\sqrt{A_2}-\sqrt{A_1}}{L\sqrt{\pi}}\right)$, deg

θ blade camber angle

Ω angular velocity of rotor

$\Omega \cdot R$ tip velocity

$\Omega \cdot r$ blade velocity at radius r

Δ signifies a pressure differential

Δp_T total pressure drop through a section

Δp_F total pressure rise across the fan

ξ stagger angle, the angle between the airfoil chord line and the fan axis

SUBSCRIPTS

0 upstream end of test section

1 inlet

2 outlet

$*$ sonic flow

BL blade (rotor and straightener)

D diffuser

F fan

P prerotator

R rotor

S straightener

T total (stagnation) conditions

CHAPTER 1

INTRODUCTION

1.1 Overview of Various Subsonic Wind Tunnels in the World

At the beginning of this thesis, subsonic wind tunnels all over the world were investigated in order to obtain general information about the wind tunnels and their fan properties. Tunnel type, tunnel speed, test section area, power of the fan, rpm of the fan, number of blades, number of stages of the fan, etc of such research establishment have been determined. Although more than one hundred subsonic wind tunnels were found, only the ones which provided the fan power data were chosen and listed in Table 1.1. Moreover, the wind tunnels that have closed test section were the primary focus because the required power for a given wind tunnel with an open jet may easily exceed three times the power required by the same tunnel at the same speed with a closed jet [4]. The wind tunnels with test section areas between 2 m^2 and 16 m^2 were considered to get an idea about the fan properties and power requirements of tunnels that are comparable with Ankara Wind Tunnel (AWT) in size. All these are given in Figs. 1-6.

Figs. 1.1 and 1.2 show the change of power with Mach number and test section area, respectively. It can be seen from these figures that the power of the fan generally increases with the Mach number. The tunnels with low

Mach number compared to AWT has also smaller test section area and power values than AWT. It is clear from these figures that there are three ways to increase the Mach number of AWT:

- decrease the test section area by keeping the power of the fan constant,
- increase the power of fan without changing the test section,
- decrease the test section area and increase the power of the fan.

Although it can also be considered to increase both test section area and power of the fan, it is not possible to increase the test section area of AWT.

The change of power with the number of blades for tunnels having different Mach numbers and test section areas is given in Fig. 1.3. When the power of fan and Mach number are greater than those of AWT, the number of blades of the fan is also higher. Although the tunnels with higher Mach numbers compared to AWT have more blades than the AWT, there is no linear relationship between the power and number of blades.

The variations of power and number of blades with mass flow parameter are shown in Figs. 1.4 and 1.5, respectively. The mass flow parameter values in these figures are calculated using the formula given below:

$$MFP = \frac{\dot{m} \cdot \sqrt{T_t}}{P_t} = M \cdot A \cdot \sqrt{\frac{\gamma}{R}} \cdot \left(1 + \frac{\gamma - 1}{2} \cdot M^2\right)^{\frac{-(\gamma+1)}{2\cdot(\gamma-1)}} \tag{1.1}$$

The mass flow parameter is related to Mach number. When the Mach number of the tunnel increases, required power also increases. On the other hand, there seems no direct relation between the number of blades and the mass flow parameter. However, it is clear that all tunnels have at least four blades.

Fig. 1.6 gives the variation of blade tip speed with Mach number. Generally, blade tip speeds are less than 180 m/s.

Table 1.1 Subsonic Wind Tunnels in the World

#	Tunnel	Country	Date Built	Type	Test Section Dimensions (m)			Mach (Speed, m/s)	Power hp (kW)	Power Type & Fan Properties
					H	W	L			
1	Ankara Wind Tunnel (AWT)	Turkey	1950	Closed	2.44	3.05	6.1	0.25 (85)	1000	Variable speed DC motor 5 m in diameter 4-bladed fan
2	NASA-Ames Research Center NFAC 80 x 120 ft	USA	1982	Open	24.38	24.38	36.58	0.15 (51.4)	135000	fan
3	University of Kansas 3 x 4 ft WT	USA	1965	Open	0.92	1.29	1.83	0.3 (90)	300	440 V
4	UC Davis Aeronautical Wind Tunnel Facility	USA	1997	Open	0.85	1.22		(73.7)	125	fan
5	DA-LSWT	Germany	1969	Open Eiffel	2.1	2.1	4.3	(75)	(500)	fan 580 rpm

Table 1.1 Subsonic Wind Tunnels in the World (Continued)

#	Tunnel	Country	Date Built	Type	Test Section Dimensions (m)			Mach (Speed, m/s)	Power hp (kW)	Power Type & Fan Properties
					H	W	L			
6	15 x 5 Foot Environmental Wind Tunnel	United Kingdom	1992	Open	4.57	1.52	9.14	(20)	(112)	3 parallel 1.8 m in diameter 10 bladed fans 112 kW motor
7	I.A.T S2	France	1936	Open Eiffel	1.8	2.2	2	(55)	(130)	4 blade 3.43 m diameter
8	Low Speed Wind Tunnel	USA	1947	Closed	2.44	3.66	4.57	0.34	2250	Variable speed 6-blade fan 3 phase AC
9	Micro Craft Technology	USA			2.44	3.66	4.57	(120.7)	2250	6.1 m in diameter 6-bladed fan 5 to 850 rpm
10	US Air Force Academy Subsonic Wind Tunnel	USA	1985	Closed	0.92	0.92	-	0.58	1000	575 V AC 2.75 m in diameter axial fan

Table 1.1 Subsonic Wind Tunnels in the World (Continued)

#	Tunnel	Country	Date Built	Type	Test Section Dimensions (m)			Mach (Speed, m/s)	Power hp (kW)	Power Type & Fan Properties
					H	W	L			
11	Boeing V/STOL Wind Tunnel (BVWT)	USA	1968	Closed	6.1	6.1	12.8	(118)	15000	9 bladed fan
12	Aerodynamic Model Test Facility	USA	1992	Closed	1.34	2.29	8.23	(80.46)	1000	fan
13	Wind Tunnel 2	USA	1958	Closed	3.81	6.1	9.14	0.2 (68)	2000	fan
14	ONERA F1	France		Closed pressurized	3.5	4.5	11	0.36	(9500)	16 bladed fan constant speed variable pitch
15	ONERA F2	France		Closed atmospheric	1.8	1.4	5	(100)	(750)	DC motor 12-bladed fan
16	GM Aerodynamics Laboratory	USA	1980	Closed	5.5	10.4	21.3	(70)	4000	Variable speed DC motor fixed pitch 6-bladed fan

Table 1.1 Subsonic Wind Tunnels in the World (Continued)

#	Tunnel	Country	Date Built	Type	Test Section Dimensions (m)			Mach (Speed, m/s)	Power hp (kW)	Power Type & Fan Properties
					H	W	L			
17	Lockheed Martin LSWT	USA	1967	Closed	5	7.1	12.8	0.26 (90)	12000	6 blade fan
18	Wright Brothers Memorial Tunnel	USA	1938	Closed	2.29	3.05	4.57	(76)	(2000)	AC
19	NASA-Glenn Research Center 9 x 15 ft LSWT	USA	1967	Closed	2.74	4.57	8.53	0.2	(35000)	7 stage axial compressor
20	NSWCCD Wind Tunnel No.1	USA	1943	Closed	2.44	3.05	4.27	0.25 (84)	1000	electric motor fan
21	INCAS Subsonic Wind Tunnel	Romania	1950	Closed	2.5	2	5	(100)	(1200)	Variable speed DC motor 3.5 m in diameter 12-bladed fan
22	Subsonic Wind Tunnel T-1	Russia		closed	3 m diameter circular		6.5	(60)	(1000)	6 bladed fan

Table 1.1 Subsonic Wind Tunnels in the World (Continued)

#	Tunnel	Country	Date Built	Type	Test Section Dimensions (m)			Mach (Speed, m/s)	Power hp (kW)	Power Type & Fan Properties
					H	W	L			
23	7 x 10 Foot Wind Tunnel	USA	1956	Closed	2.13	3.05	6.1	0.36	4000	Toshiba International wound rotor motor 4160 V rpm controlled max rpm=685 6 blade fan constant 32 deg. pitch angle
24	Auto Research Center	USA	1998	Closed	2.1	2.3	5.5	(50)	(320)	DC-electric
25	NASA-Langley Research Center 14 x 22 ft Subsonic Tunnel	USA	1970	Closed	4.42	6.63	15.24	(100)	8000	Electrical drive system 12.2 m in diameter 9-bladed fan 6650 hp AC induction motor in tandem with a 1350 hp direct current motor

Table 1.1 Subsonic Wind Tunnels in the World (Continued)

#	Tunnel	Country	Date Built	Type	Test Section Dimensions (m) H	W	L	Mach (Speed, m/s)	Power hp (kW)	Power Type & Fan Properties
26	Penn State University Subsonic WT	USA	1953	Closed	1.22 m diameter circular		4.88	(45.72)	150	Axial flow blower Variable speed
27	Texas A&M University The Oran W. Nicks LSWT	USA	1950	Closed	2.13	3.05	3.66	0.25 (90)	1500	3.81 m in diameter 4 blade Variable pitch Constant rpm(900) 1250 KVA
28	Swift Aero	USA	1994	Closed	2.74	2.44	6.71	(63)	500	Electric motor fan
29	University of Maryland GLM WT	USA	1947	Closed	2.36	3.35	3.66	0.3	2250	fan
30	University of Washington Aero Lab Kirsten Wind Tunnel	USA	1936	Closed Double return	3.7	2.4	3	(89.5)	2x500	Two electric motors Fans two sets of 4.5 m in diameter 7 bladed propellers

Table 1.1 Subsonic Wind Tunnels in the World (Continued)

#	Tunnel	Country	Date Built	Type	Test Section Dimensions (m)			Mach (Speed, m/s)	Power hp (kW)	Power Type & Fan Properties
					H	W	L			
31	Wichita State University Walter H. Beech Memorial Wind Tunnel	USA	1948	Closed	2.13	3.05		(70)	1000	2300 V 3 phase electric wound-rotor induction motor
32	NASA Langley Research Center Low Turbulence Pressure Tunnel	USA		Closed-circuit Single return	2.29	0.92	2.29	0.5	2000	20-bladed propeller
33	NASA Langley Research Center 20-Foot Vertical Spin Tunnel	USA		Closed-throat Annular return	12-sided test section 6.1 m in wide		7.62	(26)	400	DC motor 3-bladed fixed pitch fan
34	Subsonic Wind Tunnel T-101	Russia		Closed circuit Open test s.	14 m circular		24	(55)	(30000)	2 fan

Table 1.1 Subsonic Wind Tunnels in the World (Continued)

#	Tunnel	Country	Date Built	Type	Test Section Dimensions (m)			Mach (Speed, m/s)	Power hp (kW)	Power Type & Fan Properties
					H	W	L			
35	Naval Surface Warfare Center 8 by 10 Foot Subsonic Wind Tunnel	USA	1943	Closed	2.44	3.05	4.27	(80)	1000	Clymer-type main drive electric induction motor 4.88 m in diameter fans main fan: 4. 0.48 m mean chord blades windmill: 5. 0.4064 m constant chord blades
36	GALCIT Adaptive WT California Institute of Technology	USA	2002	Closed	1.52	1.83	7.62	(76.2)	670	16-blade 13 stator 2.44 m diameter fan adjustable pitch Toshiba variable frequency motor drive
37	Universiti Teknologi Malaysia UTM-LST	Malaysia	2001	Closed	1.5	2	5.8	(30)	(430)	AC motor 2.9 m in diameter 16-bladed axial fan variable rpm

Table 1.1 Subsonic Wind Tunnels in the World (Continued)

#	Tunnel	Country	Date Built	Type	Test Section Dimensions (m)			Mach (Speed, m/s)	Power hp (kW)	Power Type & Fan Properties
					H	W	L			
38	Airbus Filton Low Speed Wind Tunnel Facility	United Kingdom	1957	Closed	3.66	3.05	7.62	0.25 (97)	(1600)	fan
39	0.5 x 0.5 m Low Turbulence Wind Tunnel	United Kingdom		Closed	0.5	0.5	3	(42)	(30)	single stage 5 bladed fan tacho controlled drive
40	AVRO 9 x 7 Foot Low Speed Wind Tunnel	United Kingdom	1988	Closed	2.75	2.23	5.5	(70)	(400)	single stage 4 bladed fan tacho controlled drive
41	5 Meter Low Speed WT	United Kingdom	1977	Closed	4.2	5	8	0.34	(13600)	DC and AC on a common shaft

Table 1.1 Subsonic Wind Tunnels in the World (Continued)

#	Tunnel	Country	Date Built	Type	Test Section Dimensions (m) H	W	L	Mach (Speed, m/s)	Power hp (kW)	Power Type & Fan Properties
42	Vertical Subsonic Wind Tunnel T-105	Russia		Closed Open test section	4.5 m circular		7	(35)	(450)	fan
43	Subsonic wind tunnel T-129	Russia		Closed Open test section	1.2		1.75	(80)	(200)	fan
44	Wind Tunnel T-324	Russia		Closed	1	1	80	(80)	(640)	DC motor 1-staged axial fan 20 wooden blades
45	I.A.T S4	France	1974	Closed	3	5	10	(40)	(260)	2 fan 4 blade (each) 4.6 m in diameter
46	I.A.T S6	France	1980		4	6	17	(16)	(27x28)	27 fan
47	VIGYAN Low Speed Wind Tunnel	USA	1987	Open	0.9	1.2	1.5	(12–55)	150	Constant rpm Variable pitch

Table 1.1 Subsonic Wind Tunnels in the World (Continued)

#	Tunnel	Country	Date Built	Type	Test Section Dimensions (m) H	W	L	Mach (Speed, m/s)	Power hp (kW)	Power Type & Fan Properties
48	I.A.T S10	France	1985		3	5	10	(55)	(2x500)	2 fan 4 blade 4.8 m in diameter
49	I.A.T SVL	France	1972		1.7	2.2	15	(40)	(150)	4 blade 2.8 m in diameter
50	Institute & Chair of Aerospace Eng. (ILR)	Germany		Closed	1.5 m diameter circle		3	(70)	(500)	1 stage, 1000 rpm outer diameter: 2.4 m inner diameter: 1.4 m three phase motor hydraulic blade control
51	VKI L-2A Low Speed Wind Tunnel	Belgium		Open Suction type	octagonal test section 0.28 m in width		1.3	(45)	(10)	Axial fan Variable speed DC motor

Table 1.1 Subsonic Wind Tunnels in the World (Continued)

#	Tunnel	Country	Date Built	Type	Test Section Dimensions (m)			Mach (Speed, m/s)	Power hp (kW)	Power Type & Fan Properties
					H	W	L			
52	Aeroacoustic Wind Tunnel	Germany	1998	Closed	9	15	16	(83)	(2600)	DC-Fan
53	Wind Kanal Ut	Germany	1939	Closed	4.8	7.2	12	(70)	(4000)	fan
54	Technical University Darmstadt Unterschall-Kanal	Germany	1937	Closed	2.2	2.9	4.3	0.2 (68)	(300)	single stage axial fan
55	Volkswagen KW1	Germany	1966	Closed	5	7.5	10	(55)	(2600)	fan
56	Low Speed Tunnel (LST)	Germany & Netherlands	1983	Closed walls	2.25	3.0		0.23 (80)	(700)	fan

Table 1.1 Subsonic Wind Tunnels in the World (Continued)

#	Tunnel	Country	Date Built	Type	Test Section Dimensions (m)			Mach (Speed, m/s)	Power hp (kW)	Power Type & Fan Properties
					H	W	L			
57	Large-Low speed facility (LLF)	Germany & Netherlands		Closed walls	9.5	9.5	20	0.18 (62)	(12500)	fan
58	DNW-NWB	Germany & Netherlands	1960	Closed	3.25	2.8	8	(90)	(1400)	Tyristor controlled single stage fan DC motor
59	Railway Technical Research Institute	Japan	1996	Closed	3	5	20	(83)	(7000)	single stage fan
60	Full Scale Wind Tunnel	Japan	1981	Closed /Open	4	6	12	(60)	(2350)	8m in diameter 10 blades 20 to 260 rpm
61	Nihon University Low Speed Wind Tunnel	Japan	1975	Closed	5.3	2	2	(50)	(250)	fan

Table 1.1 Subsonic Wind Tunnels in the World (Continued)

#	Tunnel	Country	Date Built	Type	Test Section Dimensions (m)			Mach (Speed, m/s)	Power hp (kW)	Power Type & Fan Properties
					H	W	L			
62	Full-scale Aerodynamic Wind Tunnel	Japan	1985	Closed	7.4	5	12	(75)	(2200)	fan
63	NRC-CNRC 9 m x 9 m Low Speed Wind Tunnel	Canada		Closed	9.1	9.1	23.9	(55)	9000	DC motor 8-bladed fan
64	NRC Low Speed Wind Tunnel	Canada	1940	Closed	1.93	2.74	5.2	0.4	(1500)	fan
65	Agusta AWT	Italy	1940	Closed open test section	2 diameter		2.7	(70)	(800)	8 blades 2 fan
66	PF Wind Tunnel	Italy	1972	Closed	7.98	5	2.9	(55)	1675	DC motor 29 blade fan
67	LT1	Sweden	1940	Closed	3.6 m diameter circular		8	(80)	(1500)	fan

Table 1.1 Subsonic Wind Tunnels in the World (Continued)

#	Tunnel	Country	Date Built	Type	Test Section Dimensions (m)			Mach (Speed, m/s)	Power hp (kW)	Power Type & Fan Properties
					H	W	L			
68	Galleria del Vento del Politecnico di Milano	Italy	2002	Closed	3.84	13.8 4	36	(16)	(1400)	12 bladed fan 1.75 m in diameter
69	Volvo Wind Tunnel	Sweden	1986	Closed	15.2	6.6	4.1	(55)	(2700)	8.15 m fan
70	VKI Aeronautics and Aerospace Department L1A Subsonic Wind Tunnel	Belgium			3 m circular			(60)	(580)	DC motor variable speed
71	RUAG Aerospace Emmen 7x5 m	Switzerland	1945	Closed	7	5	11	(70)	(3000)	2 counter rotating fan 8 bladed 8.5 m in diameter
72	LSWT	South Africa	1964	Closed	2.1	1.5	4.5	(120)	1000	fan

Table 1.1 Subsonic Wind Tunnels in the World (Continued)

#	Tunnel	Country	Date Built	Type	Test Section Dimensions (m)			Mach (Speed, m/s)	Power hp (kW)	Power Type & Fan Properties
					H	W	L			
73	TA-1	Brazil	1930	Closed	0.1778 m octagonal			0.13 (58.11)	200	fan
74	Defence Science and Technology Organisation	Australia	1941	Closed	2.1	2.7	3.6	(100)	(660)	3.96 m in diameter 8-blades variable rpm (max rpm : 750)
75	IAI-LSWT	Israel	1973	Closed	3.66	2.59	6	(100)	1750	fan
76	4 Meter Low Speed Wind Tunnel	South Korea	1998	Closed	3	4	10	(110)	(3740)	fan
77	Indonesian Low Speed Tunnel	Indonesia	1987	Closed	3	4	10	(110)	(5000)	fan
78	Harper Wind Tunnel	USA	1931	Closed	2.13	2.74	3.2	0.2	600	AC electric motor fan

Table 1.1 Subsonic Wind Tunnels in the World (Continued)

#	Tunnel	Country	Date Built	Type	Test Section Dimensions (m)			Mach (Speed , m/s)	Power hp (kW)	Power Type & Fan Properties
					H	W	L			
79	Old Dominion University The Langley Full Scale Wind Tunnel	USA	1931	Closed Double return	9.1	18.3	17.1	(36)	2x4000	Variable speed wound rotor induction motors. each driving fixed-pitch 4 bladed 10.8 m in diameter laminated wooden propellers
80	NASA Ames Research Center 7 by 10 Foot Wind Tunnel	USA	1940	Closed	2.13	3.05	4.57	0.4 (133)	(1172)	fan
81	NASA Ames Research Center 40 by 80 Foot Wind Tunnel	USA		Closed	12.19	24.38	24.38	0.32 (107)	(6 x 4043)	6 fan

Table 1.1 Subsonic Wind Tunnels in the World (Continued)

#	Tunnel	Country	Date Built	Type	Test Section Dimensions (m)			Mach (Speed, m/s)	Power hp (kW)	Power Type & Fan Properties
					H	W	L			
82	Small Wind Tunnel of Civil Engineering Department of METU	Turkey		Closed	0.3	0.4		(30)		
83	Subsonic Wind Tunnel of Mechanical Engineering Department of METU	Turkey		Open	0.5	0.6		(40)		
84	Small Subsonic Research Wind Tunnel of Aerospace Engineering Department of METU	Turkey		Open	0.3	0.3		(30)		

Table 1.1 Subsonic Wind Tunnels in the World (Continued)

#	Tunnel	Country	Date Built	Type	Test Section Dimensions (m)			Mach (Speed, m/s)	Power hp (kW)	Power Type & Fan Properties
					H	W	L			
85	Large Subsonic Wind Tunnel of Civil Engineering Department of METU	Turkey	1950	Open	1.5	6.0		(20)		
86	Subsonic Wind Tunnel with Open Test Section of İTÜ	Turkey		Open	0.8	0.8		(40)		
87	Gümüşsuyu Closed Circuit Subsonic Wind Tunnel of İTÜ	Turkey		Closed	0.8	1.1		(40)		

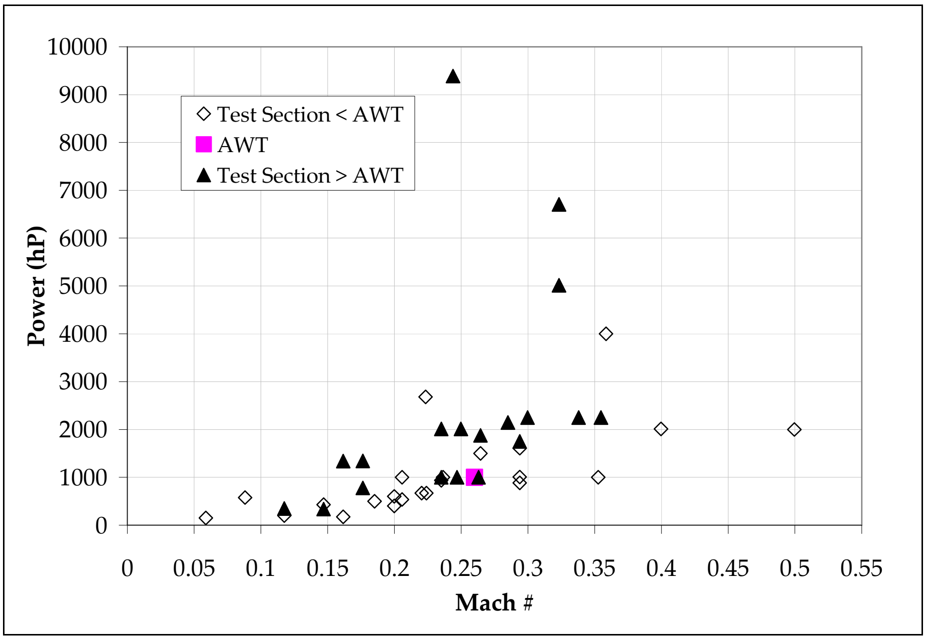

Figure 1.1 Variation of Power with Mach Number for Tunnels Having Different Test Section Areas.

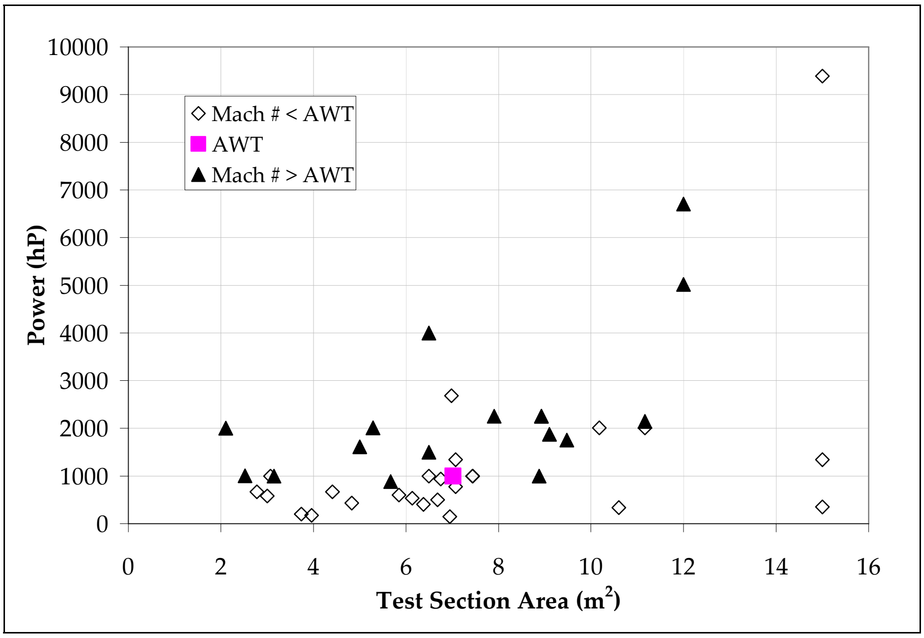

Figure 1.2 Variation of Power with Test Section Area for Tunnels Having Different Mach Numbers.

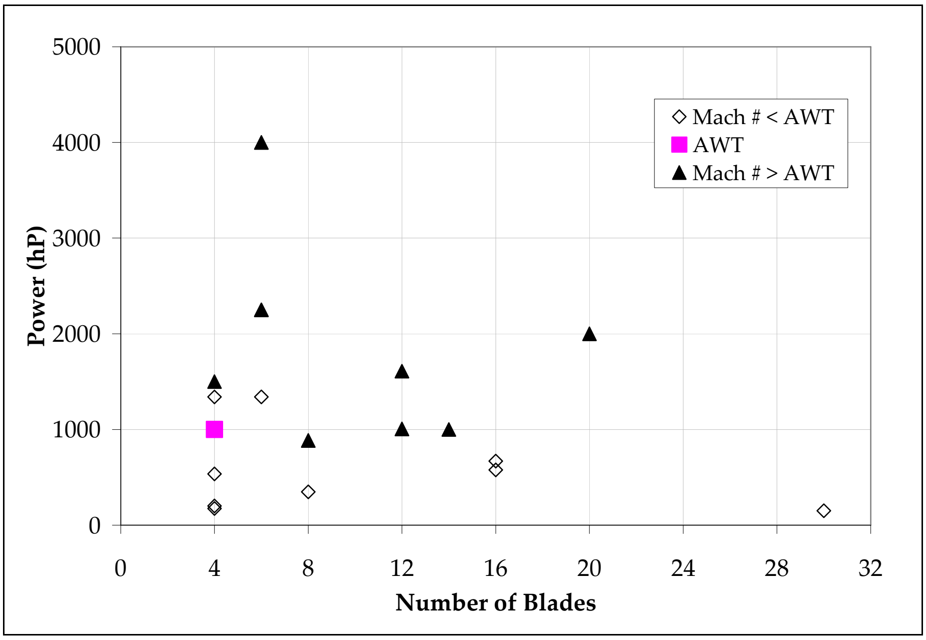

(a) For Different Mach Numbers.

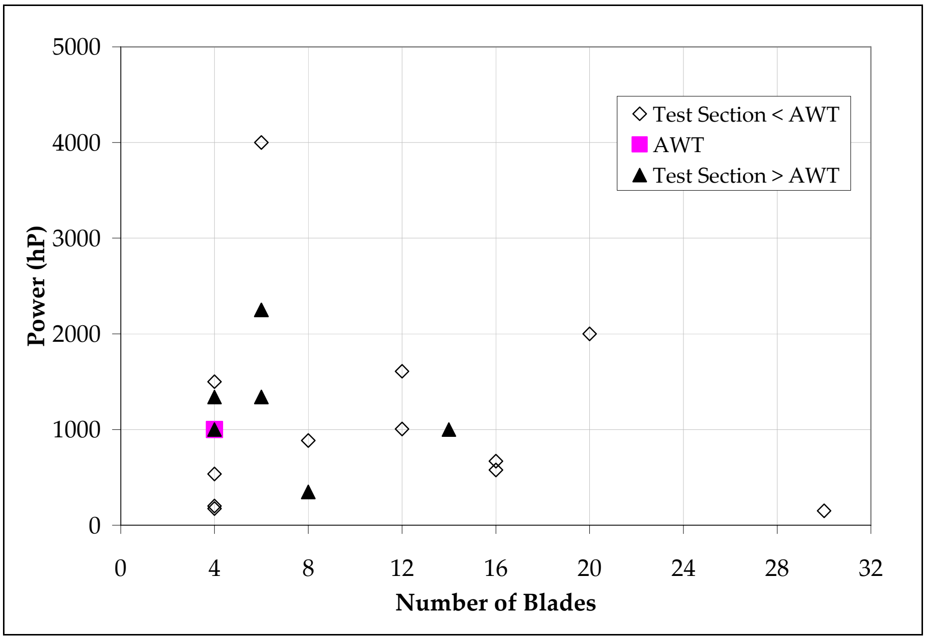

(b) For Different Test Section Areas.

Figure 1.3 Variation of Power with Number of Blades.

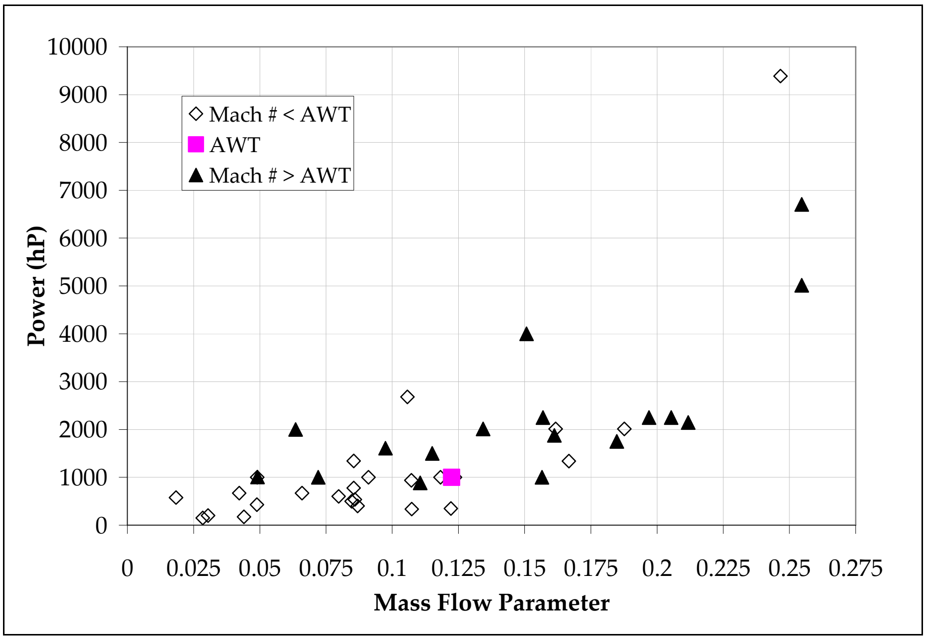

(a) For Different Mach Numbers.

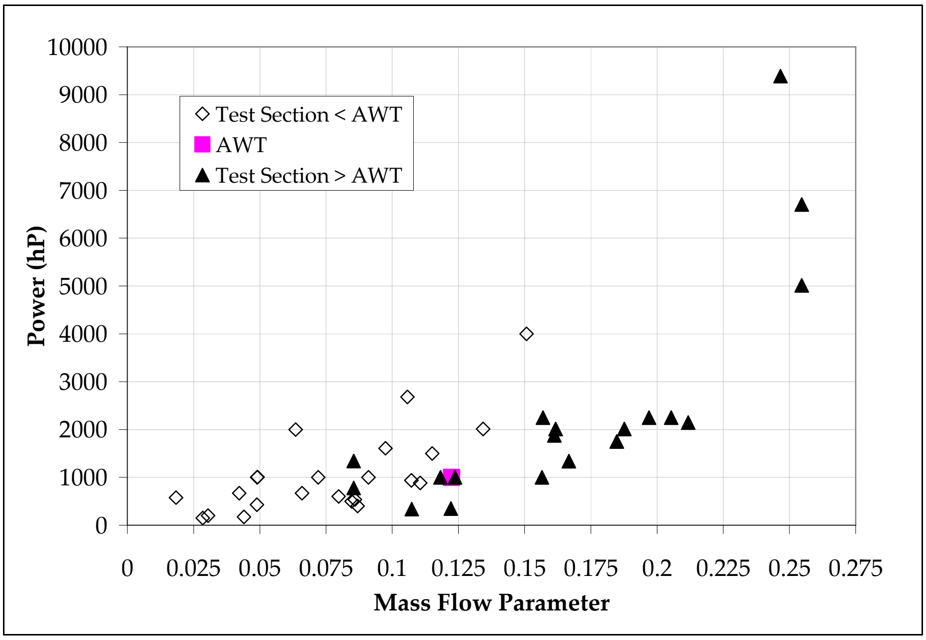

(b) For Different Test Section Areas.

Figure 1.4. Variation of Power with Mass Flow Parameter.

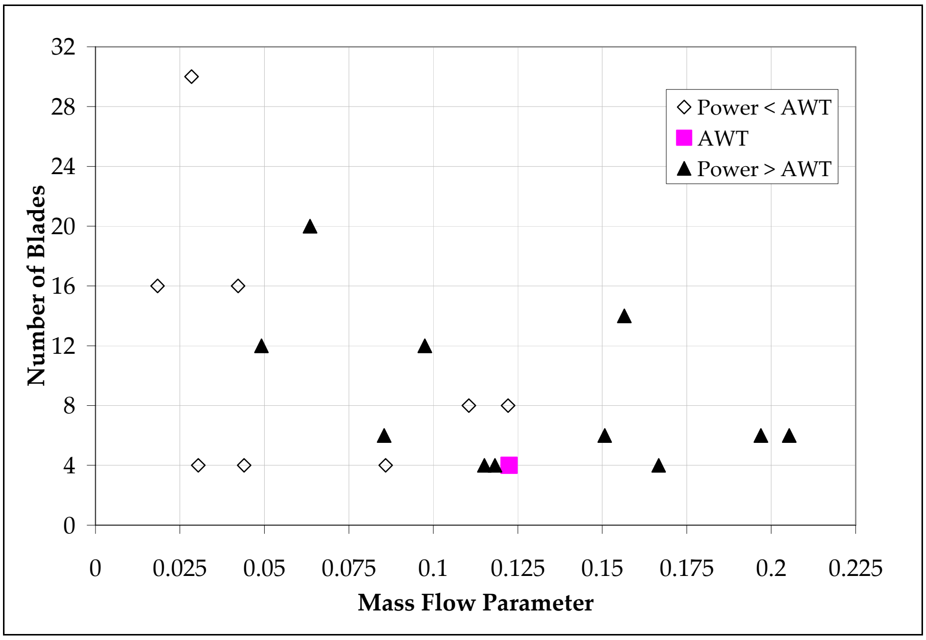

Figure 1.5 Variation of Number of Blades with Mass Flow Parameter.

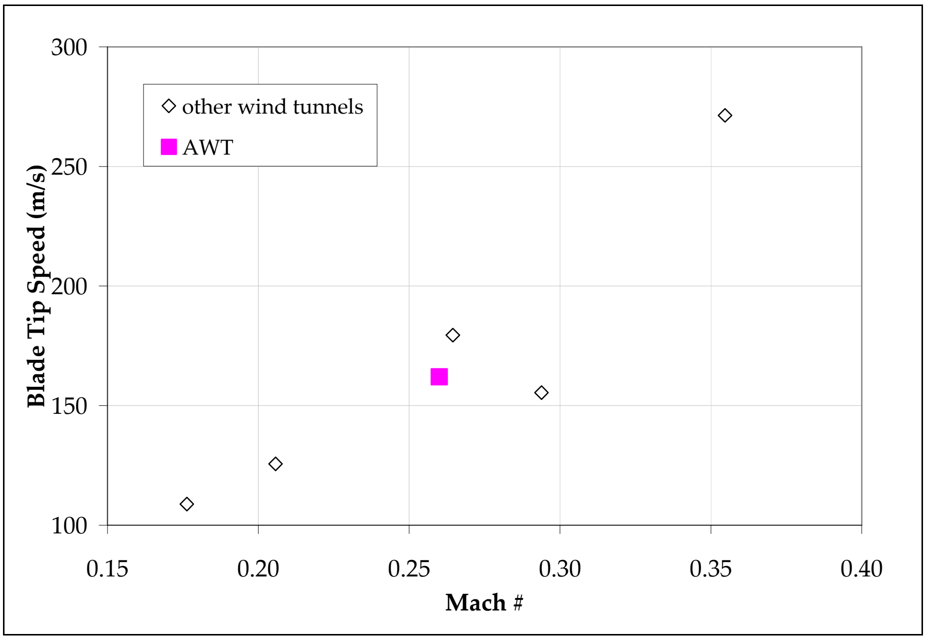

Figure 1.6 Variation of Blade Tip Speed with Mach Number.

1.2 Ankara Wind Tunnel

The Ankara Wind Tunnel was established in 1950. While establishing such a complex, it was aimed to give support to the aircraft industry and academic research and development. The wind tunnel has been managed by many government organizations. Presently, Defense Industries Research and Development Institute of the Scientific and Technological Research Council of Turkey (TÜBİTAK-SAGE) has formed a team of researchers to operate the tunnel for the needs of the aerospace industry and other applicable areas.

The chronology of Ankara Wind Tunnel is summarized below:

- 1941: Starting to Design of AWT
- 1950: Building of AWT
- 1955: Installing of External Balance System
- 1955-1993: Being idle after aircraft factory was closed
- 1993: Starting "Improvement of AWT" Project by TÜBİTAK-SAGE
- 1994: Re-operating of AWT
- 1994-1995: Calibrating and Analyzing of AWT
- 1996-1998: Operating, modernizing and calibrating the external balance system
- 1999: Opening of AWT for industrial usage
- 2000: Being a member of Subsonic Aerodynamic Testing Association (SATA)

Ankara Wind Tunnel is a horizontal, closed circuit, low subsonic (M = 0.26) wind tunnel. Test section is atmospheric and 2.44 m x 3.05 m x 6.1 m (height x width x length) in size. Tunnel circuit is concrete except the wooden test section.

A wide variety of tests can be performed in the Ankara Wind Tunnel such as the tests of

- full size and scaled model cars,
- aircraft models and components,
- weapon systems,
- buildings and building materials,
- wind turbines,
- dish antennas,
- parachutes,
- submarines,
- street lights.

The AWT was designed to be driven by an axial flow fan. The existing fan, which is shown in Fig. 1.7, is located downstream of the test section at the second corner. It consists of rotor, prerotator and straightener. The properties of the fan are summarized below:

- Number of rotor blades : 4 (wooden)
- Hub Diameter : 1.53 m
- Blade Diameter : 5.16 m
- Hub Length : 7.37 m
- Number of inlet guide vane (prerotator) : 7 (reinforced concrete)

- Number of outlet guide vane (straightener) : 7 (reinforced concrete)
- Maximum rpm : 600 (variable rpm)
- Power of the fan : 1000 hP

Figure 1.7 Ankara Wind Tunnel Fan (Looking From Downstream).

1.3 Objective of the Thesis

The objective of this thesis is to design a variable pitch axial flow fan for the Ankara Wind Tunnel (AWT) and to increase the Mach number from 0.26 to 0.52, and determine the performance characteristics of the fan over operating range. It is also aimed to determine

- the sizes of every section of AWT,
- the loss characteristics of AWT,
- aerodynamic efficiency of the existing fan,
- power requirement necessary to reach a Mach number of 0.52.

1.4 Outline of the Thesis

In Chapter 2, information is given about axial flow fans. General types of fans, ducted fan unit, types of ducted fan, fan theory, rotor and stator design methods, airfoils for rotor and stator are presented in detail.

Chapter 3 deals with the design of a variable pitch axial flow fan. First of all, loss characteristics and power requirement of the AWT are determined and design inputs and design constraints are given. The design methodology and related equations are also presented for the rotor, straightener and hub cone.

In Chapter 4, the designed fan is analyzed at different volumetric flowrates and blade angles including the design point and the overall performance characteristics of the fan are obtained.

Conclusions of this study are given in Chapter 5.

CHAPTER 2

AXIAL FLOW FANS

2.1 Overview

Computational and experimental methods are two basic tools used in aerodynamic design. Although the usage of computational fluid dynamics methods is increasing very fast in recent years thanks to the improvements in computer technology; experimental methods still play a very important role in the aerodynamic design. Flight tests, road tests, ballistic tunnels and wind tunnels are the major types of experimental methods. Because of safety, speed, reliability and low price; wind tunnels are frequently used in aerodynamic testing of different shaped bodies throughout the world such as aircrafts, missiles, space shuttles, helicopters, road vehicles, buildings and many others.

Test section size and maximum speed are two basic properties defining the capacity and reliability of a wind tunnel. Although there are some correction methods for speed, higher maximum speeds are preferred as it increases the sensitivity of results. As the test section size increases, wind tunnel models get larger. Test section size and maximum speed directly depend on fan and driving system.

The driving system and the fan are generally the most expensive and among the most critical parts of wind tunnels. Fans may be classified as centrifugal fans or axial-flow fans. In centrifugal fans, air is led through an inlet pipe to the centre or eye of the impeller, which forces it radially outward into the volute or spiral casing from which it flows to a discharge pipe. An axial flow fan may be described as a fan in which the flow of air is parallel to the axis of the rotor. In the simplest form, air approaches the rotor in the axial direction and leaves it with a rotational velocity component due to the work done by the rotor. More advanced designs have upstream and/or downstream guide vanes to obtain a higher static pressure difference across the rotor. Guide or stator vanes serve to smoothen / straighten the airflow and improve efficiency. If the pressure losses are high, multistage fans may also be used.

In general, an axial-flow fan is suitable for a larger flowrate with a relatively small pressure gain and a centrifugal fan for comparatively smaller flowrate and a large pressure rise [21].

Important factors affecting the choice of fan unit are

- manufacturing simplicity
- cost of manufacture
- power input to fan
- fan tip speed and fan noise
- required flow speed in the test section
- fan efficiency
- flow reversal in an emergency

The first two former often favour the centrifugal while the subsequent two favour the axial flow type [2].

While aircraft propeller type fans are used in most wind tunnels for circulating the air, in some cases multiblade centrifugal fan are also employed. According to wind tunnel test, the propeller fan was found to be superior to the centrifugal fan in that the efficiency was about twice as great while the flow was also much smoother [20].

Axial flow fans are finding greater acceptance in industrial applications as alternative equipment to the radial flow machinery [1].

Axial flow fans are designed by using either "free vortex flow theory" or "arbitrary vortex flow theory".

The conventional method of blade design for axial flow fans and compressors specifies a free-vortex type of blade loading, which is characterized by an essentially two dimensional flow through the rotor disk. According to free vortex theory, the blades are loaded radially so that no mutual interference exists between adjacent blade elements. This loading is accomplished by having the absolute tangential velocities in front of and behind the fan varies inversely with the radius, i.e,

$$V_\theta = \frac{Const.}{r} \tag{2.1}$$

The flow through free vortex blading in incompressible flow is essentially quasi-two dimensional in character; no radial velocities occur in the flow field outside the boundary layer regions. In incompressible flow, therefore, the axial velocities at a particular radius are the same upstream and downstream of the fan when the flow area is constant. A free vortex rotor is also characterized by a uniform total energy rise across the annulus. Free vortex flow is achieved when both the total pressure rise and axial velocity component remain constant along the blade span.

Arbitrary vortex flow theory (non-free vortex theory) is generally used in design of high pressure rise rotor [12]. In this case, spanwise load distribution differs from the free vortex type. This loading is generally accomplished by having a constant absolute tangential velocity, i.e,

$$V_\theta = Const. \tag{2.2}$$

Another distribution of load along the blade span is,

$$V_\theta = Const \times r \tag{2.3}$$

This is known as “solid rotation”, so called because in this case the air would rotate as though it were a solid body.

Free vortex flow is assumed when designing ducted axial flow fans. This theory permits simple design methods and high efficiencies [1, 2]. Tests of a series of free vortex designed fans are reported in reference 13; the experimental results therein show excellent agreement with the theory.

2.2 General Types of Axial Flow Fans

In the existing literature the axial-flow fans are generally placed in three main categories:

1. Air circulator or free fan: A free fan is one that rotates in a common unrestricted air space. Desk, wall, pedestal and ceiling fans fall into this category.
2. Diaphragm-mounted fan: This type of fan transfers air from one relatively large air space to another.
3. Ducted fan: A fan is ducted when the air is constrained by an enclosing duct to enter and leave the fan blading in an axial direction. The minimum duct length required to satisfy this condition will be in excess of the distance between inlet to and outlet from the blading.

The first two types are relatively long-established, being currently in common usage. The task that they perform, generally speaking, can not be economically performed by radial flow equipment. Although improvements have been made in the design of these unducted types, there are still many of a relatively crude type in existence. Exhaust fans that operate in short, compact ducts constitute a worthwhile improvement over the diaphragm-mounted variety and could eventually supersede the latter. Higher efficiencies and lower noise levels will, of course, be associated with the better class of air circulator and exhaust units [1].

Wind tunnel fan must be of ducted fan type whether the tunnel is open or closed circuit because the fan is located inside the tunnel circuit.

2.3 Elements of a Ducted Fan Unit

The various elements that go to make up a ducted fan unit are illustrated in Fig. 2.1. When additional fan stages are fitted in series, the pressure rise which a single unit is capable of increases, in the extreme case a multistage unit becomes a compressor.

Rotor blades are a series of airfoils that by virtue of relative motion with respect to the air mass add total pressure to the airstream. It is desirable to reach desired a uniform test section speed with minimum power input, friction, secondary flow, and flow separation losses.

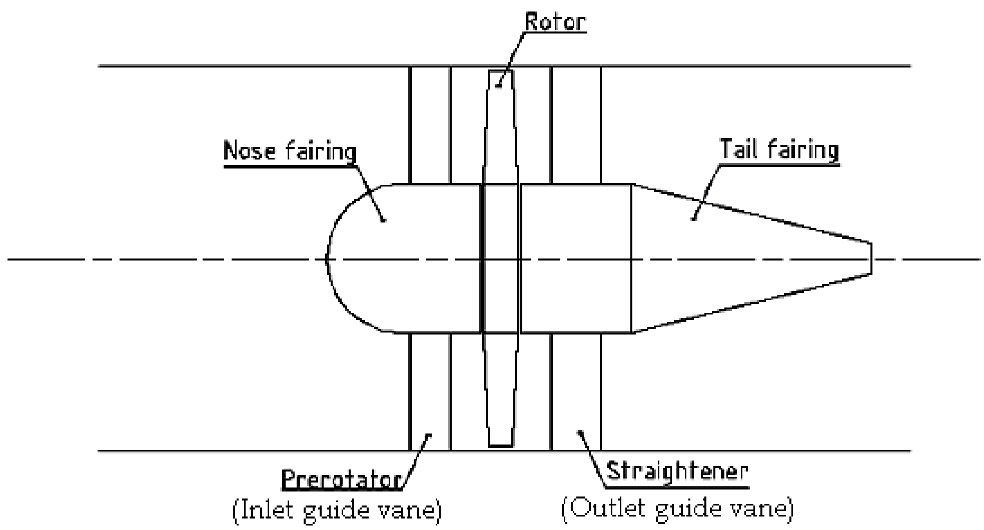

Figure 2.1 Components of Ducted Fan Unit.

Stationary vanes known as stators or guide vanes are normally located upstream and/or downstream of the rotor to achieve maximum amount of useful pressure. The air flowing through prerotating stators is accelerated and, in accordance with Bernoulli's equation, the static pressure falls. However, the reverse occurs in straighteners, where a static pressure rise accompanies the removal of the tangential velocity component.

Suitably shaped fairings upstream and downstream of the hub are an essential part of a good design. In a multistage unit of co-rotating rotors, a stator row is required between rotor stages. Contra-rotating rotors do not normally require inlet or outlet guide vanes.

The purpose of a fan is to increase the total pressure of the air to a value equal to the total resistance losses in any given duct system so as to achieve desired uniform test section speed . These losses that have to be overcome within the wind tunnel are due to skin friction, flow separation, secondary flow and energy dissipation at system discharge [1, 8].

Duct resistance increases approximately as the square of the velocity for turbulent flow, which is the type normally encountered in industrial installations. The nature of the characteristic curve for the duct system is illustrated in Fig. 2.2. The fan characteristic cuts this curve to give the operating point of the system for a given fan speed. Provided the fan is not stalled, flow conditions will be steady; this feature is emphasized by the very definite point at which the two characteristics intersect.

$$P_{input} = \frac{\left(\sum_{i=1}^{N} K_{0_i}\right) \cdot \rho_0^{\ 2} \cdot A_0 \cdot V_0^{\ 3}}{2 \cdot \rho_F} \tag{2.4}$$

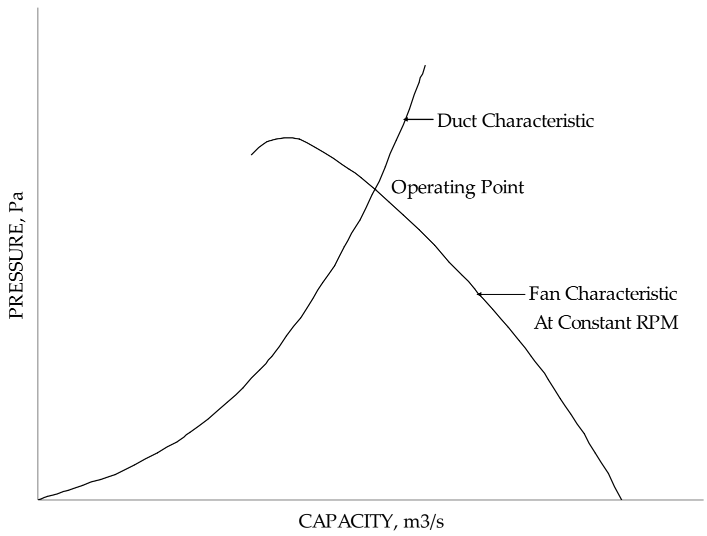

Figure 2.2 Matching of Fan and Duct System.

Denoting the mean total pressure at fan inlet and outlet by the symbols $P_{t_{in}}$ and $P_{t_{out}}$, the fan total pressure ($\Delta P_{t_{fan}}$) is given by

$$\Delta P_{t_{fan}} = P_{t_{out}} - P_{t_{in}} \tag{2.5}$$

For a given duct system the volume through the fan is normally varied by changing the rotor speed. Alternative methods which have been devised for the purpose of altering the fan characteristic utilize variable pitch rotor or stator blades. Fans provided with pitch change capability are known as adjustable-or variable pitch units, where the latter term refers to equipment in which the pitch can be changed without stopping the fan.

2.4 Types of Ducted Fan: Aerodynamic Classification

When a fan rotor adds total head to the air flowing through it, the angular momentum of the stream is increased. For example, a rotor receiving mainly an axial air flow discharges it with a tangential component of velocity, resulting in the appearance of a phenomenon which in the theory of aircraft propellers is known as “slipstream rotation”. The change of angular momentum in the airstream is directly related to the torque on the rotor shaft.

The efficiency of the fan unit is also influenced by the amount of the swirl left in the air after it has passed the last stage of blading in the unit.

Five main design possibilities arise as a result of the above mentioned aerodynamic phenomenon of slipstream rotation.

a) No-straightener rotor unit: The swirl passes downstream of the rotor and associated momentum is lost.
b) Rotor-straightener unit: The swirl is removed by the stators placed downstream of the rotor and the associated dynamic head is recovered in the form of a static pressure rise.
c) Prerotator-rotor unit: Stators are used to impart a preswirl in the opposite sense to the rotor motion and the rotor then removes the swirl.
d) Prerotator-rotor-straightener unit: A combination of the preceding two configurations.

e) Contra-rotating rotors: The second rotor removes the swirl introduced by the first.

The question is often raised whether an inlet guide vane or an outlet guide vane should be chosen. In many cases the decision is governed by the type of installation and overall arrangements. Inlet guide vane is only benefit for very low hub to rotor diameter ratios and particularly for fans having blades with small lift to drag ratios. In practice, present tendency is to design axial flow fan with outlet guide vanes. This is justified because an outlet guide vane removes the swirl component of velocity and increases the static pressure developed by the fan.

The rotors in a contra-rotating fan assembly will differ, with the rear rotor possessing blading with lower solidity and pitch settings than the leading one.

Multistage co-rotating units may be designed with identical rotors and stators, except for instances where air compressibility becomes an important factor.

The magnitude of the pressure rise required produces detailed design differences between fans that are nominally of a similar type. For example, low pressure-rise fans possess a smaller number of blades than the high pressure rise fans; the relative hub diameter will be greater in the latter case.

Comparative characteristics for fans are shown in Fig. 2.3. As seen, the highest pressure is naturally expected from a contra-rotating fan. Although fans with inlet guide vanes develop higher pressures than fans equipped with outlet guide vanes, they show marked stalling characteristic.

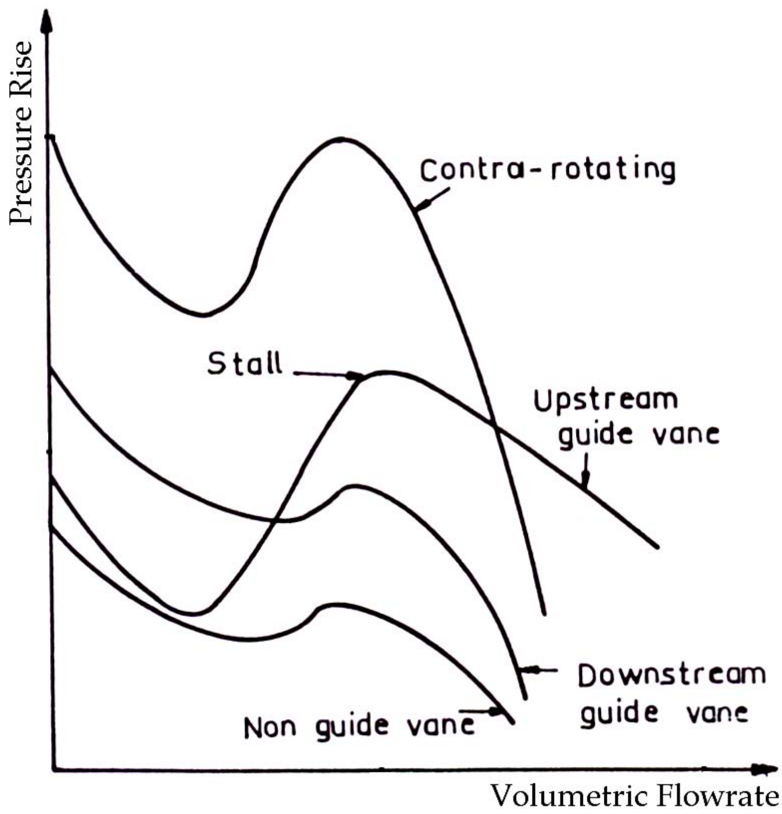

Figure 2.3 Characteristic of Axial Flow Fans.

2.5 Theoretical Considerations

Axial flow fans are designed by using either "free vortex flow theory (two dimensional flow with uniform total pressure spanwise distribution and radial equilibrium)" or "arbitrary vortex flow theory (two dimensional flow with radial gradients of axial velocity and total pressure and also radial equilibrium)".

A vortex can be qualitatively described as a circulatory flow about an axis OZ as shown in Fig. 2.4. When the fluid has a velocity component in the direction OZ, the air particles trace out helical flow paths.

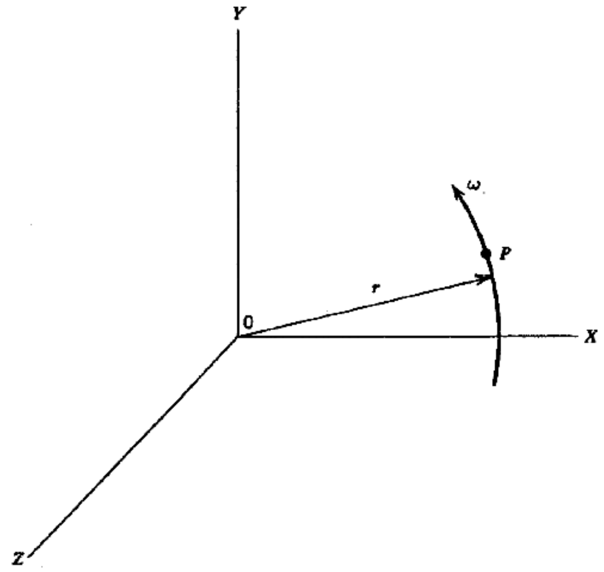

Figure 2.4 Vortex Flow.

When these paths maintain a constant radius, a condition for radial equilibrium exists, namely, a balance is maintained between the centrifugal and pressure forces acting on the particle. The equilibrium requirements for this two-dimensional balance, is termed free vortex flow.

Assume that an element of fluid at radius r with unit length in the direction OZ rotates with tangential velocity V_θ about the axis OZ as shown in Fig. 2.5. The centrifugal force acting on the element is given by

$$dF_c = s \cdot dr \cdot \rho \cdot \frac{V_\theta^2}{r} \tag{2.6}$$

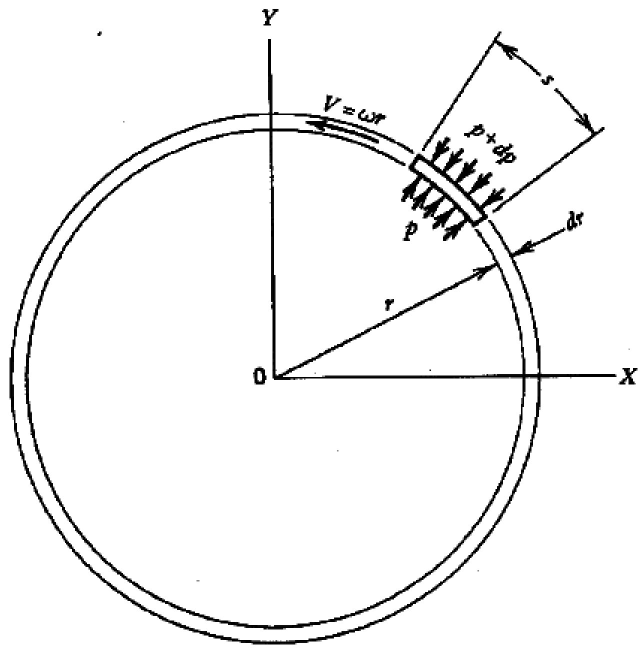

Figure 2.5 Rotating Element.

and the pressure force by

$$dF_p = dp \cdot s \tag{2.7}$$

where dp is the pressure difference between the two faces of the element. Equating the two forces gives

$$\frac{dp}{dr} = \rho \cdot \frac{V_\theta^2}{r} \tag{2.8}$$

which is a universal requirement for radial equilibrium. The total pressure of a particle in equilibrium is

$$p_T = p + \frac{1}{2}\cdot\rho\cdot V_a^{\ 2} + \frac{1}{2}\cdot\rho\cdot V_\theta^2 \tag{2.9}$$

where V_a and V_θ are the axial and tangential velocity components, respectively. Differentiating with respect to r,

$$\frac{dp_T}{dr} = \frac{dp}{dr} + \frac{1}{2}\cdot\rho\cdot\frac{dV_a^{\ 2}}{dr} + \frac{1}{2}\cdot\rho\cdot\frac{dV_\theta^2}{dr} \tag{2.10}$$

when H and V_a are constant with radius, Eqn. (2.10) reduces to

$$\frac{dp}{dr} = -\frac{1}{2}\cdot\rho\cdot\frac{dV_\theta^2}{dr} \tag{2.11}$$

Combining Eqns. (2.8) and (2.11), it follows that

$$V_\theta = \frac{Const.}{r} \tag{2.12}$$

That is, V_θ is inversely proportional to r. A vortex flow with the above requirements regarding p_T, V_a, and V_θ is commonly known as a “free vortex”.

Free vortex flow is achieved when both the total pressure rise and axial velocity component remain constant along the blade span

Departures from free vortex flow give what is commonly known as arbitrary vortex flow. Owing to its lower rotational speed, the blade root is the most aerodynamically critical design section and conditions here limit the work capacity of a rotor designed for free vortex flow. By increasing the swirl towards the tips, relative to the free vortex distribution, however, it is possible to increase the work capacity of the rotor, especially for small boss ratios that is the ratio of hub diameter to fan section diameter. The ensuing axial velocity distributions for a particular arbitrary vortex flow can readily be calculated when suitable simplifying assumptions are made.

In some instances it is necessary to design axial flow fan equipment with radial gradients of axial velocity and total pressure. Low pressure rise cooling tower fans with small boss ratio provide one example of this design requirement brought about by practical blade construction considerations. Although approximate design methods are available for use with tangential velocity distributions of the form

$$V_\theta = a + br \tag{2.13}$$

where a and b are constants, the computerized “streamline curvature” and “matrix” techniques would provide more accurate design procedures. However, these theoretical methods must be adjusted to conform to practical situations such as those arising from boundary layer growth. Experimental feedback and confirmation is usually required for fans possessing a marked departure from free vortex flow. Two well known distributions which follow from this equation are

$$V_\theta = a \quad (where\ b = 0) \tag{2.14}$$

and

$$V_\theta = b \cdot r \quad (where\ a = 0) \tag{2.15}$$

The first, of course, gives constant tangential velocity while the second is known as "solid rotation", so called because in this case the air would rotate as though it were a solid body.

When an arbitrary vortex of the above type is imparted to the air by means of fan blades or vanes, there is a radial displacement of the air particles. It has, however, been found in practice that radial equilibrium is quickly established; the flow then satisfies the equation

$$\frac{dp_T}{dr} = \rho \cdot \frac{V_\theta^2}{r} + \frac{1}{2}\rho\frac{dV_a{}^2}{dr} + \frac{1}{2}\rho\frac{dV_\theta^2}{dr} \tag{2.16}$$

which is obtained by combining Eqns. (2.8) and (2.10). This equation is a key one in developing design methods for fans with arbitrary vortex flow.

2.6 Design Methods of Fan Blade and Stators

Airfoil characteristics are available in two general classes: isolated or free airfoil data, and airfoil data. The first data are, as the name implies, obtained from wind tunnel tests on a single airfoil whilst the second result from test on multiple airfoils installed in a cascade testing tunnel. This leads to two methods of design which are designated here as the "isolated airfoil method", and the "cascade airfoil method". The former utilizes lift data in design, while the latter is based mainly on flow deflection information.

The first axial flow machines designed was of a small pressure rise variety and employed low-solidity blading. As a consequence the blading design was successfully based on two-dimensional, isolated airfoil lift and drag data. Increased pressure duties, however, resulted in larger blade solidities with a progression toward mutual flow interference between adjacent blades. An interference factor C_L/C_{L_i} was introduced on the basis of theoretical studies. However, the use of this factor failed to predict accurately the cascade effect on blade performance because of the inviscid nature of the investigations and also probably the blade interaction with the wake of the preceding blade was not modeled accurately. Hence attempts have been made to extend the scope of the isolated airfoil theory by the introduction of an interference factor such as the ratio of the actual lift of the blade to the lift it would exert in the absence of the other blades. These methods have, however, failed in general to produce consistent results [2]. The designers of axial flow compressors, therefore, were obliged to procure deflection, lift, and drag data from two-dimensional cascade wind tunnel tests [1].

Choosing of appropriate design method depends basically on the following parameters:

a) Multiplane interference
b) Blade solidity
c) Whether the fan is a high pressure or a low pressure fan

When airfoil sections are brought closer and closer to each other, there is mutual interference between the flow patterns around the airfoils. This leads to change of slope in the lift curve and a decrease in the maximum lift.

Solidity of blade is defined as

$$\sigma = \frac{c}{s}$$

where c is the chord length of the blade and s is the circumferential gap between adjacent blade elements and it is defined as

$$s = \frac{2 \cdot \pi \cdot r}{n}$$

where n is the number of blades and r is the radius of any circle on the fan blades concentric with the fan rotational axis. For low solidities, no interference is experienced and two-dimensional test data obtained for a single airfoil can be used with confidence in design. But since the interference between the blades is high for high solidities, then cascade airfoil method is used for the blade design. Although there are some theoretical methods of calculating cascade of airfoils most present day designs are based on experimental data obtained from two-dimensional cascade wind tunnels. The main application of these data has been to axial flow compressor design [2].

Observance of the following general rule should ensure a satisfactory design:

i) If $\sigma \geq 1.0$ the cascade method of design should be employed

ii) If $\sigma \leq 0.7$ the isolated airfoil method is the appropriate one

iii) $0.7 < \sigma < 1.0$ either method may be employed

It is apparent that, in view of the limited experimental data available, no single design method can cover the entire range of ducted axial flow fans. Multiplane interference prevents the use of isolated airfoil design method for solidities much above unity, while the cascade design method can not be used for solidities much less than 2/3 [2].

In reference (1) it is also stated that the cascade airfoil method is used in high pressure fans and isolated airfoil method is used for low pressure fans with large boss ratios.

2.7 Airfoils for Rotor and Stator

Any airfoil for which two-dimensional lift and drag data are available can be used in rotor blade design. However, design accuracy is improved by the use of carefully selected sections for which experimentally established performance information is available [1].

In reference 1 four general categories of airfoil are recommended for use, namely,

a) A high performance type of circular arc blading, being particularly suitable for high pressure rise units.
b) A high performance type of flat undersurface blading for low pressure rise units.
c) Elliptical sections for flow reversing design requirements.
d) A less efficient and cheaper variety of blading featuring cambered constant thickness plates.

F-Series and NACA 65-Series airfoils are generally used as circular arc blading. These airfoils are usually used for compressors operating in high

Mach numbers. F-Series airfoils meet the need for a unified approach to fan blade design, irrespective of blade solidity requirements.

Airfoils with flat undersurfaces shown in Fig. 2.6 are the Clark Y, Göttingen, and RAF 6 profiles. All possess maximum thickness at 30% chord and varying this quantity without altering the flat undersurface is equivalent to changing the camber. For 10% sections the Clark Y and Göttingen airfoils possess additional leading edge droop of approximately 1% c, while 3% c value is more relevant to the RAF 6 case. The drag coefficient data presented in Fig. 2.7 disclose differences related to leading edge shape. The RAF 6E airfoil with its greater nose droop suffers a drag penalty at low C_L but surpasses the Clark Y at high C_L, for identical Reynolds number. The Göttingen and Clark Y sections possess similar characteristics when Re effects are taken into account. For blades requiring a design C_L of about 0.8 to 0.9, there is little significant drag difference between all three sections. Also, a small delay in the stall onset is indicated for the RAF 6E section.

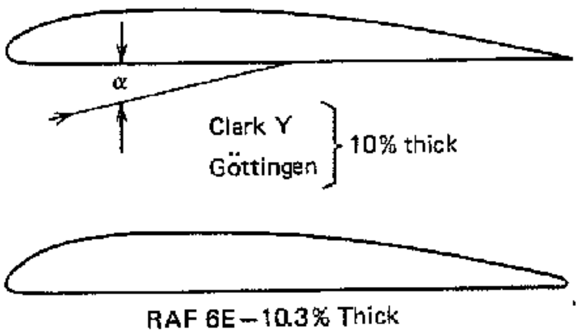

Figure 2.6 Flat Undersurface Airfoils.

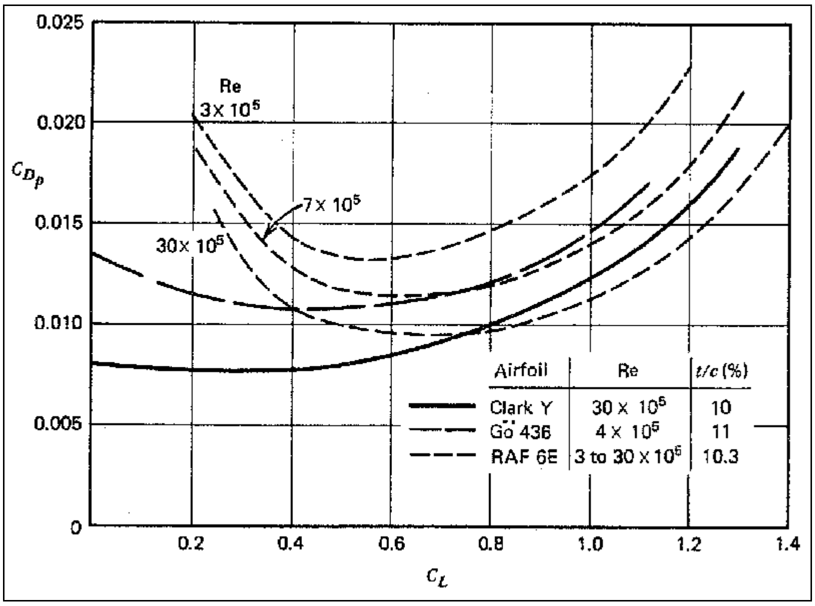

Figure 2.7 C_{D_p} versus C_L Data for Flat Undersurface Airfoils (ref.1, p. 160).

In elliptical airfoils, ellipses possess the same airfoil characteristics for reversed directions of airflow approach. They are therefore used in design situations where an identical duty condition is required for reversible fan assemblies, such as utilized in a number of preheat furnaces and drying kilns.

Cambered plate airfoils have many obvious advantages. When correctly shaped and constructed, the resulting operational characteristics and peak efficiency can be good, provided high quality inlet flow is assured in duct/fan installation. Unfortunately, many existing fans fail to meet these basic requirements and consequently are noisy, inefficient, and inadequate.

Production considerations often influence the choice of blade section. The RAF 6 and Clark Y series of airfoils are very popular as both possess a flat undersurface and are capable of high efficiency operation. When cheapness of construction is more important than the attainment of the highest possible efficiency, cambered plates of constant thickness, twisted from root to tip, are often used.

In straightener design, NACA symmetrical airfoils especially NACA 0012 and C4 symmetrical airfoil are often used when the swirl velocity is small. This type of straightener can be considered satisfactory when the swirl coefficient less than 0.4. When the value of swirl coefficient exceeds 0.4, circular arc blading in C4 thickness form is preferred.

CHAPTER 3

AERODYNAMIC DESIGN OF THE FAN

3.1 Aerodynamic Characteristics of Ankara Wind Tunnel

In order to achieve a satisfactory fan design, it is essential to prescribe the aerodynamic characteristics of the wind tunnel. This is done by either calculating or measuring the pressure losses in the wind tunnel.

In order to determine the loss characteristics of AWT, an algorithm is developed and the results are validated by two test cases. Pressure losses of every section of AWT and necessary power to drive the tunnel at 0.52 Mach are calculated by a computer program. To this end some pressure and velocity measurements are made at the fan section to find the losses experimentally.

3.1.1 Numerical Calculations

The method of loss analysis presented is a synthesis of theoretical and empirical techniques. A system of equations has been compiled and assembled into a computer program for determining the total pressure losses. The formulation presented is applicable to compressible flow through most closed or open test section, single, double, or non-return wind tunnels.

Flow-state parameters:

The basic flow-state parameters are determined from input information about the test section. These parameters are mainly derived from continuity equation and isentropic relations for compressible flow.

$$\rho_T = \frac{p_T}{R \cdot T_T} \tag{3.1}$$

$$a_T = \sqrt{\gamma \cdot R \cdot T_T} \tag{3.2}$$

$$\mu_T = \mu_{STD} \cdot \left(\frac{T_T}{T_{STD}} \right)^{0.76} \tag{3.3}$$

$$a_0 = \frac{a_T}{\sqrt{1 + \left(\frac{\gamma - 1}{2} \cdot M_0{}^2 \right)}} \tag{3.4}$$

$$\rho_0 = \frac{\rho_T}{\left[1 + \left(\frac{\gamma - 1}{2} \cdot M_0{}^2 \right) \right]^{\frac{1}{\gamma - 1}}} \tag{3.5}$$

$$A_* = M_0 \cdot A_0 \cdot \left\{ \frac{\gamma + 1}{2 \cdot \left[1 + \left(\frac{\gamma - 1}{2} \cdot M_0{}^2 \right) \right]} \right\}^{\frac{\gamma + 1}{2 \cdot (\gamma - 1)}} \tag{3.6}$$

Local conditions:

The local flow conditions are determined at the end of every section of the wind tunnel. Each section of AWT is depicted in Fig. 3.3 and for the test cases; sections are illustrated in Figs. 3.1 and 3.2. Calculations and determination of the main variables proceed according to following formulas;

1. Mach number: The local Mach number is found from a Newton's-method solution of the relationship (ref. 9, p. 6)

$$M^2 - \left[\frac{\gamma+1}{\gamma-1} \cdot \left(\frac{A}{A_*} \cdot M \right)^{\frac{2\cdot(\gamma-1)}{\gamma+1}} \right] + \frac{2}{\gamma-1} = 0 \tag{3.7}$$

2. Reynolds number: The Reynolds number based on the characteristic length ℓ, usually the local hydraulic diameter, is determined from (ref. 9, p. 6)

$$\mathrm{Re} = \frac{\rho_0 \cdot V_0 \cdot \ell}{\mu_T} \left(\frac{A_0}{A} \right) \left[1 + \left(\frac{\gamma-1}{2} \cdot M^2 \right) \right]^{0.76} \tag{3.8}$$

3. Friction coefficient: A Newton's-method solution is used to determine the friction coefficient for smooth walls from the expression (ref. 9, p. 6)

$$\left[\log_{10}\left(\lambda \cdot \mathrm{Re}^2 \right) - 0.8 \right]^{-2} - \lambda = 0 \tag{3.9}$$

<u>Calculation of the pressure losses for each section:</u>

The loss in total pressure caused by each section is calculated in a form non-dimensionalized by local dynamic pressure: $K = \Delta p_T / q$. In this study the smallest-area end of each section is used as the local reference position. The individual losses are based on the nature of the section, local flow conditions, input geometry and parameter information.

1. Constant-area ducts: For closed, constant area sections the pressure loss due to the friction is given by (ref. 9, p. 6)

$$K = \frac{\lambda \cdot L}{D_h} \tag{3.10}$$

2. Contractions: In contraction sections, where the major part of the losses is due to the friction, the local loss may be approximated as (ref. 9, p. 6)

$$K = 0.32 \cdot \frac{\lambda \cdot L}{D_h} \tag{3.11}$$

3. Corners with no net area change ("constant areas"): A duct can change direction with or without the aid of the flow guide vanes. For a constant-area turn employing turning vanes for efficiency, with a "normal" number of vanes and with chord-to-gap ratios between 2-to-1 and 4-to-1, the losses resulting from friction and rotation caused by the vanes are (ref. 9, p. 7)

$$K = \frac{K_{TV}}{3}\left[2 + \left(\frac{\log_{10}\mathrm{Re}_{REF}}{\log_{10}\mathrm{Re}}\right)^{2.58}\right] \tag{3.12}$$

The Reynolds number used for the turning vane loss is based on the vane chord. The turning vane loss parameter K_{TV} is a function of turning angle and $K_{TV} = 0.15$ is a reasonable value for a $90°$ corner. Re_{REF} is the reference Reynolds number and $\mathrm{Re}_{REF} = 0.5 \cdot 10^6$ at which turning vane $90°$ loss parameter, $K_{TV_{90}}$, was determined. Corners without turning vanes are less efficient and the loss function related to turn angle, ϕ, may be approximated by a sixth order polynomial as (ref. 9, p. 7)

$$\begin{aligned} K = {} & 4.313761\cdot 10^{-5} - 6.021515\cdot 10^{-4}\cdot\phi + 1.693778\cdot 10^{-4}\cdot\phi^2 \\ & - 2.755078\cdot 10^{-6}\phi^3 + 2.323170\cdot 10^{-7}\phi^4 - 3.775568\cdot 10^{-9}\phi^5 \\ & + 1.796817\cdot 10^{-11}\phi^6 \end{aligned} \tag{3.13}$$

4. Diffusers: Diffusion produces both expansion and friction losses in the duct given by (ref. 9, p. 7)

$$K = \left[K_{EXP} + \left(\frac{\lambda}{8\cdot\sin\theta}\cdot\frac{AR+1}{AR-1}\right)\right]\left(\frac{AR-1}{AR}\right)^2 \tag{3.14}$$

where K_{EXP} is the expansion parameter, AR is the ratio of cross sectional areas at upstream and downstream ends of section, and θ is the diffuser half angle in radian.

The determination of the diffuser loss parameter, K_{EXP}, is complex. It depends on the cross-sectional shape and equivalent cone angle of the section and it is being given by (ref. 9, p. 38)

$$K_{EXP} = K_{EXP_{basic}} + (1-\delta_s)\cdot\left(K_{EXP_{Additional}} - K_{EXP_{basic}}\right) \tag{3.15}$$

where δ_s is the diffuser side length ratio (ratio of change in height to change in width from upstream to downstream end, or its inverse, whichever is less than or equal to unity). If the ratio is negative, $\delta_s = 0$. For different cross-sectional shapes formulations on determination of K_{EXP}, are given in Table 3.1 and 3.2.

Table 3.1 $K_{EXP_{basic}}$ and $K_{EXP_{Additional}}$ Definitions for Different Cross Sectional Shapes.

Cross-Sectional Shape		$K_{EXP_{basic}}$	$K_{EXP_{Additional}}$
Upstream	**Downstream**		
Circular	Circular	$K_{EXP_{Circular}}$	$K_{EXP_{2D_{Circular}}}$
Circular	Rectangular	$K_{EXP_{3D_{Average}}}$	$K_{EXP_{2D_{Average}}}$
Circular	Flat oval	$K_{EXP_{Circular}}$	$K_{EXP_{2D_{Circular}}}$
Rectangular	Rectangular	$K_{EXP_{Square}}$	$K_{EXP_{2D_{Rectangular}}}$
Rectangular	Circular	$K_{EXP_{3D_{Average}}}$	$K_{EXP_{2D_{Average}}}$
Flat oval	Flat oval	$K_{EXP_{Circular}}$	$K_{EXP_{2D_{Circular}}}$
Flat oval	Circular	$K_{EXP_{Circular}}$	$K_{EXP_{2D_{Circular}}}$

Table 3.2 Formulations Related to K_{EXP} for Different Cross Sectional Shapes.

$3^\circ \le 2\theta \le 10^\circ$	$K_{EXP_{Circular}} = 1.70925 \cdot 10^{-1} - 5.84932 \cdot 10^{-2} \cdot (2 \cdot \theta) + 8.14936 \cdot 10^{-3} \cdot (2 \cdot \theta)^2 + 1.34777 \cdot 10^{-4} \cdot (2 \cdot \theta)^3 - 5.67258 \cdot 10^{-5} \cdot (2 \cdot \theta)^4 - 4.15879 \cdot 10^{-7} \cdot (2 \cdot \theta)^5 + 2.10219 \cdot 10^{-7} \cdot (2 \cdot \theta)^6$	(3.16)
$0^\circ < 2\theta < 3^\circ$	$K_{EXP_{Circular}} = 1.033395 \cdot 10^{-1} - 1.19465 \cdot 10^{-2} \cdot (2 \cdot \theta)$	(3.17)
$2\theta^\circ > 10^\circ$	$K_{EXP_{Circular}} = -9.66135 \cdot 10^{-2} + 2.336135 \cdot 10^{-2} \cdot (2 \cdot \theta)$	(3.18)
$3^\circ \le 2\theta \le 10^\circ$	$K_{EXP_{Square}} = 1.22156 \cdot 10^{-1} - 2.29480 \cdot 10^{-2} \cdot (2 \cdot \theta) + 5.50704 \cdot 10^{-3} \cdot (2 \cdot \theta)^2 - 4.08644 \cdot 10^{-4} \cdot (2 \cdot \theta)^3 - 3.84056 \cdot 10^{-5} \cdot (2 \cdot \theta)^4 + 8.74969 \cdot 10^{-6} \cdot (2 \cdot \theta)^5 - 3.65217 \cdot 10^{-7} \cdot (2 \cdot \theta)^6$	(3.19)
$0^\circ < 2\theta < 3^\circ$	$K_{EXP_{Square}} = 9.62274 \cdot 10^{-2} - 2.07582 \cdot 10^{-3} \cdot (2 \cdot \theta)$	(3.20)
$2\theta^\circ > 10^\circ$	$K_{EXP_{Square}} = -1.321685 \cdot 10^{-1} + 2.93315 \cdot 10^{-2} \cdot (2 \cdot \theta)$	(3.21)
$3^\circ \le 2\theta \le 9^\circ$	$K_{EXP_{3D,rectangular}} = 3.23334 \cdot 10^{-1} - 5.82939 \cdot 10^{-2} \cdot (2 \cdot \theta) - 4.97151 \cdot 10^{-3} \cdot (2 \cdot \theta)^2 + 1.99093 \cdot 10^{-4} \cdot (2 \cdot \theta)^3 + 1.98630 \cdot 10^{-5} \cdot (2 \cdot \theta)^4 + 2.06857 \cdot 10^{-6} \cdot (2 \cdot \theta)^5 + 3.81837 \cdot 10^{-7} \cdot (2 \cdot \theta)^6$	(3.22)
$9^\circ \le 2\theta \le 10^\circ$	$K_{EXP_{3D,rectangular}} = 5.72853 - 1.21832 \cdot (2 \cdot \theta) + 7.08483 \cdot 10^{-2} \cdot (2 \cdot \theta)^2$	(3.23)
$0^\circ < 2\theta < 3^\circ$	$K_{EXP_{3D,rectangular}} = 1.0 \cdot 10^{-1} - 5.333333 \cdot 10^{-3} \cdot (2 \cdot \theta)$	(3.24)
$2\theta > 10^\circ$	$K_{EXP_{3D,rectangular}} = -1.36146 + 1.986460 \cdot 10^{-1} \cdot (2\theta)$	(3.25)
$K_{EXP_{3D,Circular}} = K_{EXP_{3D,rectangular}} \cdot K_{EXP_{Circular}} / K_{EXP_{Square}}$		(3.26)
$K_{EXP_{3D,average}} = (K_{EXP_{3D,rectangular}} + K_{EXP_{3D,Circular}})/2$		(3.27)
$K_{EXP_{2D,average}} = (K_{EXP_{Square}} + K_{EXP_{Circular}})/2$		(3.28)

5. Fan (power) section: Fan drive sections are commonly made up of contractions, constant-area annular ducts, and diffusers. Therefore analysis of this section is handled by dividing the fan into contraction, constant area duct, and diffuser sections for which the corresponding formulas have already been given above.

6. Internal flow obstruction-drag items: The loss due to the drag of internal structure such as struts or models has the form (ref. 9, p. 9)

$$K = C_D \cdot \frac{S}{A_{FLOW}} \cdot \varepsilon \tag{3.29}$$

7. Mesh screen: The losses produced by a mesh screen may be expressed as (ref. 9, p. 9)

$$K = K_{\mathrm{Re}} \cdot K_{MESH} \left(1 - \frac{A_{FLOW}}{A}\right) + \left(\frac{A}{A_{FLOW}} - 1\right)^2 \tag{3.30}$$

where the mesh constant, K_{MESH}, is 1.3 for average circular metal wire, 1.0 for new metal wire, and 2.1 for silk thread and the Reynolds number influence factor, K_{Re}, is related to Reynolds number based on mesh diameter as

for $0 \le \mathrm{Re} < 400$

$$K_{\mathrm{Re}} = \frac{78.5 \cdot \left(1 - \frac{RN}{354}\right)}{100} + 1.01 \tag{3.31}$$

for $\mathrm{Re} \ge 400$

$$K_{\mathrm{Re}} \equiv 1.0 \tag{3.32}$$

8. Calculation method for transferring loss values to reference location: Each local loss parameter is calculated based on local conditions at the smallest-area end of each section and may then be referenced to the test section conditions by the formula (ref. 9, p. 33)

$$K_0 = \frac{\Delta p_T}{q} \cdot \left(\frac{q}{q_0} \right) = K \cdot \left(\frac{q}{q_0} \right) = K \cdot \left[\frac{A_0 \cdot M}{A \cdot M_0} \sqrt{\frac{1 + \left(\frac{\gamma - 1}{2} \cdot M_0{}^2 \right)}{1 + \left(\frac{\gamma - 1}{2} \cdot M^2 \right)}} \right] \tag{3.33}$$

9. Overall and summary performance: The energy ratio of the wind tunnel under consideration is given by (ref. 9, p. 10)

$$ER = \frac{1}{\sum_{i=1}^{N} K_{0_i}} \tag{3.34}$$

Total pressure rise across the fan is equal to total pressure drop through the wind tunnel and it is given by (ref. 9, p. 34)

$$\Delta p_{T_F} = q_0 \cdot \sum_{i=1}^{N} K_{0_i} \tag{3.35}$$

The power required to be input into the flow in order to drive the flow through the wind tunnel at a specified test section speed is expressed as (ref. 9, p. 10)

$$P_{input} = \frac{\left(\sum_{i=1}^{N} K_{0_i} \right) \cdot \rho_0{}^2 \cdot A_0 \cdot V_0{}^3}{2 \cdot \rho_F} \tag{3.36}$$

The actual drive power required is dependent on the efficiency of the fan/motor system:

$$P_{required} = \frac{P_{input}}{\eta_F} \tag{3.37}$$

To calculate the pressure losses at AWT an algorithm is developed based on these equations. Firstly results of the algorithm are validated by two test cases. Two (40 by 80 Foot and 7 by 10 Foot) Wind Tunnels belonging to NASA-Ames Research Center are selected as test cases because they bear close similarity with AWT. These tunnels are shown in Figs. 3.1 and 3.2 and the algorithm results belonging to these facilities are given in Table 3.4 and 3.5 respectively. Some of the component losses could not be calculated due to the lack of available data so that related columns are left blank.

The performance calculations, based on three different flow conditions at the test section of AWT, are made once the circuit geometry of AWT is determined (Fig. 3.3). The flow conditions in the test section (velocity, and stagnation temperature and pressure) and the external atmospheric pressure that are input to the algorithm are determined experimentally. The total pressure and temperature for the Condition-3 are found by curve fitting (Table 3.3).

Table 3.3 Flow Conditions Input to the Algorithm.

Condition	1	2	3
Velocity (m/s)	72	90	180
Total Pressure (Pa)	94166	95353	105291
Total Temperature (°K)	302.8	303.2	306
Atmospheric Pressure (Pa)	91840	91840	91840

The aims of the choosing three different flow conditions are three folds: (1) to compare with experimental data, (2) to find aerodynamic efficiency of the existing fan, and (3) to find required power for a test section Mach number of 0.52 respectively. Results of the algorithm for all three conditions of AWT are listed in Table 3.6. Loss at the fan section part of AWT could not be calculated by dividing this section into three parts (contraction, constant area duct, and diffuser) because there is no data corresponding to the center body and struts. Since the NASA-Ames Research Center 7 by 10 Foot Wind Tunnel is very similar to AWT and its fan section loss is about 0.89% in overall, the fan section loss of AWT is taken conservatively to be 1% of the overall loss value.

All results are summarized in Table 3.7.

Table 3.4 Components Losses of NASA-Ames Research Center

40 by 80 Foot Wind Tunnel (Test Case-1).

No	Section Type	K0 (Ref. 9)	%	K0 Eqn. (3.33)	Difference %
1	Constant Area Duct	0.00003	0.02	0.00003	0
2	Contraction	0.00501	3.99	0.00502	0.200
3	Test Section, Diffusion	0.00835	6.65	0.00836	0.120
4	Diffuser	0.04514	35.95	0.04515	0.022
5	Corner With Vanes	0.01995	15.89	0.01999	0.201
6	Constant Area Duct	0.00123	0.98	0.00123	0.000
7	Corner With Vanes	0.01995	15.89	0.01999	0.201
8	Diffuser	0.00191	1.52	0.00191	0
9	Fan Contraction	0.00050	0.40	0.00050	0
10	Fan Duct & Struts	0.00279	2.22	0.00279	0
11	Fan Diffuser & Center Body	0.01431	11.40	0.01541	7.687
12	Multi Internal Structure	0.00060	0.48		
13	Diffuser	0.00123	0.98	0.00123	0
14	Corner With Vanes	0.00227	1.81	0.00227	0
15	Constant Area Duct	0.00004	0.03	0.00004	0
16	Corner With Vanes	0.00227	1.81	0.00227	0.044

Table 3.5 Components Losses of NASA-Ames Research Center

7 by 10 Foot Wind Tunnel (Test Case-2).

No	Section Type	K0 (Ref. 9)	%	K0 Eqn. (3.33)	Difference %
1	Constant Area Duct	0.00003	0.02	0.00003	0
2	Contraction	0.01213	9.81	0.01214	0.082
3	Test Section, Diffusion	0.01322	10.69	0.01322	0
4	Diffuser	0.00096	0.78	0.00083	-13.542
5	Internal Structure	0.00224	1.81		
6	Diffuser	0.07838	63.38	0.06888	-12.120
7	Corner With Vanes	0.00799	6.46	0.00799	0
8	Diffuser	0.00076	0.61	0.00077	1.316
9	Corner With Vanes	0.00448	3.62	0.00448	0
10	Diffuser	0.00066	0.53	0.00066	0
11	Fan Contraction	0.00001	0.01	0.00001	0
12	Fan Duct & Struts	0.00017	0.14	0.00017	0
13	Multi Internal Structure	0.00021	0.17		
14	Fan Diffuser & Center Body	0.00071	0.57		
15	Contraction	0.00001	0.01	0.00001	0
16	Diffuser	0.00002	0.02	0.00002	0
17	Diffuser	0.00003	0.02	0.00003	0
18	Constant Area Duct	0.00001	0.01	0.00001	0
19	Corner With Vanes	0.00079	0.64	0.00079	0
20	Constant Area Duct	0.00002	0.02	0.00002	0
21	Corner With Vanes	0.00084	0.68	0.00084	0

Table 3.6 Components Losses of Ankara Wind Tunnel.

No	Section Type	K0 Eqn. (3.33)			%
		Cond. 1	Cond. 2	Cond. 3	Cond. 1
1	Constant Area Duct	0.00007	0.00006	0.00005	0.03
2	Contraction	0.00892	0.00867	0.00786	3.78
3	Test Section, Diffusion	0.01911	0.01856	0.01683	8.09
4	Diffuser	0.07194	0.07148	0.06924	31.16
5	Corner With Vanes	0.01896	0.01858	0.01639	8.10
6	Diffuser	0.00094	0.00091	0.00075	0.4
7	Corner With Vanes	0.01852	0.01814	0.01598	7.91
8	Fan Contraction	0.02127	0.02101	0.00194	1.0
9	Fan Duct & Struts				
10	Fan Diffuser & Center Body				
11	Constant Area Duct	0.00037	0.00036	0.00029	0.16
12	Diffuser.	0.00659	0.00647	0.00577	2.82
13	Corner With Vanes	0.00263	0.00257	0.00224	1.12
14	Constant Area Duct	0.00002	0.00002	0.00001	0.01
15	Corner With Vanes	0.00263	0.00257	0.00224	1.12
16	Screen, Fine Mesh	0.02546	0.02518	0.02278	10.98
17	Screen, Fine Mesh	0.02546	0.02518	0.02278	10.98
18	Screen, Coarse Mesh	0.00972	0.00961	0.00869	4.12

Table 3.7 Summarized Results of the Algorithm.

Parameter	Test Case-1	Test Case-2	AWT Cond. 1	AWT Cond. 2	AWT Cond. 3
Total pressure loss coefficient, Eqn. (3.33)	0.12559	0.12387	0.2137	0.2105	0.1938
Energy ratio, Eqn. (3.34)	7.962	8.073	4.68	4.75	5.16
Total Pressure Rise (Pa), Eqn. (3.35)	840	1238.7	589.3	900.4	3278.3
Input power (kW), Eqn. (3.36)	23044	996.6	293.2	552.3	3667.2
Required Power (kW), Eqn. (3.37)	24257	1172.5	-	750	4314.4
Fan aerodynamic efficiency	%95	%85	-	%74	%85

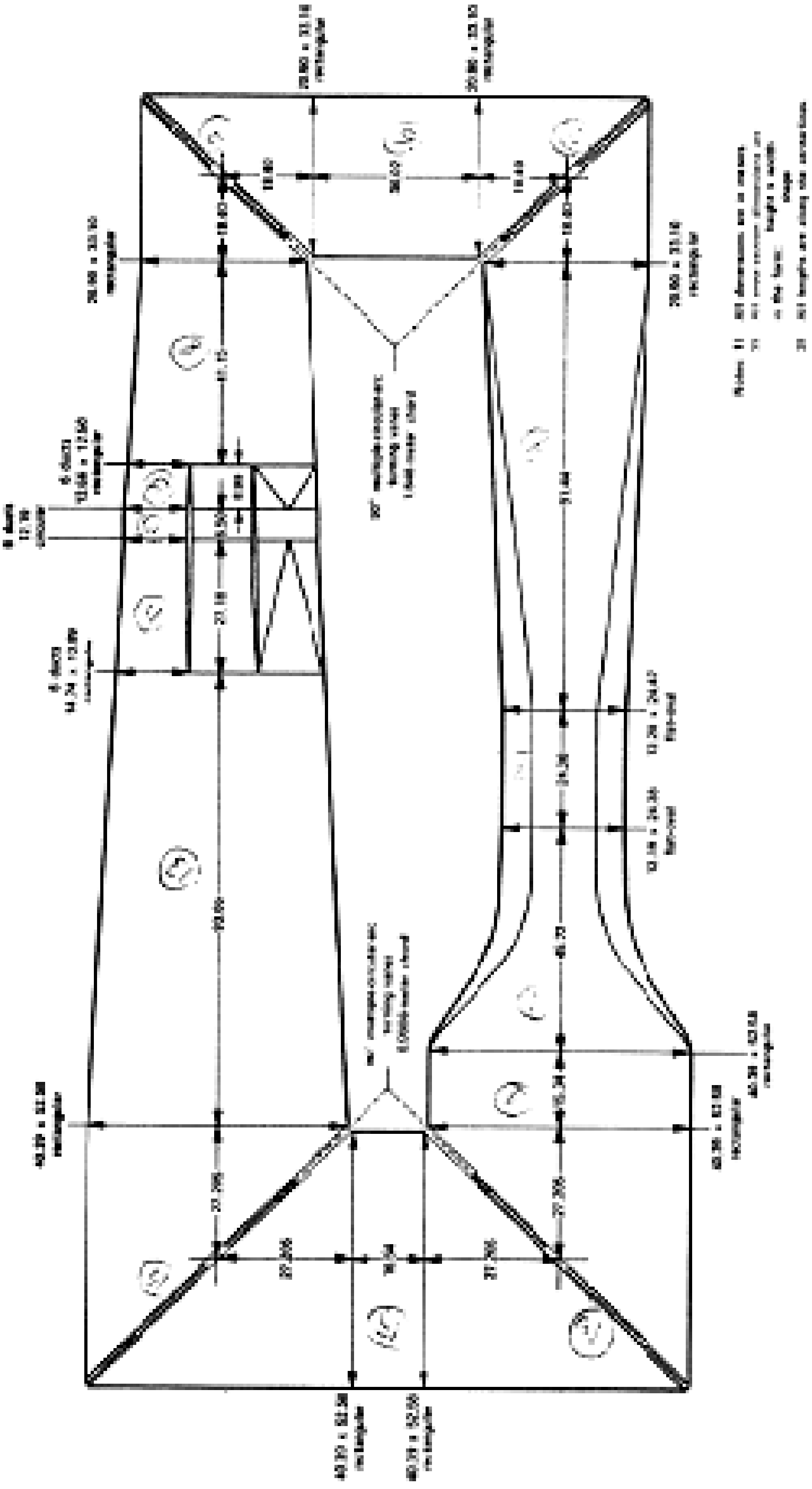

Figure 3.1 NASA-Ames Research Center 40 by 80 Foot Wind Tunnel Outline.

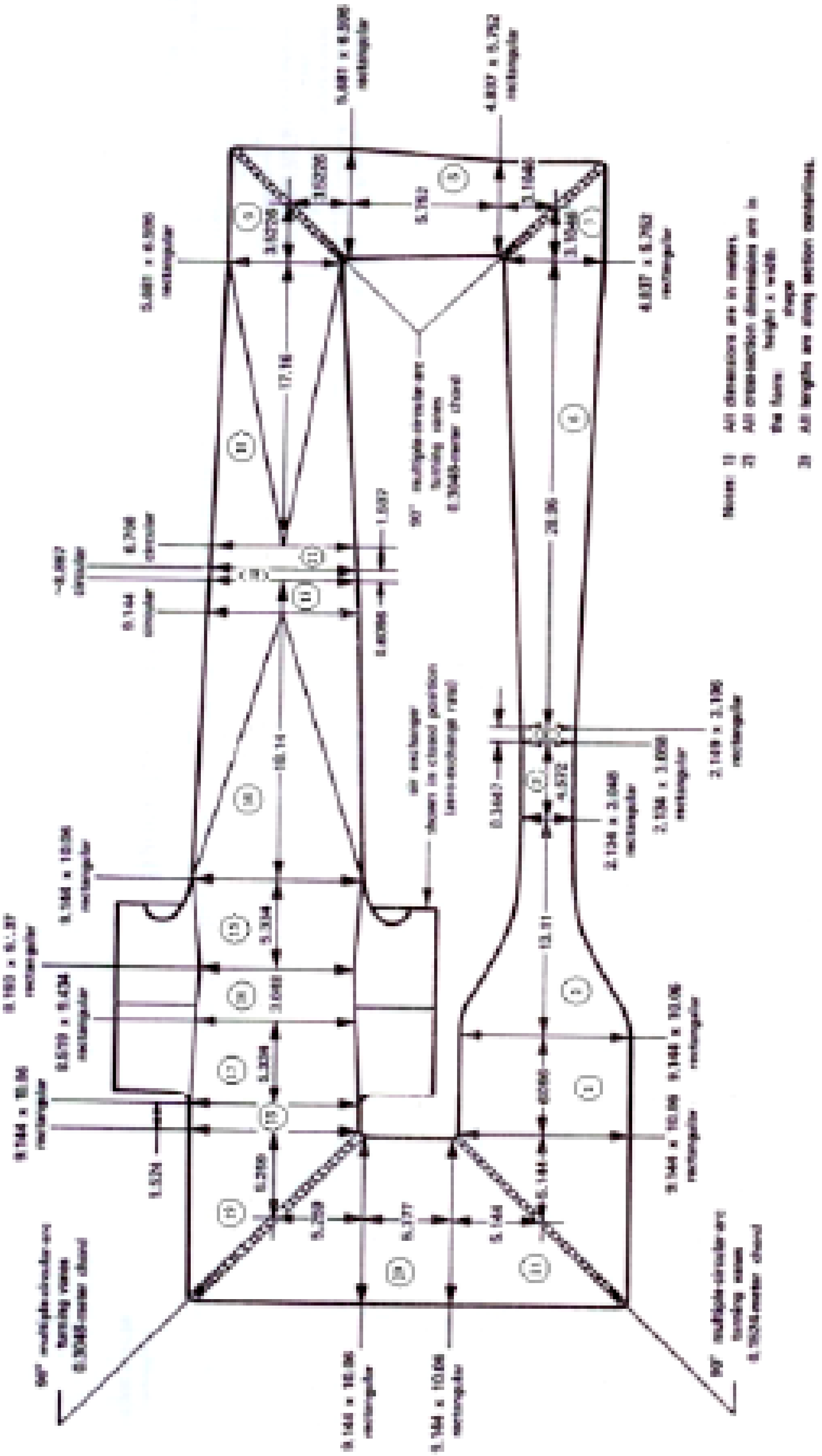

Figure 3.2 NASA-Ames Research Center 7 by 10 Foot Wind Tunnel Outline

Table 3.2 Formulations Related to K_{EXP} for Different Cross Sectional Shapes.

TÜBİTAK-SAGE ANKARA WIND TUNNEL

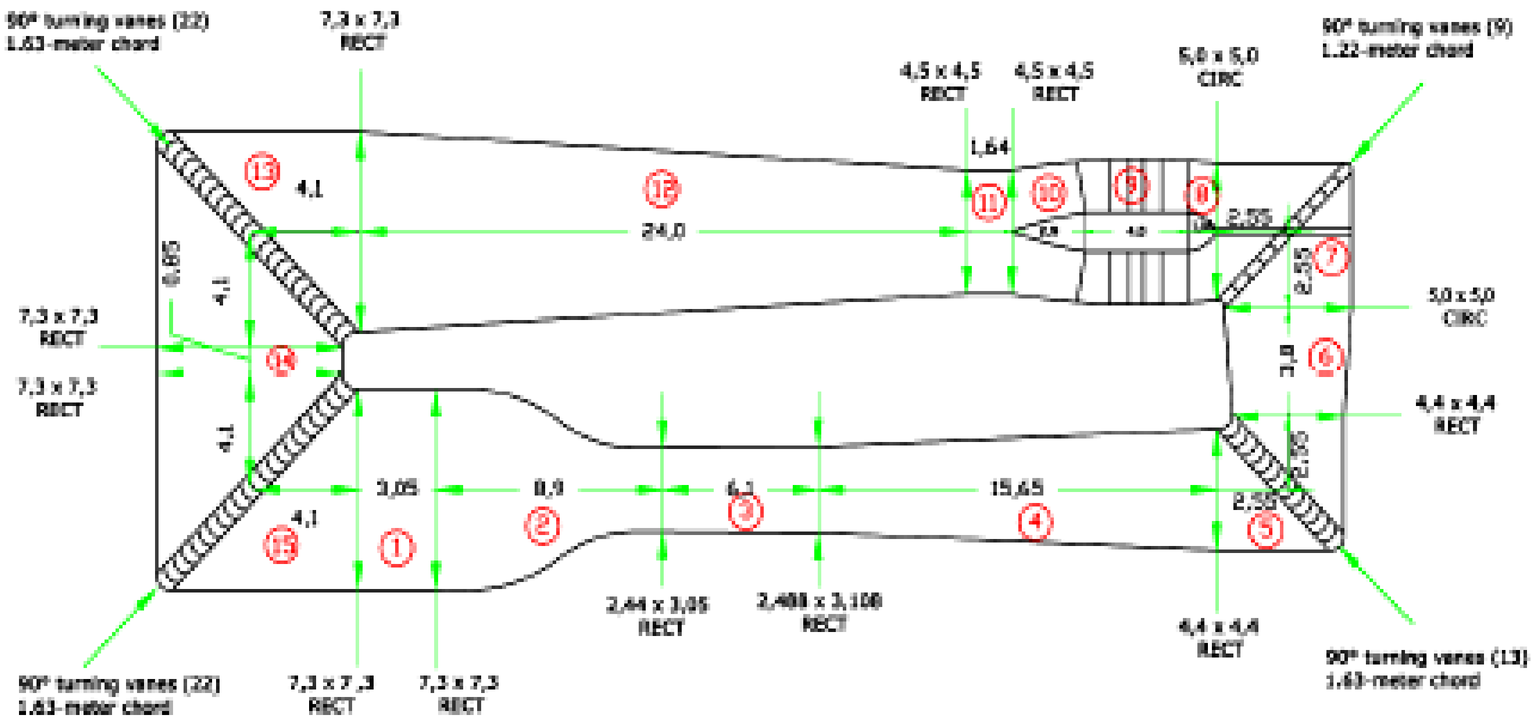

Notes: 1) All dimensions are in meters.
2) All cross-section dimensions are in the form:
height x width
shape
3) All lengths are along section centerlines.

3.1.2 Experimental Measurements

In order to determine the loss characteristics of AWT, some pressure and velocity measurements are made at the fan section. In this measurements two pitot tube shown in Fig. 3.4 and a pressure transducer (±0.5 psid) are used as experimental apparatus.

Figure 3.4 Pitot Tube Used in Experimental Measurements.

The upstream velocity profile is measured at a section 60 cm upstream of the inlet guide vanes after performing some pretests for determining the axial location. Sensor-blade proximity sensitivity is also carried out: It is clear from the results that flow is not disturbed by the inlet guide vanes when the pitot tube is at least 40 cm far away (Fig. 3.5). The axial velocity profile is also measured at a section 150 cm downstream of the outlet guide vanes. Although there are not many alternative axial locations for downstream axial velocity profile measurements because of the difficulty of fixing the pitot tube supports to the thick concrete walls, the distance from the outlet guide vane is still taken to be larger than the chord of outlet guide vane. Pitot tubes are traversed starting from 33.5 cm from the tunnel floor up to 173.5 cm with 20 cm intervals at both sections (Fig. 3.6). Test pictures are shown in Figs. 3.7 and 3.8. Measurements are performed at 7 different fan speeds.

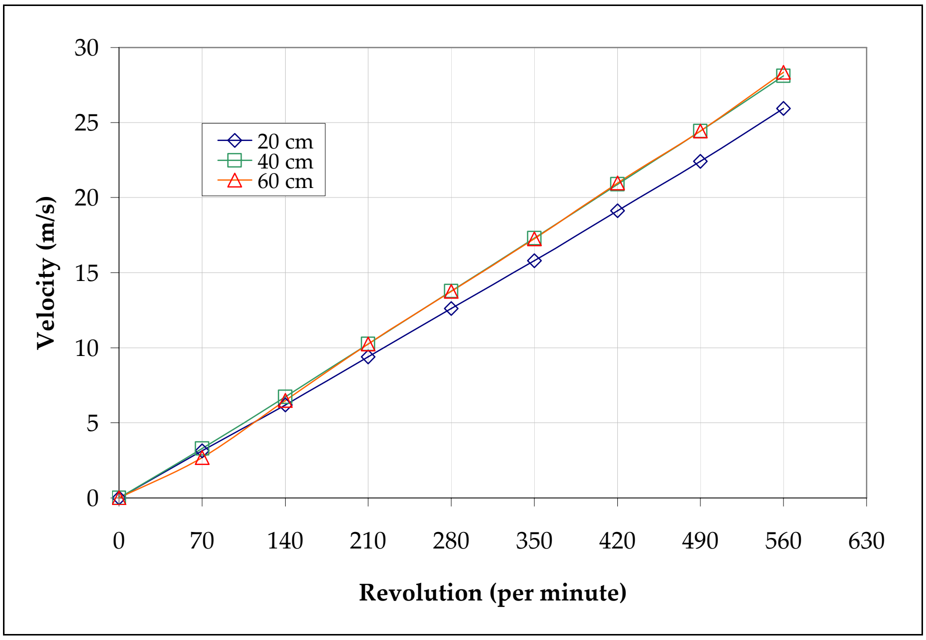

Figure 3.5 Determination of Upstream Axial Measurement Location.

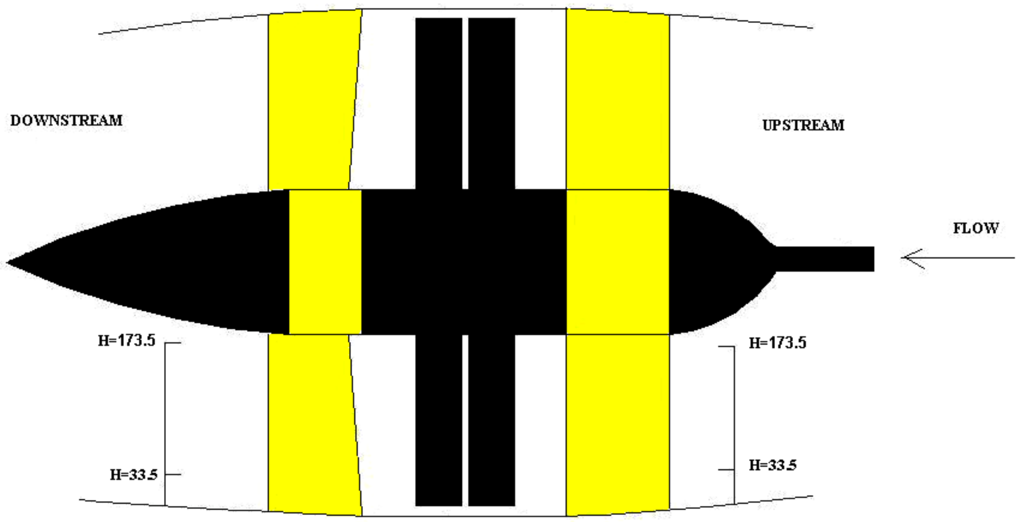

Figure 3.6 Velocity and Total Pressure Rise Measurement Points.

Figure 3.7 Test Picture (Up and Downstream of the Fan).

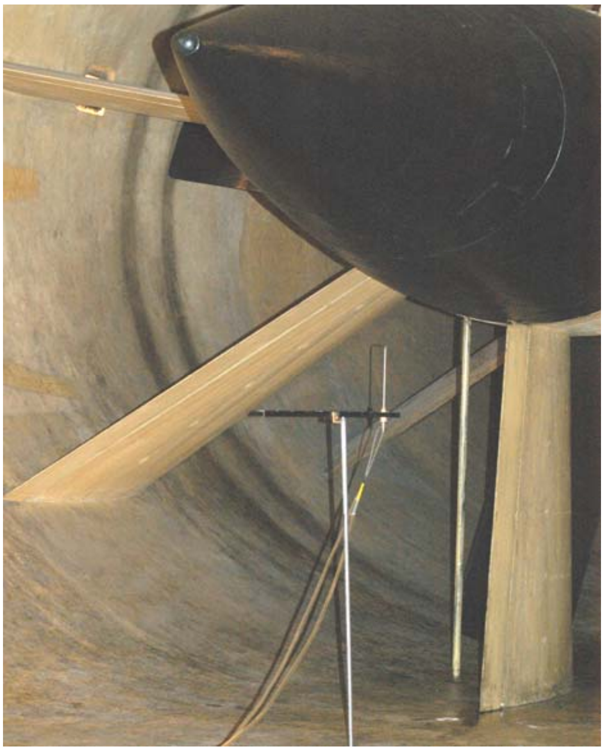

Figure 3.8 Test Picture (Downstream of the Fan).

Upstream velocity profile is presented in Fig. 3.9. Nonuniformities in upstream velocity are found to be low, and it is about 11% at the highest fan speed.

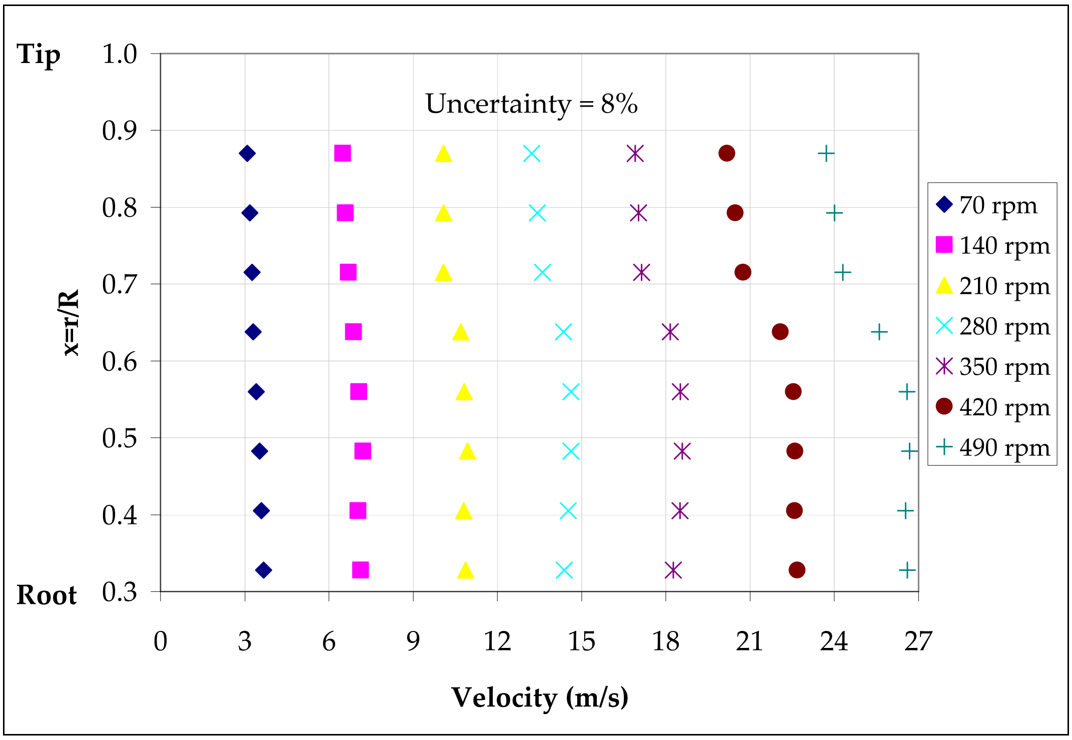

Figure 3.9 Upstream Velocity Profile.

Downstream velocity profile is presented in Fig. 3.10. Nonuniformities are found to be relatively high compared to upstream values. One of the reasons may be the flow separation near the root.

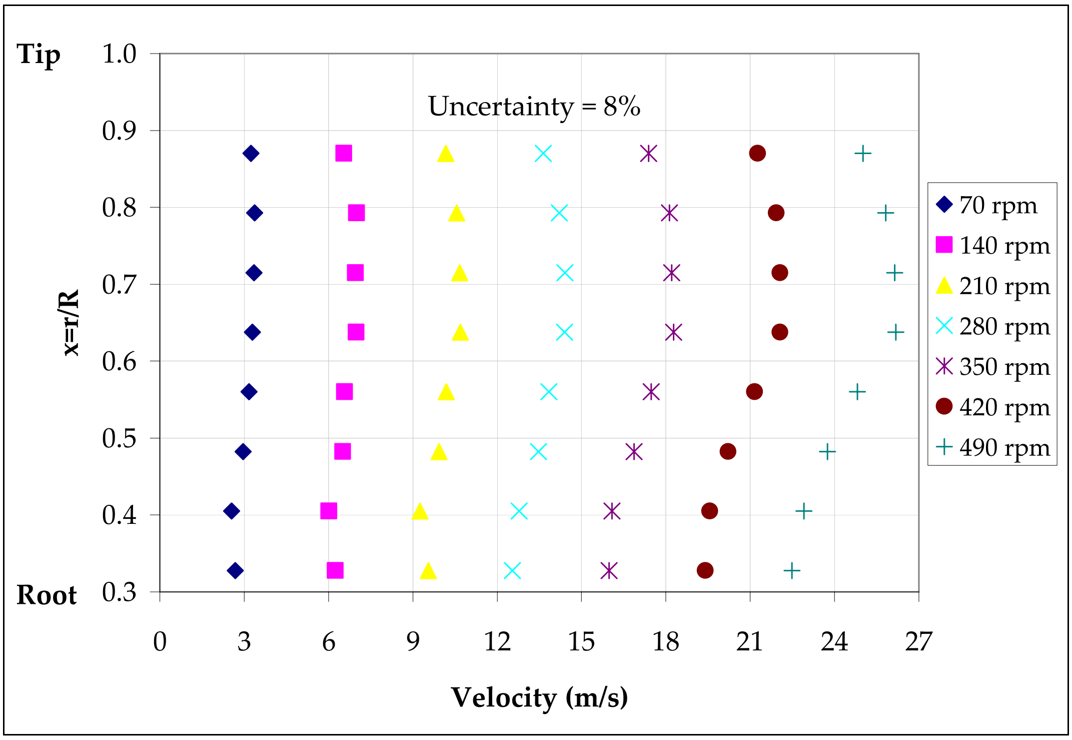

Figure 3.10 Downstream Velocity Profile.

Total pressure rise across the fan is presented in Fig. 3.11. As seen from this figure, total pressure rise changes largely from root to tip. High total pressure rise occurs near the midspan and this is compatible with the typical total pressure contours aft of straightener which is given in Reference 1 (Fig. 3.12).

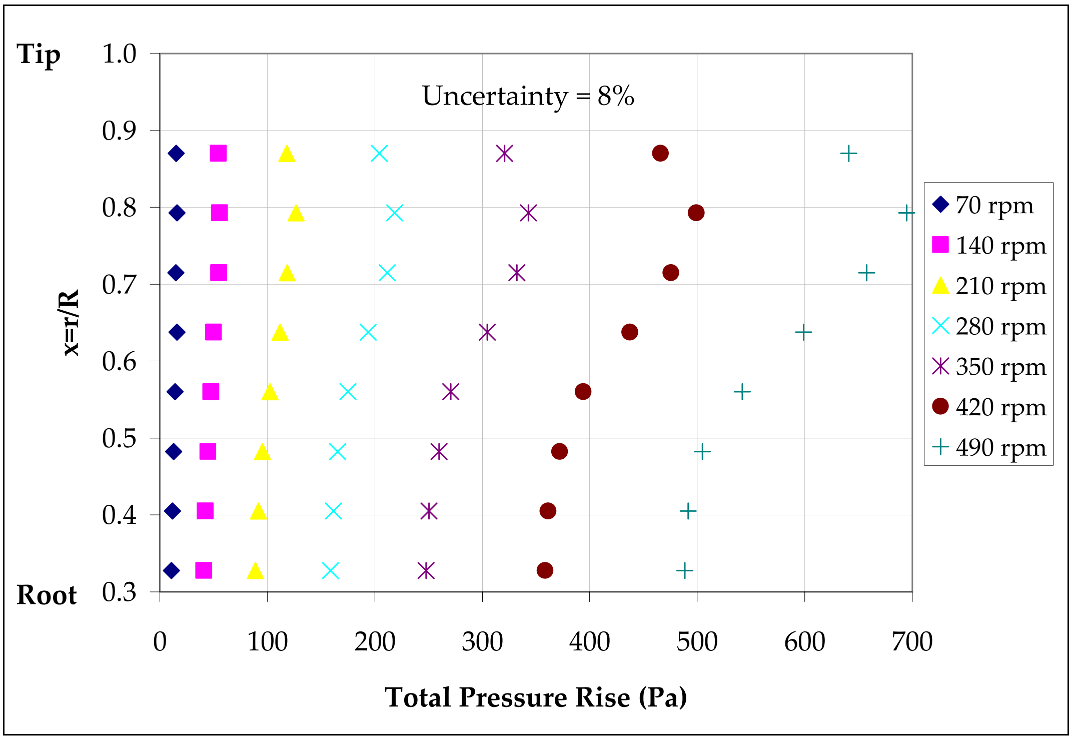

Figure 3.11 Total Pressure Rise.

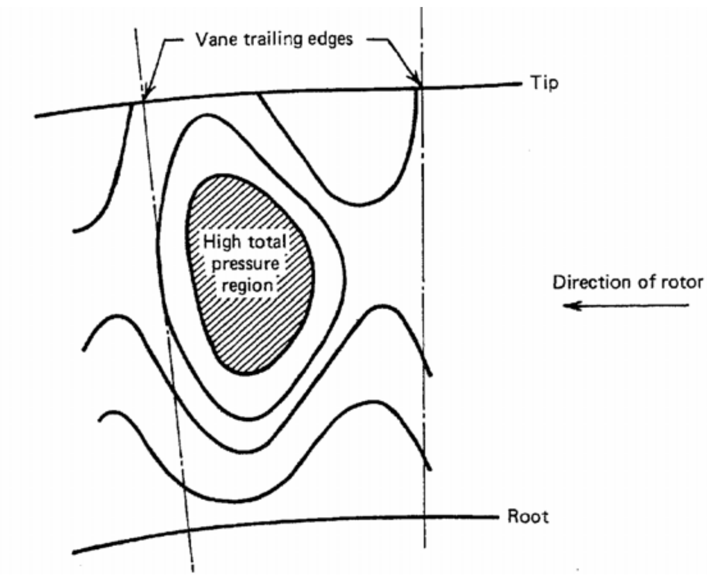

Figure 3.12 Typical Total Pressure Contours Aft of Straighteners

(ref. 1, p. 375).

Mean axial velocity at the upstream of the fan and the mean total pressure rise across the fan may be calculated respectively as:

$$\overline{V}_f = \frac{2}{1-{x_b}^2}\int_{x_b}^{1} V_f \cdot x \cdot dx \tag{3.38}$$

$$\Delta\overline{p}_T = \frac{2}{1-{x_b}^2}\int_{x_b}^{1} \Delta p_T \cdot x \cdot dx \tag{3.39}$$

Volumetric flowrate at the upstream of the fan is calculated by

$$Q = \overline{V}_f \cdot \left(\frac{\pi \cdot D^2}{4}\right) \tag{3.40}$$

where D is the diameter of the fan section entire and it is equal to 5 m. Experimental results based on formulations given above are listed in Table 3.8.

Table 3.8 Experimental Results for the Losses of AWT.

$\overline{V}_f\ (m/s)$	$Q\ \left(m^3/s\right)$	$\Delta\overline{p}_T\ (Pa)$	$k = \Delta\overline{p}_T / Q^2$
3.21	63.00	14.83	0.003737
6.69	131.27	51.83	0.003008
10.29	201.96	113.28	0.002777
13.69	268.57	196.80	0.002728
17.40	341.56	308.42	0.002644
20.99	411.84	446.30	0.002631
24.65	483.68	614.24	**0.002626**

Since the loss through a duct system is proportional to the square of the volumetric flowrate, the loss characteristics of the tunnel is parabolic. It may be given in the following form.

$$\Delta p_T = k \cdot Q^2 \tag{3.41}$$

where k is the constant of proportionality. The value of k in Eqn. (3.41) may be estimated by taking k for the highest velocity in Table 3.8 and accordingly the total pressure loss can be defined as

$$\Delta p_T = 0.002626 \cdot Q^2 \tag{3.42}$$

Then, AWT loss characteristics curve that simulated by Eqn. (3.42) is plotted in Fig 3.13.

Models with different sizes are going to be tested in the test section of AWT. These models will cause blockage losses. According to reference 9, this blockage loss is estimated to be between 10% and 15% of the total tunnel loss. In the present case the tunnel loss is increased by 10% for each flowrate because of large tunnel size and the actual tunnel loss characteristics is determined in Table 3.9. It is plotted in Fig. 3.13 and may be expressed as

$$\Delta p_T = 0.002888 \cdot Q^2 \tag{3.43}$$

Table 3.9 Actual Loss Characteristics of AWT.

$\overline{V}_f \ (m/s)$	$Q \ (m^3/s)$	$\Delta\overline{p}_T \ (Pa)$	$k = \Delta\overline{p}_T / Q^2$
3.21	63.00	16.31	0.004111
6.69	131.27	57.01	0.003309
10.29	201.96	124.60	0.003055
13.69	268.57	216.48	0.003001
17.40	341.56	339.26	0.002908
20.99	411.84	490.93	0.002894
24.65	483.68	675.67	**0.002888**

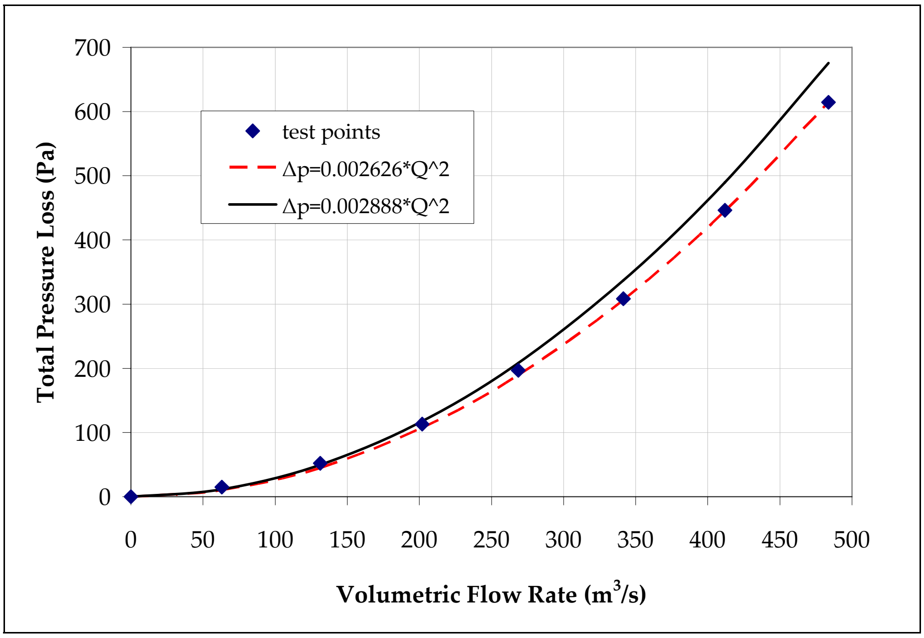

Figure 3.13 AWT Loss Characteristics Curve.

3.2 Design Inputs

- Selection of the Ducted Fan Type
- Selection of Design Theory
- Selection of Rotor Blade and Straightener Design Method
- Selection of Airfoils for Rotor and Straightener
- Selection of Speed Control Method

The chosen fan configuration consists of rotor and straightener unit because it provides flow stability. This configuration is the common choice for high power axial flow fan wind tunnel applications and if correctly designed, these units of rotor and straightener are potentially the most efficient [1].

For the present design, free vortex theory is used for the fan design because spanwise nonuniformity of axial velocity at the fan section is not high.

Since it is a low pressure fan, the isolated aerofoil design method is found to be suitable. Choice of the straightener design method depends on the swirl values produced by the rotor. If swirl coefficient is equal or lower than 0.4, the isolated airfoil method is suitable otherwise cascade airfoil method must be used. For the straightener case cascade airfoil design method is found to be suitable because of high swirl (that greater than 0.4).

As for the rotor blade design method, it is appropriate to consider each rotor blade element as an isolated two dimensional airfoil. Production considerations often influence the choice of blade section. The RAF 6E and Clark Y series of airfoils are very popular as both has flat (pressure side) undersurfaces and is capable of high efficiency operation [2]. The RAF 6E airfoil is selected for the rotor blade because its aerodynamic characteristics is available at design Reynolds number and stall limit is higher than the Clark Y. The experimental two dimensional aerodynamic characteristics of the RAF 6E airfoil plotted against the angle of attack at different Reynolds number are shown in Fig. 3.14. Circular arc blading in C4 thichkness form is selected for straightener because of high swirl. The section coordinates of RAF 6E and C4 airfoils are given in Table 3.10.

The flowrate through a fan unit is normally varied by changing the rotor speed. An alternative method for changing the flowrate is to use variable pitch rotor blades. Since variable pitch fan allows more efficiency in large working range, it is found to be more suitable for the present fan. Also, a variable pitch fan is of great value even when a variable rpm drive is available since it gives much quicker speed control than variable rpm drive [4].

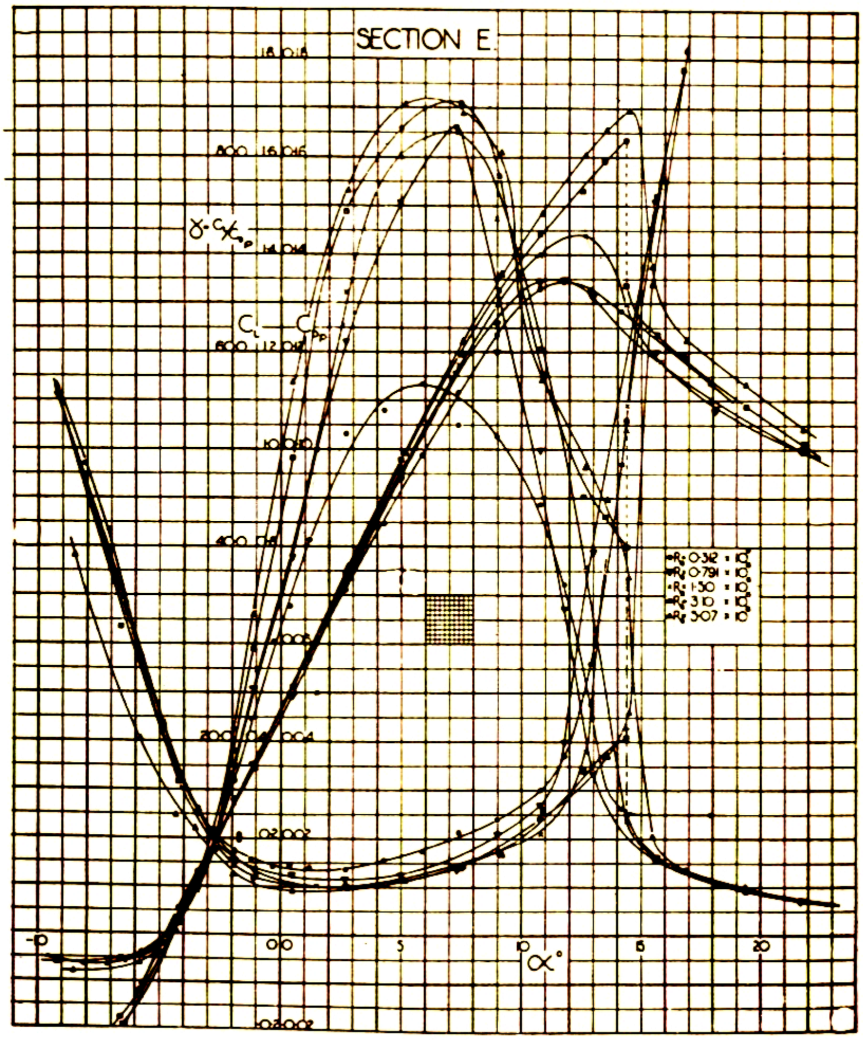

Figure 3.14 Airfoil Characteristics of RAF 6E Section.

Table 3.10 Section Coordinates of RAF 6E and C4 Airfoils.

Distance from leading edge	Distance from chord line	
	RAF 6E	C4
0	1.15	0
1.25	3.19	1.65
2.5	4.42	2.27
5.0	6.10	3.08
7.5	7.24	3.62
10	8.09	4.02
15	9.28	4.55
20	9.90	4.83
30	10.30	5.00
40	10.22	4.89
50	9.80	4.57
60	8.98	4.05
70	7.70	3.37
80	5.91	2.54
90	3.79	1.60
95	2.58	1.06
100	0.76	0
L.E. radius	1.15	1.2
T.E. radius	0.76	0.60

3.3 Design Constraints

- Fan Hub Ratio
- Solidity
- Lift Coefficient
- Loading Factor
- Flow and Swirl Coefficients
- Aspect Ratio

- Number of Blades and Straighteners
- Blade Tip Speed

In most fans, hub diameter is usually 40 to 70% of the rotor diameter [1]. The larger hub diameters are usually associated with fans designed for high pressure rises.

Blade solidity is defined as the ratio of the blade chord to circumferential gap between adjacent blade elements. The solidity σ is kept below unity in the blade design because the isolated airfoil method is selected. For solidities approaching unity or greater than unity there is an aerodynamic interference between the adjacent blades which usually results in a marked reduction in lift for a given blade incidence.

Because of the influence of the boundary layers on the hub and duct, the maximum lift coefficient of the blade section near root and tip will be less than in two dimensional flow, and the maximum lift to drag ratio will occur at a smaller lift coefficient. There is no general information to correct the two dimensional characteristics, even if the inlet boundary layer profile were known accurately. It is suggested that the fan blade lift coefficients should not exceed 0.9 or 1.0 at the root and 0.7 at the tip in order to avoid stalling due to boundary layer influence at the tip and a combination of this effect and blade interference at the root [1]. A survey of recommended C_L values in fan design indicates a range from 0.6 to 1.0 [2].

Because of the restriction on the lift coefficient C_L and solidity σ at the blade root, the product of lift coefficient and solidity known as loading factor $C_L \cdot \sigma$ do not exceed unity.

For flow coefficient λ; there is a lower limit of 0.2 fixed by efficiency considerations and there is an upper limit of 1.5, due to design difficulties. For swirl coefficient ε_s; there is an upper limits of 1.5 and 1.0 for prerotators and straighteners respectively. This value is very much fixed by blade stalling characteristics [1, 2].

Aspect ratio of a blade is defined as the ratio of the blade span to chord. The choice of blade aspect ratio is influenced by a number of factors. With the object of keeping annulus and secondary drags to a reasonable level it is generally accepted that the aspect ratio should be at least 2 [2]. From the practical point of view, increasing the aspect ratio reduces the axial dimension of the hub to which the blades are attached. Very large aspect ratios are undesirable for reasons of blade multiplicity, loss of blade stiffness and reduction in aerodynamic efficiency due to the low blade Reynolds number which follow from small chord blades.

The choice of blade numbers depends mainly on practical considerations such as root fixing details and boss depth. However, aerodynamic matters are also not to be neglected. For instance, a decreasing number of blades will reduce the aspect ratio and eventually lead to an efficiency decrease. On the other hand, a greater number would result in higher blade drag counts. The product of the blade number and chord values represent the total blade area which must be in accordance with thrust requirements. To avoid excessive blade passing pulsations, a minimum number of 4 blades are used in wind tunnel fans. The maximum number is limited by strength and Reynolds number considerations. The minimum Reynolds number based on the relative velocity and blade chord should be 7×10^5 in order to keep the sectional drag to a low level [2]. The number of straighteners differs from that used in the rotor design; this is done to reduce beat noise [1].

The effect of compressibility of the fluid on fan performance is important. The compressibility of the fluid becomes significant when the relative fluid velocity at the rotor blade tip speed exceed 167 m/s (550 ft/s), or the tip speed is greater than half of the local speed of sound [1]. Fan noise is also increased with increased rotor tip speed.

3.4 Rotor and Straightener Design Equations

Design equations from momentum considerations will be presented in detail for the general case of a rotor with preswirl and afterswirl. When appropriate, the preswirl or afterswirl may be equated to zero; e.g. in a rotor-straightener unit the preswirl is zero.

It is assumed that both the total pressure rise and the axial velocity component remain constant along the blade span and, that there is no radial component of flow. The latter condition is a consequence of the two former assumptions and is a requirement for free vortex flow. Constant axial velocity is never fully achieved but it has been demonstrated in practice that moderate departures from it are relatively unimportant.

Conditions in an elementary annulus of width dr and constant radius r are given in Fig. 3.15 at various stations in the fan unit. Air entering the prerotators axially is deflected tangentially in a direction opposite to the rotation of the fan. It is assumed that the air leaves the fan rotor with a swirl component in the direction of rotation, and hence the straighteners are left with the task of deflecting it back into the axial direction.

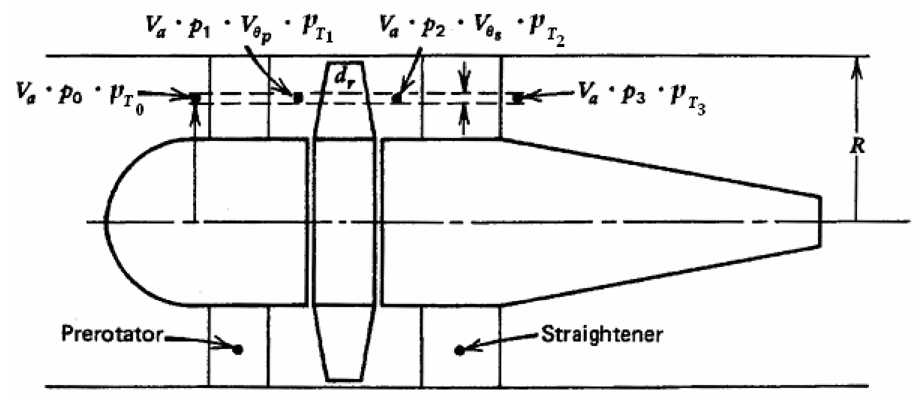

Figure 3.15 Blading Arrangements (General Blading Case)

It is convenient to take the preswirl and afterswirl as both positive values although strictly their respective positive directions are opposite sense to each other.

The Bernoulli relationships at the four stations in Fig. 3.15 assuming spanwise constant total pressure at each cross-sectional plane is

$$p_{T_0} = p_0 + \frac{1}{2} \cdot \rho \cdot V_a^{\,2} \tag{3.44}$$

$$p_{T_1} = p_1 + \frac{1}{2} \cdot \rho \cdot V_a^{\,2} + \frac{1}{2} \cdot \rho \cdot V_{\theta_p}^{\,2} \tag{3.45}$$

$$p_{T_2} = p_2 + \frac{1}{2} \cdot \rho \cdot V_a^{\ 2} + \frac{1}{2} \cdot \rho \cdot V_{\theta_s}^{\ 2} \tag{3.46}$$

$$p_{T_3} = p_3 + \frac{1}{2} \cdot \rho \cdot V_a^{\ 2} \tag{3.47}$$

where p_T, p, V_a, V_θ are the total pressure, static pressure, axial velocity component, and swirl velocity component, respectively. The overall change in total pressure in the annulus can be written

$$p_{T_3} - p_{T_0} = \Delta p_{th} - \Delta p_R - \Delta p_p - \Delta p_s \tag{3.48}$$

where Δp_{th} is the theoretical mean total pressure rise, the other terms denoting the losses in the rotor, prerotators, and straighteners, respectively, which have a spanwise variation.

The following nondimensional equation is obtained by dividing Eqn. (3.48) by $\frac{1}{2} \cdot \rho \cdot V_a^{\ 2}$, where V_a is the mean axial velocity through the fan.

$$\frac{p_{T_3} - p_{T_0}}{\frac{1}{2} \cdot \rho \cdot V_a^{\ 2}} = K_{th} - k_R - k_P - k_S \tag{3.49}$$

where $k = \Delta p \Big/ \frac{1}{2} \cdot \rho \cdot V_a^{\ 2}$, for example, $k_R = \Delta p_R \Big/ \frac{1}{2} \cdot \rho \cdot V_a^{\ 2}$

From Eqns. (3.44) and (3.47) it follows that $\left(p_{T_3} - p_{T_0}\right) \Big/ \frac{1}{2} \cdot \rho \cdot V_a^{\ 2}$ is also the nondimensional static pressure rise for the unit. Defining the swirl coefficient as

$$\varepsilon = V_\theta / V_a \tag{3.50}$$

the static pressure rise across the fan rotor at radius r is then given by

$$p_2 - p_1 = \Delta p = \frac{1}{2} \cdot \rho \cdot V_a^{\;2} \cdot \left(K_{th} - k_R + \varepsilon_p^{\;2} - \varepsilon_s^{\;2}\right) \tag{3.51}$$

The output of the work done from the rotor in the elementary annulus is defined as;

$$\left(p_{T_2} - p_{T_1}\right) \cdot 2 \cdot \pi \cdot r \cdot dr \cdot V_a \tag{3.52}$$

and the input is $\Omega \cdot dT$, where Ω is the rotational speed of the rotor in radians per second and dT is the element of torque. From the rate of change angular momentum,

$$dT = \rho \cdot V_a \cdot 2 \cdot \pi \cdot r \cdot dr \cdot \left(V_{\theta_s} + V_{\theta_p}\right) \cdot r \tag{3.53}$$

Replacing $\left(p_{T_2} - p_{T_1}\right)$ by the theoretical total pressure rise in Eqn. (3.52) and equating the new relation to $\Omega \cdot dT$,

$$\left(p_{T_2} - p_{T_1} + \Delta p_R\right) \cdot 2 \cdot \pi \cdot r \cdot dr \cdot V_a = \rho \cdot V_a \cdot 2 \cdot \pi \cdot r \cdot dr \cdot \left(V_{\theta_s} + V_{\theta_p}\right) \cdot \Omega \cdot r \tag{3.54}$$

and therefore

$$\Delta p_{th} = \rho \cdot \Omega \cdot r \cdot \left(V_{\theta_s} + V_{\theta_p}\right) \tag{3.55}$$

Nondimensionally,

$$K_{th} = \frac{2}{\lambda} \cdot \left(\varepsilon_s + \varepsilon_p\right) \tag{3.56}$$

where the flow coefficient is defined by

$$\lambda = V_a / \Omega \cdot r \tag{3.57}$$

The resultant velocity vector V_m, which determined the lift on the blade element, is shown in Fig. 3.16 together with the velocity components at inlet and outlet from the blade element.

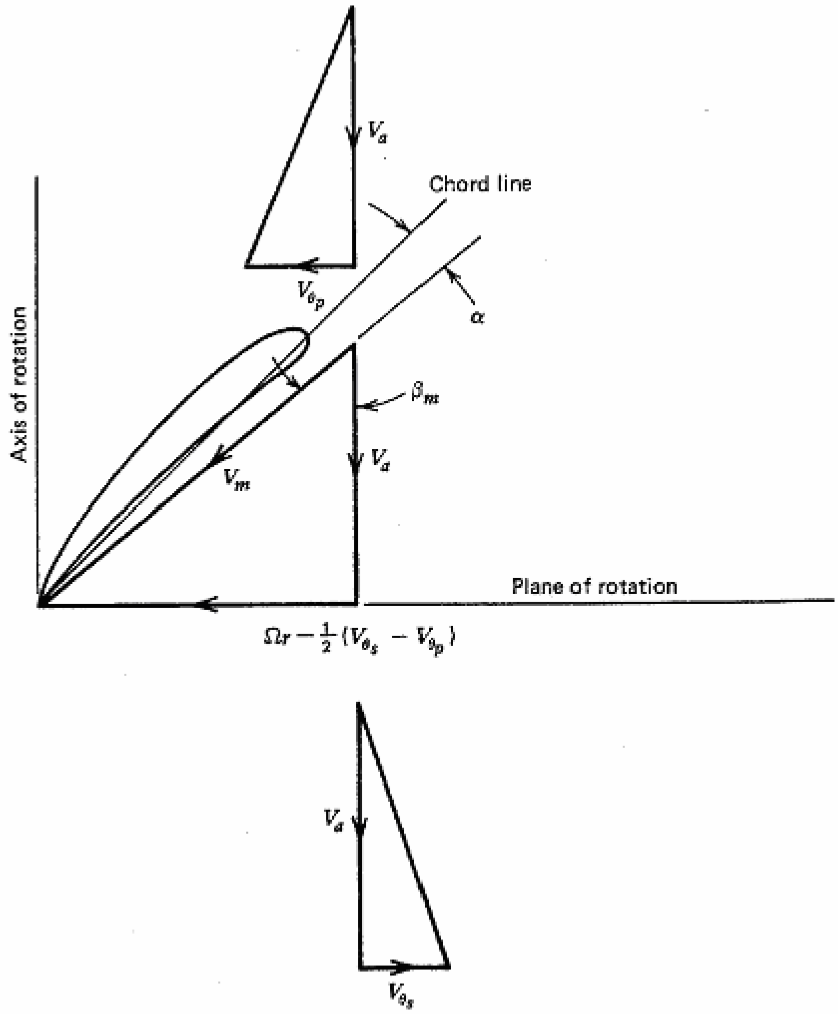

Figure 3.16 Relative Velocity Vectors, Rotor Blade Element.

The tangential velocity component of the air relative to the blade is given by

$$\Omega \cdot r - \frac{1}{2} \cdot \left(V_{\theta_s} - V_{\theta_p} \right) \tag{3.58}$$

where the second term is the mean swirl between the rotor inlet and outlet. The angle β_m that the resultant velocity V_m makes with the plane of rotation is obtained from

$$\tan \beta_m = \frac{\Omega \cdot r - \frac{1}{2} \cdot \left(V_{\theta_s} - V_{\theta_p} \right)}{V_a} \tag{3.59}$$

or

$$\tan \beta_m = \frac{1 - \frac{1}{2} \cdot \left(\varepsilon_s - \varepsilon_p \right) \cdot \lambda}{\lambda} \tag{3.60}$$

It can be shown from Eqn. (3.55) that $\left(V_{\theta_s} + V_{\theta_p} \right)$ is inversely proportional to the radius r when Δp_{th} is constant along the blade. It is usual to make one of these swirls zero or inversely proportional to the radius; in both cases the flow satisfies the condition for free vortex flow.

The general momentum theory is applied to a blade possessing relative motion, as illustrated in Fig 3.17.

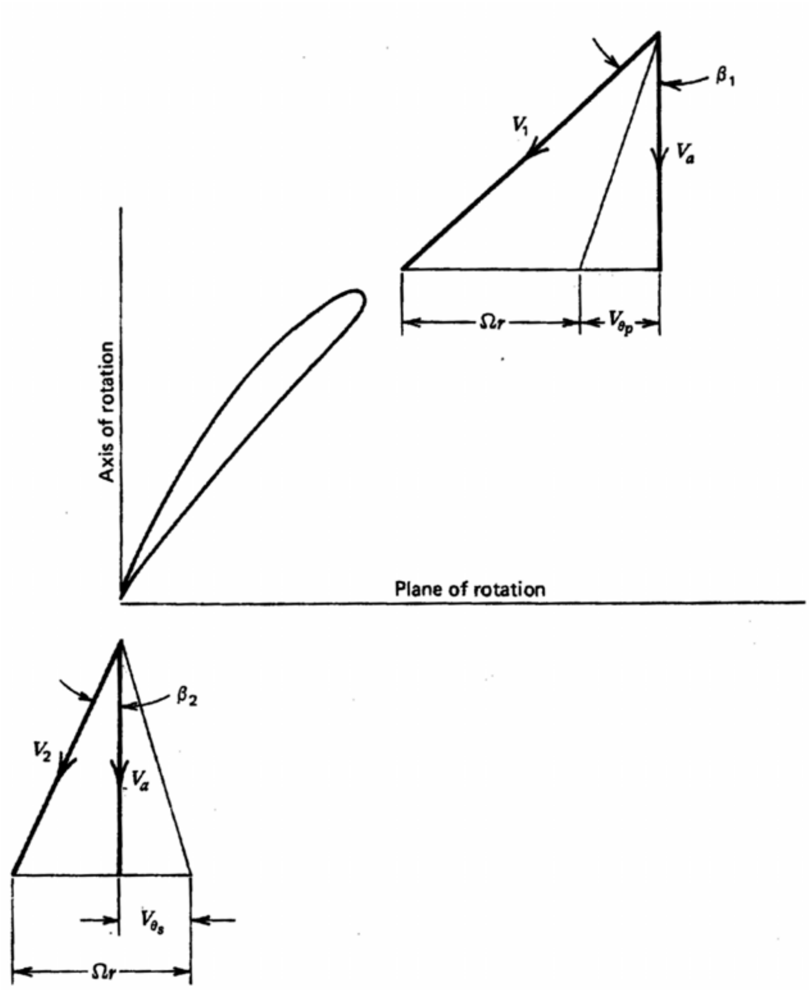

Figure 3.17 Absolute Velocity Vectors, Rotor Blade Element.

The change in the tangential velocity component from blade inlet to outlet is

$$(\Omega \cdot r + V_{\theta_p}) - (\Omega \cdot r - V_{\theta_s}) = V_{\theta_p} + V_{\theta_s} \tag{3.61}$$

In addition, the theoretical static pressure rise $(\Delta p_{th})_s$ is equal to the change in dynamic pressure, namely,

$$(\Delta p_{th})_s = \frac{1}{2} \cdot \rho \cdot V_1^{\,2} - \frac{1}{2} \cdot \rho \cdot V_2^{\,2} \tag{3.62}$$

a relationship that can alternatively be obtained by combining Eqns. (3.51) and (3.55) and by using the vector diagrams of Fig 3.15.

From the force vector diagram (Fig. 3.18) it follows that the axial force Z is given by

$$Z = \int_{r_b}^{R} \Delta p \cdot s \cdot dr \tag{3.63}$$

and the tangential force Y by

$$Y = \int_{r_b}^{R} s \cdot \rho \cdot V_a \cdot \left(V_{\theta_p} + V_{\theta_s}\right) \cdot dr = s \cdot p \cdot V_a^{\ 2} \cdot \left(\varepsilon_s + \varepsilon_p\right) \cdot dr \tag{3.64}$$

From Fig. 3.16, the drag of a blade element is

$$D = \int_{r_b}^{R} s \cdot \rho \cdot V_a^{\ 2} \cdot \left(\varepsilon_s + \varepsilon_p\right) \cdot dr \cdot \sin\beta_m - s \cdot \Delta p \cdot dr \cdot \cos\beta_m \tag{3.65}$$

Substituting for Δp from Eqn. (3.51), writing V_a / V_m as $\cos\beta_m$ (Fig. 3.13) and dividing by $\frac{1}{2} \cdot \rho \cdot V_m^{\ 2} \cdot c \cdot dr$ in order to obtain a drag coefficient,

$$\begin{aligned} C_D = {} & \frac{s}{c} \cdot \cos^2\beta_m \cdot \left[2 \cdot \left(\varepsilon_s + \varepsilon_p\right) \cdot \sin\beta_m - \left(K_{th} - \varepsilon_s^{\ 2} + \varepsilon_p^{\ 2}\right) \cdot \cos\beta_m\right] \\ & + \frac{s}{c} \cdot k_R \cdot \cos^3\beta_m \end{aligned} \tag{3.66}$$

Eliminating K_{th} by Eqn. (3.56) and using Eqn. (3.60)

$$C_D = 2 \cdot \frac{s}{c} \cdot \cos^2 \beta_m \cdot \left(\varepsilon_s + \varepsilon_p\right) \cdot \left[\sin \beta_m - \frac{\cos \beta_m}{\cot \beta_m}\right] + \frac{s}{c} \cdot k_R \cdot \cos^3 \beta_m \qquad (3.67)$$

and hence

$$C_D = \frac{s}{c} \cdot k_R \cdot \cos^3 \beta_m \qquad (3.68)$$

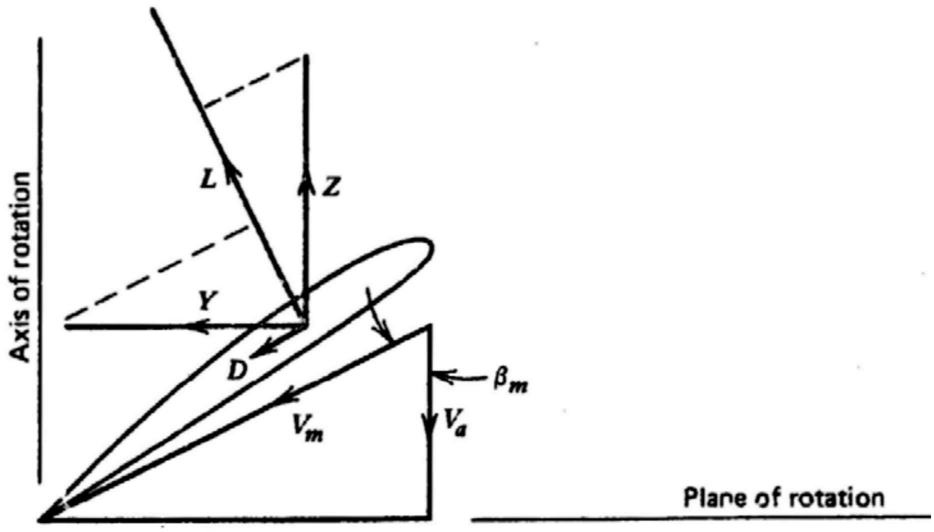

Figure 3.18 Rotor Blade Element Force Vectors.

Similarly, the lift is

$$\begin{aligned} L &= Y \cdot \cos \beta_m + Z \cdot \sin \beta_m \\ &= \int_{r_b}^{R} s \cdot \rho \cdot V_a^{\,2} \cdot \left(\varepsilon_s + \varepsilon_p\right) \cdot dr \cdot \cos \beta_m + \int_{r_b}^{R} s \cdot \Delta p \cdot dr \cdot \sin \beta_m \end{aligned} \qquad (3.69)$$

and hence

$$C_L = \frac{s}{c} \cdot \cos^2 \beta_m \cdot \left[2 \cdot \left(\varepsilon_s + \varepsilon_p\right) \cdot \cos \beta_m + \left(K_{th} - {\varepsilon_s}^2 + {\varepsilon_p}^2\right) \cdot \sin \beta_m\right]$$
$$- \frac{s}{c} \cdot k_R \cdot \cos^2 \beta_m \cdot \sin \beta_m \qquad (3.70)$$

Making substitutions similar to previous ones and using Eqn. (3.68)

$$C_L = 2 \cdot \frac{s}{c} \cdot \left(\varepsilon_s + \varepsilon_p\right) \cdot \cos \beta_m - C_D \cdot \sin \beta_m \qquad (3.71)$$

or

$$C_L \cdot \sigma = 2 \cdot \left(\varepsilon_s + \varepsilon_p\right) \cdot \cos \beta_m - \sigma \cdot C_D \cdot \tan \beta_m \qquad (3.72)$$

where $\sigma = c/s = solidity$. The last term is usually small, being ignored in most design methods. Hence

$$C_L \cdot \sigma = 2 \cdot \left(\varepsilon_s + \varepsilon_p\right) \cdot \cos \beta_m \qquad (3.73)$$

From Fig. 3.17 blade inlet and outlet angles in terms of λ and ε,

$$\tan \beta_1 = \frac{1 + \varepsilon_p \cdot \lambda}{\lambda} \qquad (3.74)$$

$$\tan \beta_2 = \frac{1 - \varepsilon_s \cdot \lambda}{\lambda} \qquad (3.75)$$

$$\tan \beta_1 - \tan \beta_2 = \varepsilon_s + \varepsilon_p \qquad (3.76)$$

and when combined with Eqn. (3.60)

$$\tan \beta_m = \frac{1}{2} \cdot \left(\tan \beta_1 + \tan \beta_2\right) \qquad (3.77)$$

The drag coefficient for a blade element is given in Eqn. (3.68). Multiplying by C_L/K_{th} and writing γ for C_L/C_D,

$$\gamma \cdot \frac{k_R}{K_{th}} = \frac{C_L \cdot \sigma}{K_{th} \cdot \cos^3 \beta_m} \tag{3.78}$$

Substituting for $C_L \sigma$ (Eqn. (3.73)) and K_{th} (Eqn. (3.56))

$$\gamma \cdot \frac{k_R}{K_{th}} = \frac{\lambda}{\cos^2 \beta_m} \tag{3.79}$$

Making the design assumption that the mean drag coefficient for the rotor is given by

$$C_D = C_{D_P} + C_{D_s} \tag{3.80}$$

where C_{D_P} is the profile drag coefficient at mid blade span, and the secondary drag coefficient C_{D_S} is suitably calculated, then the mean total pressure loss coefficient k_R for the rotors follows from Eqn. (3.79), namely,

$$\frac{k_R}{K_{th}} = \left(\frac{C_D \cdot \lambda}{C_L \cdot \cos^2 \beta_m} \right)_{MS} \tag{3.81}$$

This expression can alternatively be written

$$\frac{k_R}{K_{th}} = \frac{k_{R_P}}{K_{th}} + \frac{k_{R_S}}{K_{th}} = \left(\frac{C_{D_P}}{C_L} + \frac{C_{D_S}}{C_L} \right) \left(\frac{\lambda}{\cos^2 \beta_m} \right)_{MS} \tag{3.82}$$

where MS denotes the midspan.

The estimation of efficiency loss due to profile drag will depend on whether the fan is designed by the isolated aerofoil or the cascade design method. In the former case, profile drag coefficient can be ascertained from the experimental aerofoil data once the design midspan lift coefficient has been chosen.

Boundary layers of both duct and fan hub cause secondary flows that appear on the surfaces of the blades at their extremities and constitute momentum losses which reduce fan efficiency. The drag due to secondary flows is known as secondary drag. The secondary drag for the rotor blade is given by (ref. 1, p. 222)

$$C_{D_S} = a \cdot {C_L}^2 \tag{3.83}$$

where a is a function of chord Reynolds number only, and C_L is a mean value for the blade. The coefficient a varies from 0.019 at $\text{Re} = 1x10^5$ to 0.015 at $5x10^5$.

From momentum considerations with Fig. 3.19, similarly with the rotor blade element, the following relations are obtained for straighteners.

$$\beta_{m_S} = \tan^{-1}\left(\frac{\varepsilon_s}{2}\right) \tag{3.84}$$

$$C_L = 2 \cdot \frac{s}{c} \cdot \varepsilon_s \cdot \cos\beta_{m_S} - C_D \cdot \frac{\varepsilon_s}{2} \tag{3.85}$$

$$C_D = \frac{s}{c} \cdot k_S \cdot \cos^3 \beta_{m_S} \tag{3.86}$$

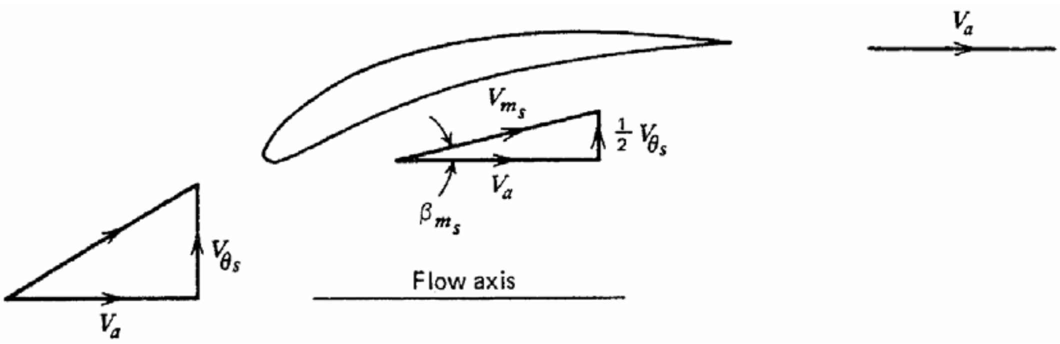

Figure 3.19 Velocity Vectors for Straightener Vane Element.

Since the last term in Eqn. (3.61) is usually much smaller than the preceding one

$$C_L \cdot \sigma = 2 \cdot \varepsilon_S \cdot \cos \beta_{m_S} \tag{3.87}$$

The important flow and geometric parameters controlling straightener design are defined Fig. 3.20.

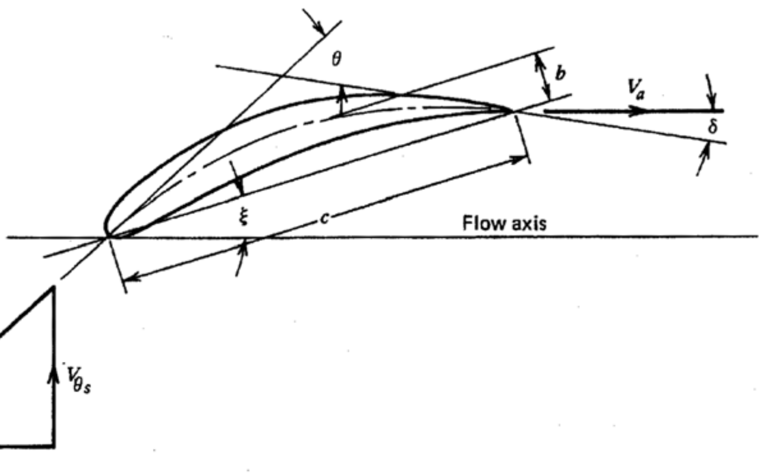

Figure 3.20 Straightener Vane Element Geometry.

From Fig. 3.20, following relationships are obtained.

$$\beta_1 = \tan^{-1} \varepsilon_S \tag{3.88}$$

$$\theta = \beta_1 + \delta \tag{3.89}$$

$$\delta = 0.26 \cdot \theta \cdot \sqrt{\frac{s}{c}} \tag{3.90}$$

$$\theta = \frac{\beta_1}{1 - 0.26\sqrt{s/c}} \tag{3.91}$$

$$\xi = \beta_1 - \frac{\theta}{2} \tag{3.92}$$

$$b = \frac{1}{2} \cdot c \cdot \tan\frac{\theta}{4} \tag{3.93}$$

In equations given above; θ, δ, ξ, b are the camber angle, deviation angle, stagger angle and radius of curvature respectively. If the swirl coefficient is known, corresponding values of $s/c, C_L$ and θ, ξ are determined from Figs. 3.21 and 3.22 respectively.

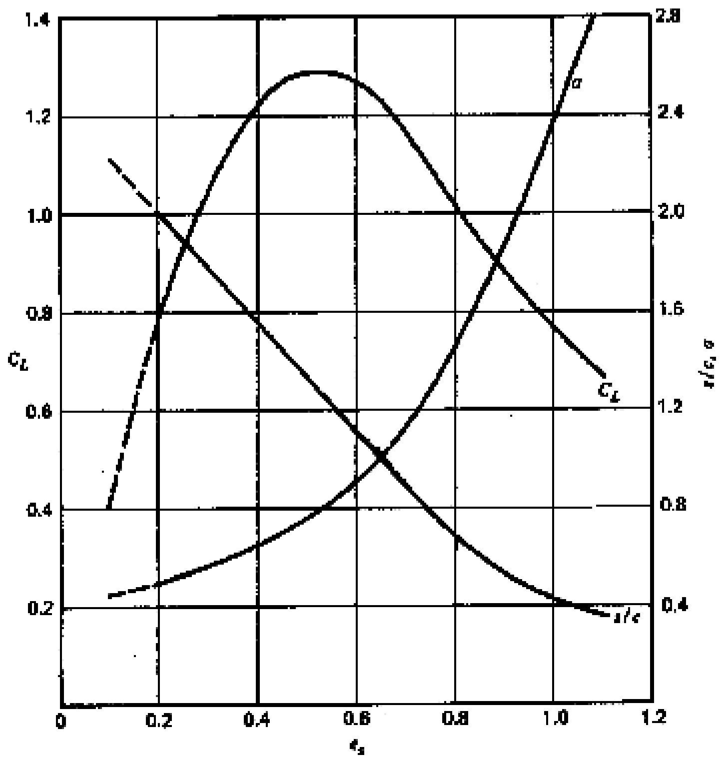

Figure 3.21 Straightener Vane Design Data (ref. 1, p. 233).

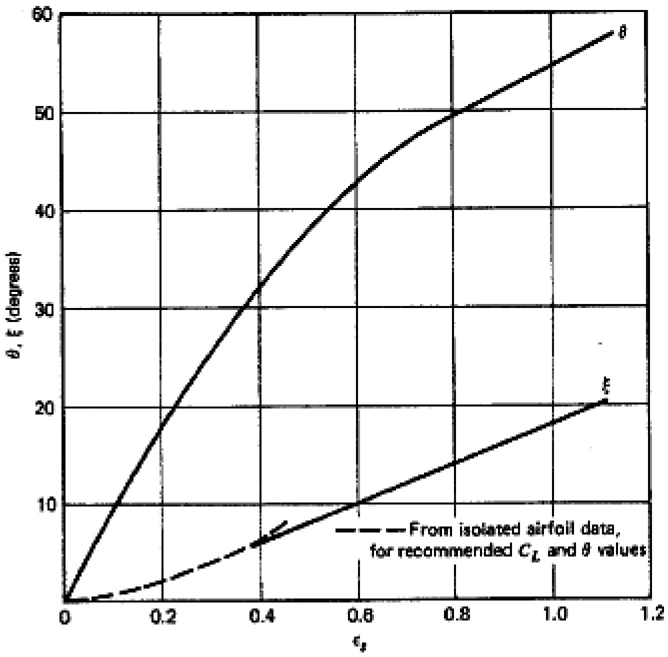

Figure 3.22 Straightener Vane Camber and Stagger Angle (ref. 1, p. 234).

Straightener losses from momentum considerations,

$$\frac{k_S}{K_{th}} \cdot \left(\frac{C_L}{C_D} + \frac{\varepsilon_S}{2} \right) = \frac{\lambda}{\cos^2 \beta_{m_S}} \cdot \frac{\varepsilon_S}{\varepsilon_S + \varepsilon_P} \tag{3.94}$$

and since $C_L / C_D >> \varepsilon_S / 2$

$$\frac{k_S}{K_{th}} \cdot \frac{C_L}{C_D} = \frac{\lambda}{\cos^2 \beta_{m_S}} \cdot \frac{\varepsilon_S}{\varepsilon_S + \varepsilon_P} \tag{3.95}$$

The profile drag coefficient C_{D_P} is assumed to be given by

$$C_{D_P} = 0.016 \tag{3.96}$$

This value corresponds to blading of moderate to high solidity at Re of $2x10^5$ approximately. Reductions of 20 to 25% in profile drag coefficient can be expected at Reynolds numbers of around $6x10^5$. The adoption of the above value for C_{D_P} therefore ensures an increasing degree of conservatism, for advancing Re.

The secondary drag coefficient C_{D_S} for straightener is assumed to be given by

$$C_{D_S} = 0.018 \cdot C_L{}^2 \tag{3.97}$$

Mean drag coefficient is given in same equation with rotor blade by.

$$C_D = \left(C_{D_P} + C_{D_S} \right)_{MS} \tag{3.98}$$

and hence

$$\frac{k_S}{K_{th}} \cdot \frac{C_L}{C_D} = \left(\frac{\lambda}{\cos^2 \beta_{m_S}} \cdot \frac{\varepsilon_S}{\varepsilon_S + \varepsilon_P} \right)_{MS} \tag{3.99}$$

3.5 Rotor and Straightener Design

Fan applications can be divided roughly into three categories, in terms of flow coefficient and pressure rise capability. These are follows [1]:

1. Λ<0.2. These low pressure rise fans which usually possess a small boss ratio (≈0.4) are frequently operated as exhaust fans, without guide vanes.
2. Λ≈0.2 to 0.4. These units normally have boss ratio between 0.5 and 0.7 and incorporate guide vanes; they are capable of substantial pressure rise, gaining from an optimum efficiency design approach.
3. Λ>0.4. Fans in this category are usually of the multistage in-line type, as single stage total pressure coefficient capability is restricted.

Since the rotor-straightener unit is selected as the ducted fan type, our fan belongs to the second category.

Rotor design is almost exclusively a function of swirl and flow coefficients and straightener design is largely a function of the former parameter. The quantity that is common to the flow and swirl coefficients is the axial velocity component.

It is known that the maximum desired velocity at the test section of AWT is assumed that 180 m/s ($M = 0.52$). Response to this velocity, the axial velocity at the fan entry is calculated using the calculations steps explained in section 3.1.1 which also takes compressibility into account. Based on these calculations, maximum axial velocity at the fan entry is 56.97 m/s. Maximum flowrate is 1118.7 m^3/s (Eqn. 3.40). The maximum axial velocity at the fan annulus can be written as

$$V_{a\max} = \frac{Q_{\max}}{\pi \cdot R^2 \cdot \left(1 - x_b^2\right)} \tag{3.100}$$

Then,

$$V_{a\max} = \frac{1118.7}{3.14 \cdot 2.58^2 \cdot \left(1 - 0.5^2\right)} = 71.32\ m/s$$

Rotor tip speed is

$$\Lambda_{\max} = \frac{V_{a_{\max}}}{V_{tip}} = 0.4\ \Rightarrow V_{tip} = \frac{71.32}{0.4} = 178.3\ m/s$$

Fan rotational speed is calculated from:

$$V_{tip} = \Omega \cdot R \Rightarrow \Omega = \frac{V_{tip}}{R} = \frac{178.3}{2.58} = 69.1\ rad/s = 660\ rpm$$

To find minimum axial velocity, minimum flow coefficient is used;

$$\Lambda_{\min} = \frac{V_{a_{\min}}}{V_{tip}} = 0.2 \Rightarrow V_{a_{\min}} = 178.3 \cdot 0.2 = 35.66\ m/s$$

The velocity at the fan entry, from continuity equation assuming no density change

$$V_f = V_{a_{\min}} \cdot \frac{A}{A_f} = V_{a_{\min}} \cdot \frac{\pi \cdot R^2 \cdot \left(1 - x_b^2\right)}{\pi \cdot R_f} = 35.66 \cdot \frac{3.14 \cdot 2.58^2 \cdot \left(1 - 0.5^2\right)}{3.14 \cdot 2.5^2} = 28.49\ m/s$$

And similarly minimum test section velocity is 79.7 m/s.

Required total pressure rises in the operating range of the fan are given in Table 3.11.

Table 3.11 Required Total Pressure Rises in the Operating Range.

Λ	$V_a\,(m/s)$	$V_t\,(m/s)$	$Q\,(m^3/s)$ (Eqn. 3.100)	$\Delta p_T = 0.002828 \cdot Q^2\ (Pa)$
0.2	35.66	79.7	559.3	903.47
0.25	44.58	-	699.2	1411.98
0.3	53.50	-	839	2033.05
0.35	62.41	-	978.8	2767.02
0.4	71.32	180	1118.7	3614.53

At the design point of a subsonic wind tunnel fan mostly maximum velocity is taken. In this study firstly maximum velocity is taken as design point but after interpreting the analysis result it is concluded that this design point is not feasible because some inefficient data and some impossible results are included in the operating range. For this reason midpoint of the flow coefficient ($\Lambda = 0.3$) is taken as design point instead.

An algorithm consists of preliminary design, rotor design and straightener design is developed to design the fan (Fig. 3.23).

After the design flow coefficient and the rotor tip speed have been fixed, for five different fan hub ratios preliminary design is carried out to determine the fan hub ratio which gives the highest overall efficiency (Table 3.11). Preliminary design is performed at midspan station of the rotor. According to preliminary design, the fan hub ratio is selected as 0.5. The next design phase concerns the detailed design of the rotor blade elements at chosen radii. First, the appropriate Reynolds number can, when blade chord is assumed to equal half the blade span, be determined for midspan station from the relation

$$\mathrm{Re} = \frac{\rho \cdot V_m \cdot c}{\mu} = \frac{\rho \cdot V_a \cdot c}{\cos \beta_m \cdot \mu} = 5.8x10^6$$

where $\mu = 1.78x10^{-5}\, N \cdot s/m^2$, $\rho = 1.17\, kg/m^3$, $V_a = 53.5\ m/s$ (Table 3.11), $\beta_m = 67.02^\circ$ (Table 3.12) and $c = 0.645\,m$. Hence the lift and drag data of RAF 6E given in Fig. 3.14 for $\mathrm{Re} = 5.07x10^6$ are suitable for design use providing that chord length is less than 0.645. Thereafter rotor blade design is performed. Rotor design details are given in Table 3.12.

It is desirable that for the straightener vanes to have a fixed pitch and yet, within acceptable limits, to still remove the swirl downstream of the rotor over the entire operating range. To achieve this goal along the entire blade span, for the rotor which is analyzed over the operating range, the swirl coefficients are calculated at the highest swirl location that is the rotor blade root. It is decided to design the straightener at 0.2 flow coefficient and zero pitch angle. Straightener design results are given in Table 3.13.

At the end of the design, efficiency of rotor and straightener system at the rotor design point is obtained (Table 3.14).

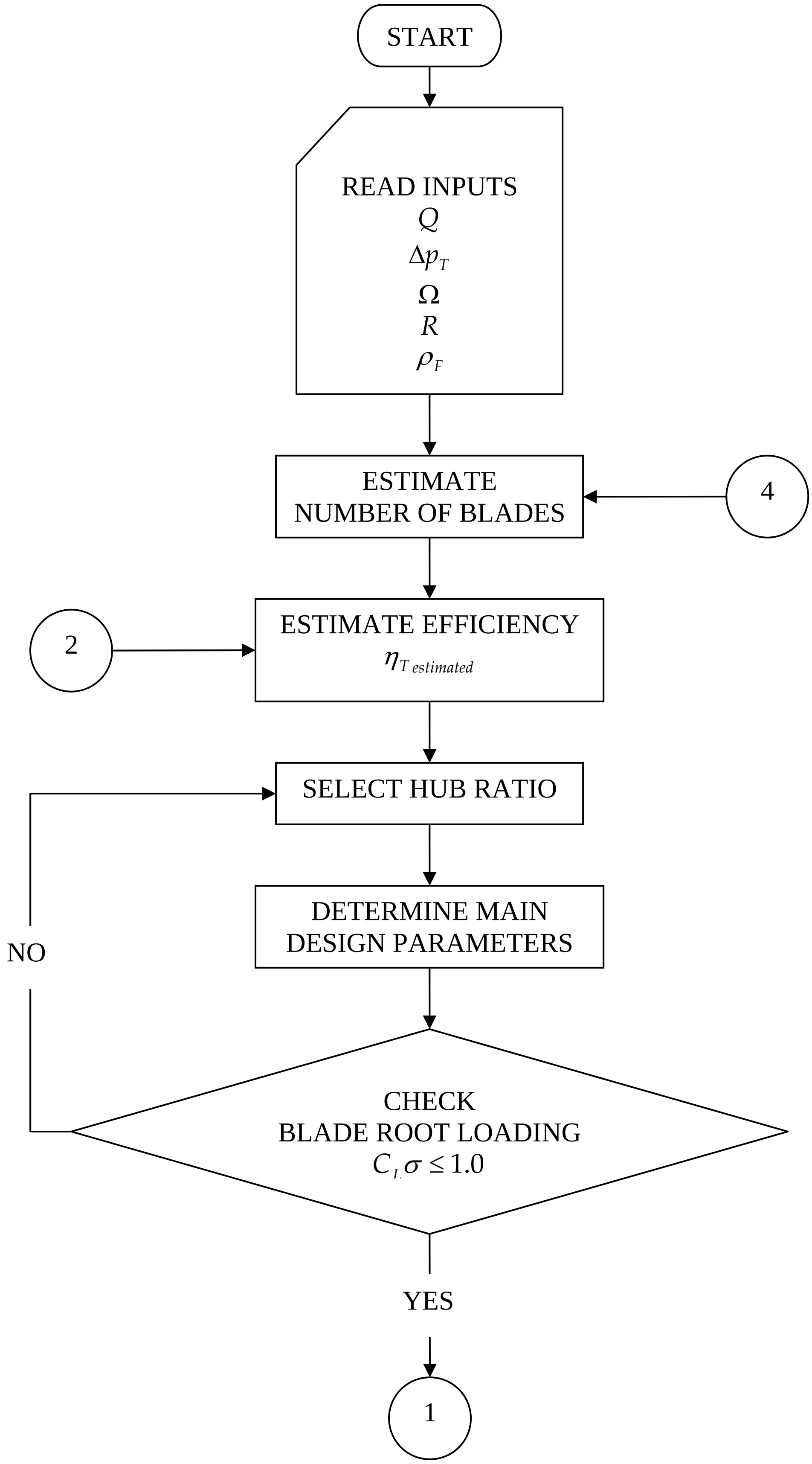
START
READ INPUTS
Q
Δp_T
Ω
R
ρ_F
ESTIMATE
NUMBER OF BLADES
4
2
ESTIMATE EFFICIENCY
$\eta_{T\,estimated}$
SELECT HUB RATIO
DETERMINE MAIN
DESIGN PARAMETERS
NO
CHECK
BLADE ROOT LOADING
$C_L\sigma \leq 1.0$
YES
1

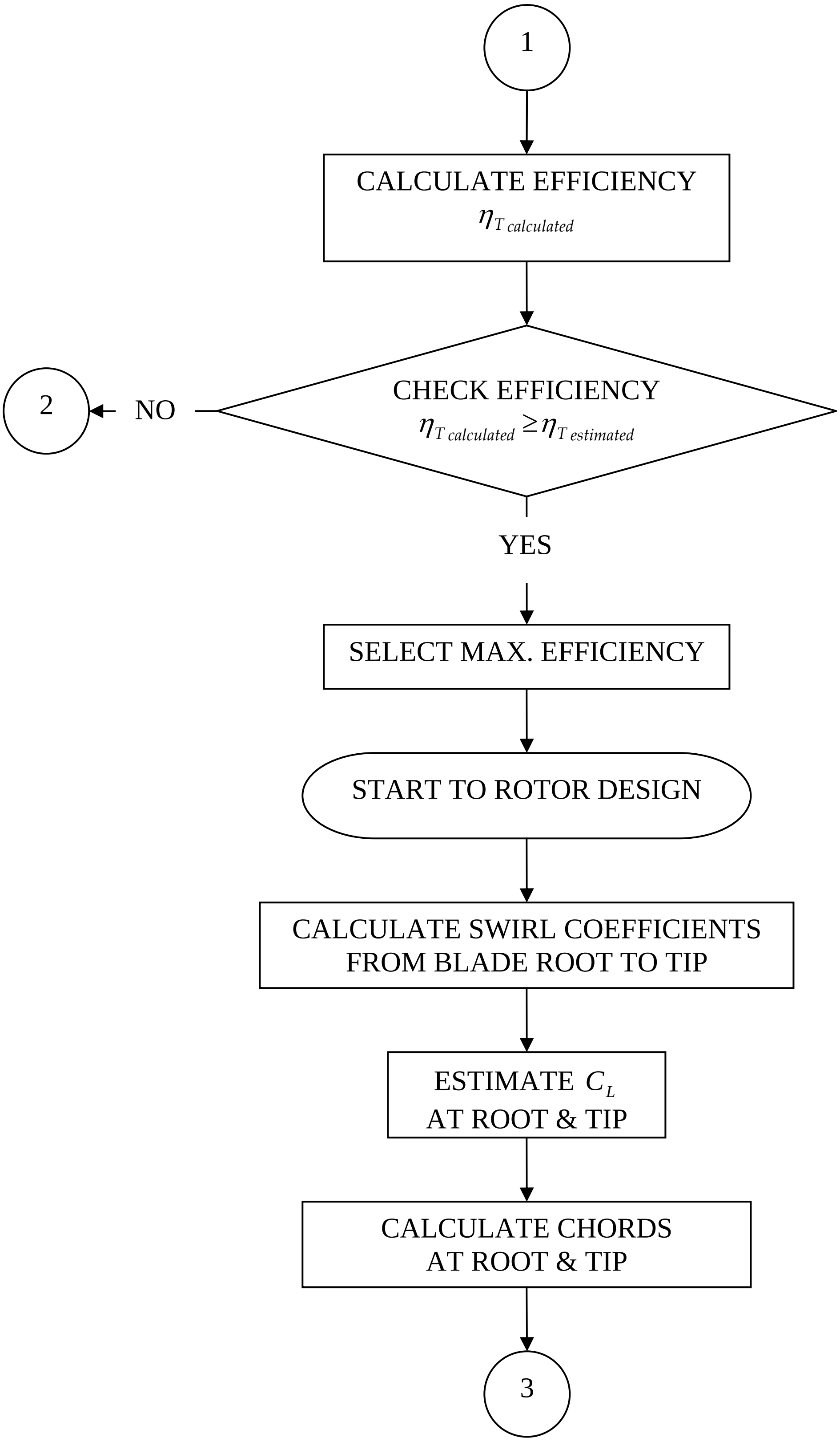
1
CALCULATE EFFICIENCY
$\eta_{T\,calculated}$
CHECK EFFICIENCY
$\eta_{T\,calculated} \geq \eta_{T\,estimated}$
NO
2
YES
SELECT MAX. EFFICIENCY
START TO ROTOR DESIGN
CALCULATE SWIRL COEFFICIENTS
FROM BLADE ROOT TO TIP
ESTIMATE C_L
AT ROOT & TIP
CALCULATE CHORDS
AT ROOT & TIP
3

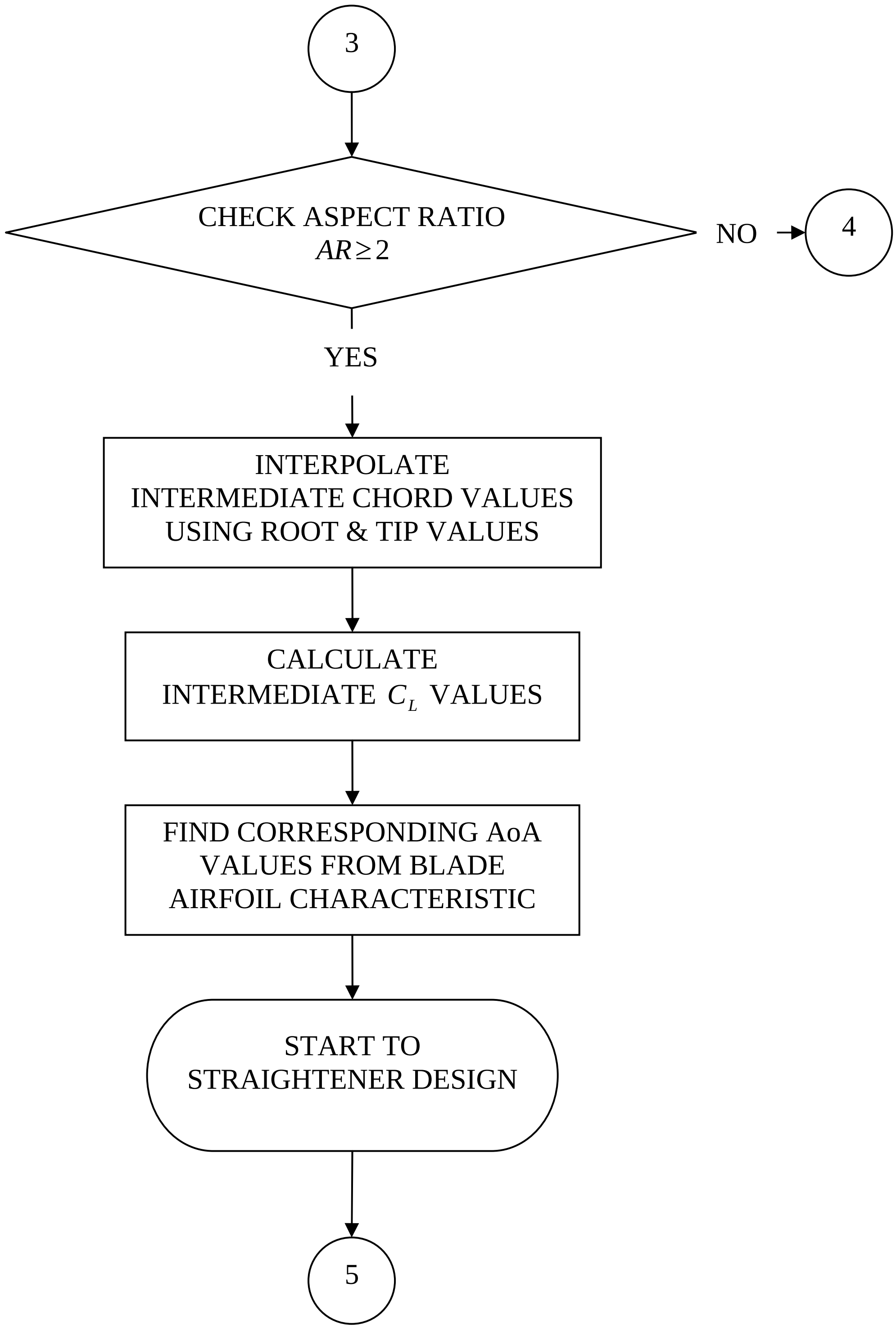
3
CHECK ASPECT RATIO
$AR \geq 2$
NO
4
YES
INTERPOLATE
INTERMEDIATE CHORD VALUES
USING ROOT & TIP VALUES
CALCULATE
INTERMEDIATE C_L VALUES
FIND CORRESPONDING AoA
VALUES FROM BLADE
AIRFOIL CHARACTERISTIC
START TO
STRAIGHTENER DESIGN
5

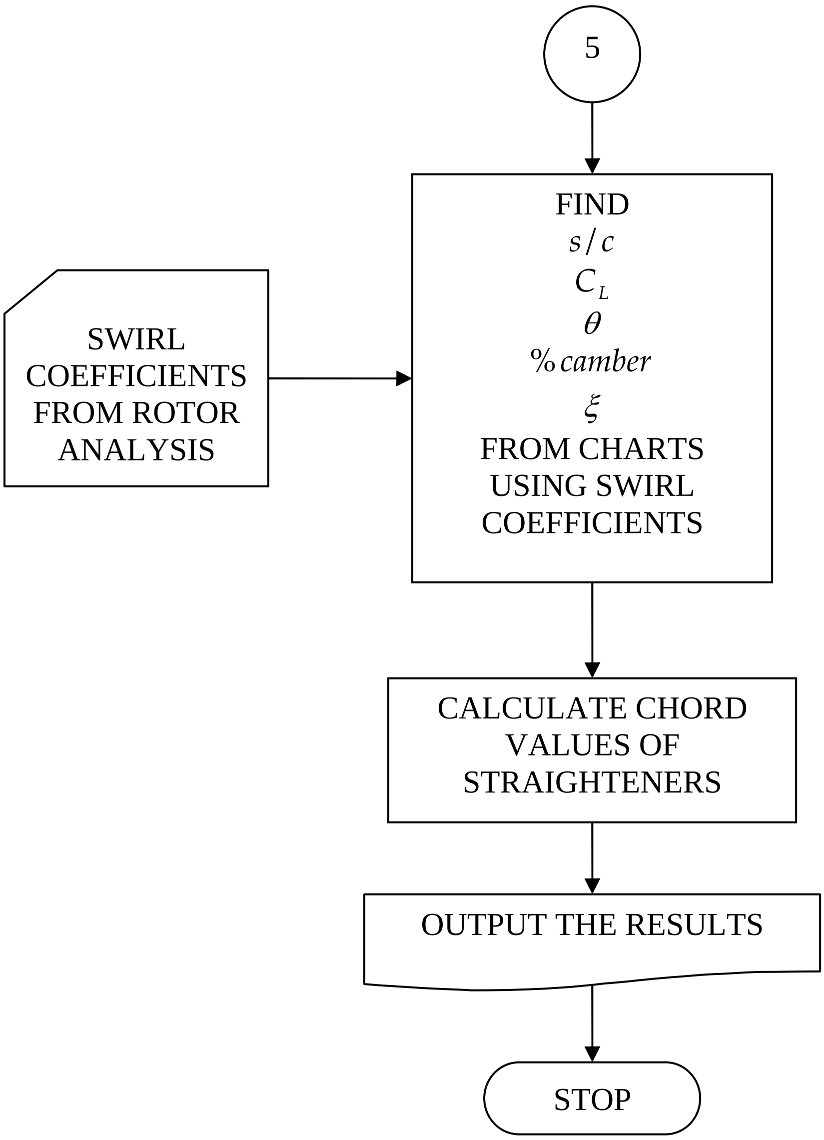

Figure 3.23 Rotor and Straightener Design Algorithm.

Table 3.12 Preliminary Design Results.

Determination of Main Design Parameters					
$x_b = r_b/R$ **(Fan boss ratio)**	**0.5**	**0.55**	**0.6**	**0.65**	**0.7**
R	2.58	2.58	2.58	2.58	2.58
r_b	1.29	1.42	1.55	1.68	1.81
$V_a = Q/\pi \cdot R^2(1-x_b^2)$	53.5	57.55	62.7	69.5	78.7
$\frac{1}{2}\cdot\rho\cdot V_a^2$	1687	1951	2317	2846	3649
Δp_T	2033	2033	2033	2033	2033
$K_{th} = \left(\Delta p_T \Big/ \frac{1}{2}\cdot\rho\cdot V_a^2\right) \Big/ \eta_{T_{estimated}}$	1.42	1.23	1.03	0.84	0.66
$V_{tip} = \Omega \cdot R$	178.3	178.3	178.3	178.3	178.3
$\Lambda = V_a/V_{tip}$	0.3	0.32	0.35	0.39	0.44
Check on Blade Root Loading					
$\lambda_b = \Lambda/x_b$	0.60	0.59	0.59	0.60	0.63
$\varepsilon_{s_b} = K_{th}\cdot\lambda_b/2$	0.43	0.36	0.30	0.25	0.21
$(\beta_m)_b = \tan^{-1}\left[\left(1-\frac{1}{2}\cdot\varepsilon_{s_b}\cdot\lambda_b\right)\Big/\lambda_b\right]$	55.5	56.8	57.3	57.0	56.0
$(C_L\cdot\sigma)_b = 2\cdot\varepsilon_{s_b}\cdot(\cos\beta_m)_b$	0.48	0.39	0.33	0.27	0.23
Efficiency Estimation					
$x_{MS} = (1+x_b)/2$	0.75	0.78	0.80	0.83	0.85
$\lambda_{MS} = \Lambda/x_{MS}$	0.40	0.42	0.44	0.47	0.52
$(\varepsilon_s)_{MS} = (K_{th}\cdot\lambda_{MS})/2$	0.28	0.26	0.23	0.20	0.17
$(\beta_m)_{MS} = \tan^{-1}\left[\left(1-\frac{1}{2}\cdot(\varepsilon_s)\cdot\lambda\right)\Big/\lambda\right]_{MS}$	67.0	66.3	65.2	63.6	61.5
$\left(\gamma\frac{k_R}{K_{th}}\right)_{MS} = \frac{\lambda_{MS}}{\cos^2(\beta_m)_{MS}}$	2.63	2.57	2.49	2.40	2.28
$\gamma_{MS} = \left[C_L/\left(C_{D_p}+C_{D_S}\right)\right]_{MS}$	42	42	42	42	42
$\left(\frac{k_R}{K_{th}}\right)_{MS}$	0.062	0.061	0.059	0.057	0.054
$(\beta_{mS})_{MS} = \tan^{-1}\left[(\varepsilon_s)_{MS}/2\right]$	8.1	7.3	6.5	5.7	4.9
$\left(\gamma\frac{k_S}{K_{th}}\right)_{MS} = \frac{\lambda_{MS}}{\cos^2(\beta_{mS})_{MS}}$	0.41	0.42	0.45	0.48	0.52

Table 3.12 Preliminary Design Results (Continued).

$\gamma_{MS} = \left[C_L/\left(C_{D_p} + C_{D_S}\right)\right]_{MS}$	28	28	28	28	28
$\left(\frac{k_S}{K_{th}}\right)_{MS}$	0.015	0.015	0.016	0.017	0.019
η_D	0.825	0.825	0.825	0.825	0.825
$k_D = (1-\eta_D)\left[x_b^2\left(2-x_b^2\right)\right]$	0.077	0.09	0.103	0.117	0.129
$\frac{k_D}{K_{th}}$	0.054	0.073	0.100	0.139	0.198
$(\eta_R)_{MS} = \left[1-\left(\frac{k_R}{K_{th}}\right)\right]_{MS}$	0.938	0.939	0.941	0.943	0.946
$(\eta_S)_{MS} = \left[1-\left(\frac{k_S}{K_{th}}\right)\right]_{MS}$	0.985	0.985	0.984	0.983	0.981
$(\eta_{BL})_{MS} = \left[1-\left(\frac{k_R+k_S}{K_{th}}\right)\right]_{MS}$	0.923	0.924	0.925	0.926	0.927
$(\eta_T)_{MS} = \left[1-\left(\frac{k_R+k_S+k_D}{K_{th}}\right)\right]_{MS}$	0.869	0.85	0.825	0.787	0.73

Table 3.13 Rotor Design Details.

$x = r/R$	0.5	0.6	0.75	0.9	1.0
$\lambda = \Lambda/x$	0.6	0.5	0.4	0.33	0.3
$K_{th} = \left(\Delta p_T \Big/ \frac{1}{2} \cdot \rho \cdot V_a^2 \right) \Big/ \eta_{T_{calculated}}$	1.387	1.387	1.387	1.387	1.387
$\varepsilon_s = K_{th} \cdot \lambda\ /2$	0.416	0.347	0.277	0.231	0.208
$\beta_m = \tan^{-1}\left[\left(1 - \frac{1}{2} \cdot (\varepsilon_s) \cdot \lambda \right) \Big/ \lambda \right]$	55.6	61.3	67.1	70.9	72.8
$C_L \cdot \sigma = 2 \cdot \varepsilon_s \cdot \cos \beta_m$	0.470	0.333	0.216	0.151	0.123
$\beta_1 = 1/\lambda$	59.0	63.4	68.2	71.6	73.3
$\beta_2 = (1 - \varepsilon_s)/\lambda$	51.4	58.8	65.8	70.1	72.3
$\beta_1 - \beta_2$	7.6	4.6	2.4	1.5	1.0
C_L	0.9	0.842	0.697	0.624	0.6
σ	0.523	0.395	0.311	0.243	0.205
α	3.87	3.37	2.01	1.35	1.13
$\xi = \beta_m - \alpha$	51.70	57.93	65.04	69.53	71.66
$\phi = 90^\circ - \xi$	38.31	32.07	24.96	20.47	18.34
$n \cdot c/R = 2 \cdot \pi \cdot \sigma \cdot x$	1.64	1.57	1.50	1.36	1.29
$c\ (n = 6,\ AR < 2)$	0.706	0.676	0.630	0.585	0.554
$c\ (n = 8,\ AR > 2)$	0.530	0.507	0.473	0.438	0.416
$c\ (n = 10,\ AR > 2)$	0.424	0.405	0.378	0.351	0.332
$c\ (n = 12,\ AR > 2)$	0.353	0.338	0.315	0.292	0.277

Table 3.14 Straightener Design Details.

$x = r/R$	0.5	0.6	0.75	0.9	1.0
ε_s	0.955	0.83	0.709	0.6	0.535
$\beta_1 = \tan^{-1}\varepsilon_S$	43.7	39.7	35.3	31.0	28.2
s/c	0.480	0.642	0.862	1.140	1.374
θ	53.2	50.0	46.6	42.9	40.4
$b/c(\%) = \frac{1}{2}\cdot\tan\frac{\theta}{4}$	11.76	11.04	10.28	9.47	8.92
ξ	17.0	14.7	12.0	9.50	7.9
C_L	0.822	0.978	1.149	1.31	1.406
$n\cdot c/R = 2\cdot\pi\cdot x/(s/c)$	6.552	5.877	5.464	4.96	4.573
n	13	13	13	13	13
c	1.3	1.166	1.084	0.984	0.908

Table 3.15 Efficiency of Rotor-Straightener System at Rotor Design Point.

$x = r/R$	0.5	0.6	0.75	0.9	1.0
$(C_{D_p})_R$	0.01	0.01	0.009	0.009	0.009
$(C_{D_S})_R = 0.015\cdot C_L^2$	0.012	0.011	0.007	0.006	0.005
$\gamma_R = [C_L/(C_{D_p} + C_{D_S})]_R$	40.44	41.19	42.41	42.34	41.87
$\frac{k_R}{K_{th}}$	0.046	0.053	0.062	0.074	0.082
$(C_{D_p})_S$	0.016	0.016	0.016	0.016	0.016
$(C_{D_S})_S = 0.018\cdot C_L^2$	0.001	0.002	0.003	0.006	0.008
$\gamma_S = [C_L/(C_{D_p} + C_{D_S})]_S$	13.57	17.47	21.83	24.65	27.81
$\frac{k_S}{K_{th}}$	0.046	0.029	0.019	0.013	0.011
$\frac{k_D}{K_{th}}$	0.054	0.054	0.054	0.054	0.054
η_R	0.954	0.947	0.938	0.926	0.918
η_S	0.954	0.971	0.981	0.987	0.989
η_{BL}	0.907	0.918	0.919	0.913	0.907
η_T	0.853	0.864	0.865	0.859	0.853

3.6 Hub Cone Design

The nose and tail fairings should preferably be good streamlined shapes. For the hub cone shape, any efficient streamlined body of revolution may be used [2]. One such shape is illustrated in Fig. 3.24 and its coordinates are given in Table 3.16.

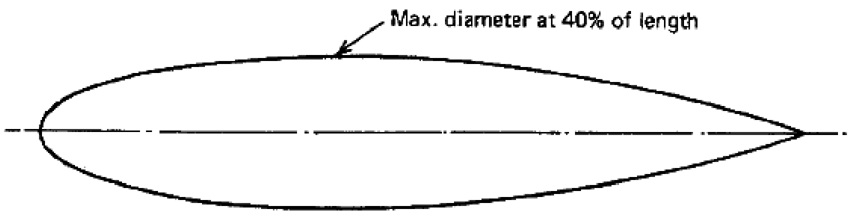

Figure 3.24 Streamlined Body of Revolution.

Table 3.16 Streamlined Body of Revolution Coordinates.

DIAMETER AT POINT / MAX. DIAMETER	*DISTANCE FROM NOSE / TOTAL LENGTH*
PERCENT	
0	0
24.8	1.25
34.8	2.5
48.4	5
66.2	10
86.6	20
96.8	30
100	40
97.7	50
90.5	60
78.2	70
60.0	80

34.7	90
18.7	95
0	100

The diameter of the streamlined body illustrated in Fig. 3.24 reaches a maximum at the 40 percent length position; the forward and rearward portions of the body can be considered separately when designing the nose and tail fairings. Nose fairing should be kept relatively short, while tail fairings may have to be long if flow separation is to be avoided. In the design of nose and tail fairings, the term fineness ratio, f, is defined as;

$$f = \frac{l}{2 \cdot r_b} \tag{3.101}$$

where l is the length of nose or tail fairing, and r_b is the radius of the hub. Experiment has shown that streamlined shapes with a total length to diameter ratio of 3 are the most efficient [2]. Assuming that the maximum diameter occurs at the 40 per cent length position, the fineness ratios of the nose and tail fairings will be 1.2 and 1.8 respectively. The ratio of 1.2 provides a good entry to the fan.

Fan diffuser efficiency is given by [1, 2]

$$\eta_D = 1 - \frac{\Delta p_D}{\frac{1}{2} \cdot \rho \cdot V_a^{\,2} \cdot \left[1 - \left(A_A / A_B\right)^2\right]} \tag{3.102}$$

where Δp_D is the mean total head loss, V_a is mean axial velocity through rotor, and A_A, A_B are the rotor annulus and duct areas respectively. In design, Δp_D is obtained by assuming the diffuser efficiency. Unfortunately, very little experimental information is available but from the existing evidence it appears that $\eta_D = 0.8 \ to \ 0.85$, provided flow separation is avoided. The loss of total head, Δp_D, can be expressed non-dimensionally as

$$k_D = \frac{\Delta p_D}{\frac{1}{2} \cdot \rho \cdot {V_a}^2} \tag{3.103}$$

and hence Eqn. (3.102) can be written

$$k_D = (1 - \eta_D) \cdot \left[1 - \left(\frac{A_A}{A_B} \right)^2 \right] \tag{3.104}$$

When the duct diameter of the fan unit remains constant, we have

$$k_D = (1 - \eta_D) \cdot \left[{x_b}^2 \cdot \left(2 - {x_b}^2 \right) \right] \tag{3.105}$$

After the determination of hub cone geometry, eight rotor blades and thirteen straighteners are located on the hub. Designed fan is illustrated in Figs. 3.25 and 3.26.

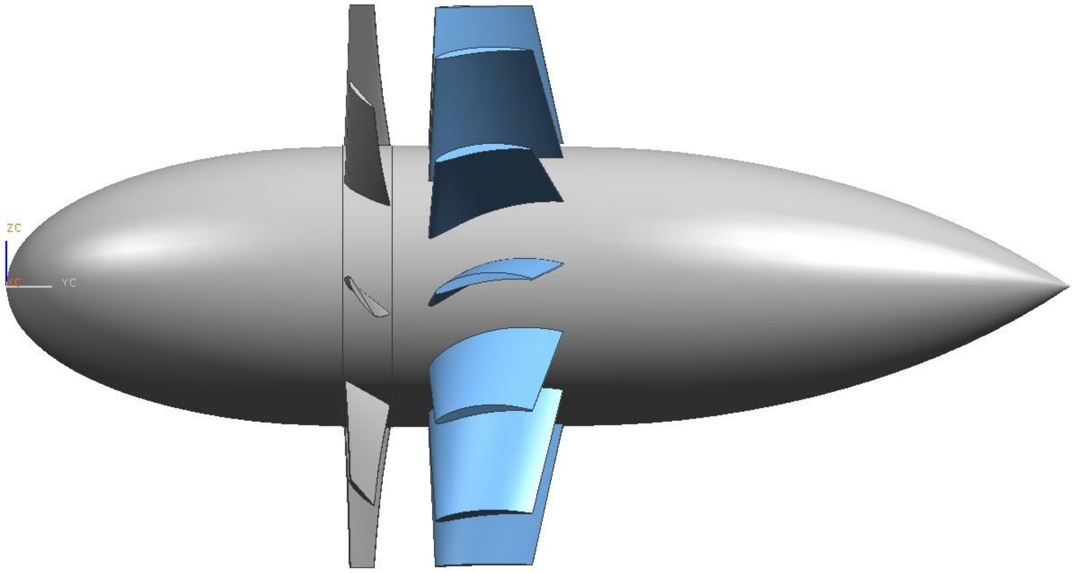

Figure 3.25 Designed Fan (Side View).

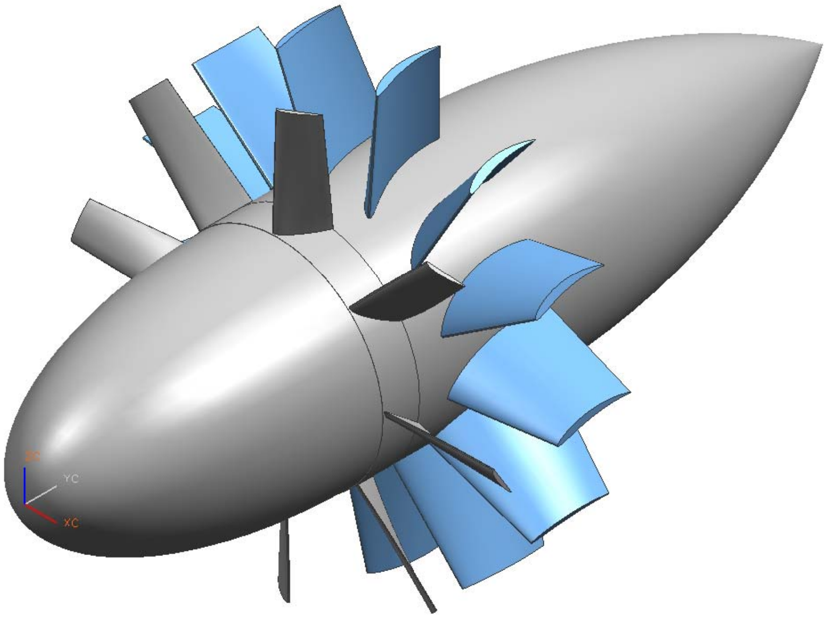

Figure 3.26 Designed Fan (Isometric View).

CHAPTER 4

PERFORMANCE ANALYSIS OF THE FAN

4.1 Introduction

An analytical method for establishing off-design duty performance is as important as the evaluation of the fan design point. It permits the construction of characteristics curves for a wide range of blade settings and enables fan stall approximations to be obtained. The procedure is invaluable in relation to the development of variable pitch axial flow fans. In addition, from measurement of blade profile, solidity, and stagger angle, the likely performance of a rotor can be estimated in the absence of aerodynamic design data.

The method proposed is centered on mean flow and pressure rise calculations. Provided the design meets free vortex flow conditions, the midspan station is a possible choice. At the mean station it is only necessary to calculate swirl coefficient ε as a function of flow coefficient λ, for a given blade geometry, in order to compute all other variables involved in characteristic curve construction except the estimation of the stall point. This latter point requires load limit studies at the blade extremities, normally the blade root.

In rotor analysis there are two major variable, the flow coefficient and the swirl coefficient. The problem of analysing stators is a relatively simple once since there is only one major variable, the swirl coefficient.

4.2 Analysis Equations

The rotor vector diagram of Fig. 3.16 is modified in manner shown in Fig. 4.1. An essential part of the analysis problem is to find the rotor no-work point. For such a condition the velocity vector diagram is reduced to the velocity triangle EBG, where

$$\text{Mean resultant velocity} = V_{m_N} = \text{EB}$$

$$\text{Axial velocity} = V_{\alpha_N} = \text{BG}$$

$$\text{Tangential velocity} = \Omega \cdot r + \left(V_{\theta_p}\right)_N = \text{EG}$$

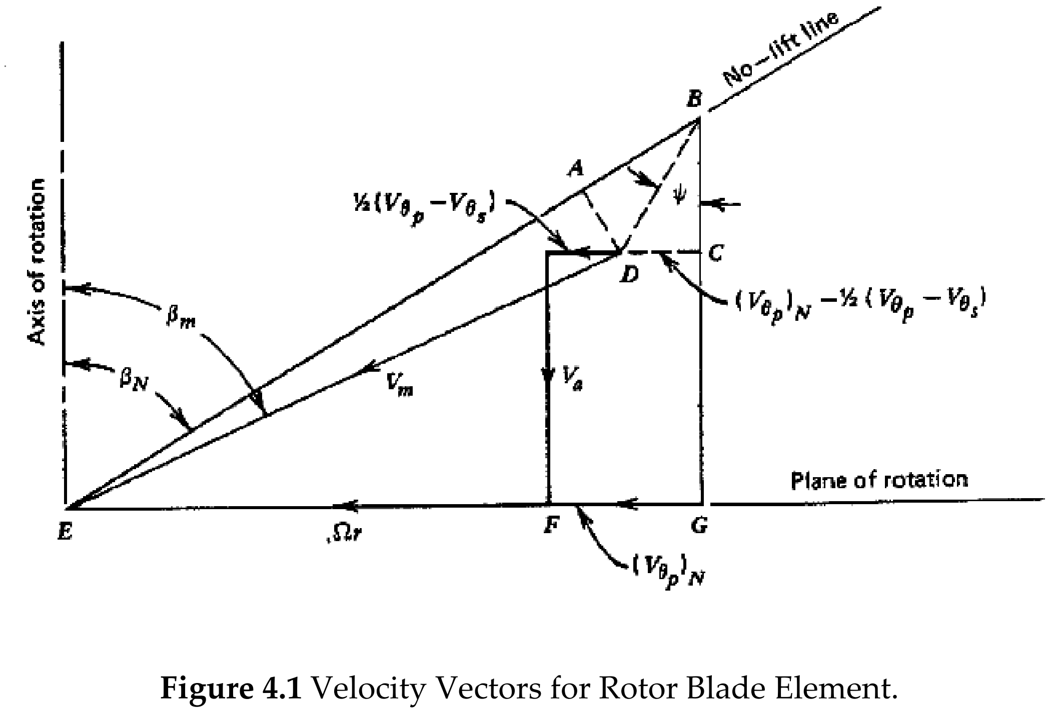

Figure 4.1 Velocity Vectors for Rotor Blade Element.

With increasing load the point D will move away from B and hence

$$V_m = ED$$

$$V_a = CG = BG - BC$$

$$\Omega \cdot r + \frac{1}{2} \cdot \left(V_{\theta_p} - V_{\theta_s}\right) = EG - CD$$

Expressions for flow coefficient λ and swirl coefficient ε_s are now developed from

$$V_a = \left[\Omega \cdot r + \left(V_{\theta_p}\right)_N\right] \cdot \cot \beta_N - \frac{\varepsilon_p \cdot \lambda_N - \frac{1}{2} \cdot \lambda \cdot \left(\varepsilon_p - \varepsilon_s\right)}{\tan \psi}$$

Dividing by $\Omega \cdot r$

$$\lambda = \left(1 + \varepsilon_p \cdot \lambda_N\right) \cdot \cot \beta_N - \frac{\varepsilon_p \cdot \lambda_N - \frac{1}{2} \cdot \lambda \cdot \left(\varepsilon_p - \varepsilon_s\right)}{\tan \psi} \qquad (4.1)$$

where

$$\frac{\left(V_{\theta_p}\right)_N}{\Omega \cdot r} \cdot \frac{V_{a_N}}{V_{a_N}} = \varepsilon_p \cdot \lambda_N$$

and

$$\lambda_N = \left(1 + \varepsilon_p \cdot \lambda_N\right) \cdot \cot \beta_N = \frac{1}{\tan \beta_N - \varepsilon_p} \qquad (4.2)$$

Eqn. (4.1) can be rewritten as

$$\varepsilon_s = 2 \cdot \tan\psi \cdot \left[\frac{\lambda_N}{\lambda} - 1\right] - \varepsilon_p \cdot \left[\frac{2 \cdot \lambda_N}{\lambda} - 1\right] \tag{4.3}$$

in which ψ is the only unknown being a function of blade element load capability.

Assuming that the lift coefficient can be expressed as a simple function of incidence angle, then

$$C_L = m \cdot \sin(\beta_m - \beta_N) \tag{4.4}$$

where m is a constant and $\beta_m - \beta_N$ is the incidence relative to the no-lift chord line. For airfoils of low to moderate camber, of faired shape, and not subject to multiplane interference, the lift proportionality constant is 5.7.

An expression for $\sin(\beta_m - \beta_N)$ is obtained as follows:

$$\begin{aligned} AD &= V_m \cdot \sin(\beta_m - \beta_N) \\ &= BD \cdot \sin(\beta_N - \psi) \\ &= \frac{DC \cdot \sin(\beta_N - \psi)}{\sin\psi} \end{aligned}$$

Substituting the velocity vector of Fig. 4.1 for DC

$$V_m \cdot \sin(\beta_m - \beta_N) = \left[\left(V_{\theta_p}\right)_N - \frac{1}{2} \cdot \left(V_{\theta_p} - V_{\theta_s}\right)\right] \cdot \frac{\sin(\beta_N - \psi)}{\sin\psi} \tag{4.5}$$

Momentum considerations are satisfied when Eqns. (3.73) and (4.4) are equated. Rearrangement gives

$$\sin(\beta_m - \beta_N) = \frac{2 \cdot (\varepsilon_p + \varepsilon_s) \cdot \cos\beta_m}{m \cdot \sigma} \tag{4.6}$$

Substitution in Eqn. (4.5) produces the expression

$$\tan\psi = \frac{\sin\beta_N}{\dfrac{4 \cdot (\varepsilon_p + \varepsilon_s)}{m \cdot \sigma \cdot [\varepsilon_p \cdot (2 \cdot \lambda_N/\lambda - 1) + \varepsilon_s]} + \cos\beta_N} \tag{4.7}$$

where $(V_{\theta_p})_N / V_a = \varepsilon_p \cdot \lambda_N / \lambda$

Introducing Eqn. (4.7) into Eq. (4.3) gives

$$\begin{aligned} \varepsilon_s &= \frac{2 \cdot \sin\beta_N \cdot [\lambda_N/\lambda - 1]}{\dfrac{4 \cdot (\varepsilon_p + \varepsilon_s)}{m \cdot \sigma \cdot [\varepsilon_p \cdot (2 \cdot \lambda_N/\lambda - 1) + \varepsilon_s]} + \cos\beta_N} - \varepsilon_p \cdot \left(\frac{2 \cdot \lambda_N}{\lambda} - 1 \right) \\ &= \frac{2 \cdot \sin\beta_N \cdot (\lambda_N/\lambda - 1) - 4 \cdot \varepsilon_p / m \cdot \sigma - \varepsilon_p \cdot \cos\beta_N \cdot (2 \cdot \lambda_N/\lambda - 1)}{4/m \cdot \sigma + \cos\beta_N} \end{aligned} \tag{4.8}$$

In the absence of prerotation Eqn. (4.3) reduces to

$$\varepsilon_s = 2 \cdot \tan\psi \cdot \left[\frac{\cot\beta_N}{\lambda} - 1 \right] \tag{4.9}$$

Eqn. (4.7) reduces to

$$\tan\psi = \frac{\sin\beta_N}{4/m \cdot \sigma + \cos\beta_N} \tag{4.10}$$

And Eqn. (4.8) reduces to

$$\varepsilon_s = \frac{2 \cdot \sin\beta_N \cdot \left(\cot\beta_N / \lambda - 1\right)}{4/m \cdot \sigma + \cos\beta_N} \tag{4.11}$$

4.3 Rotor and Straightener Analysis

The thickness to chord ratio of the selected airfoil, RAF 6E, is 10.3%. According to the Fig. 4.1, no lift incidence angle, α_N, is approximately -4.5°.

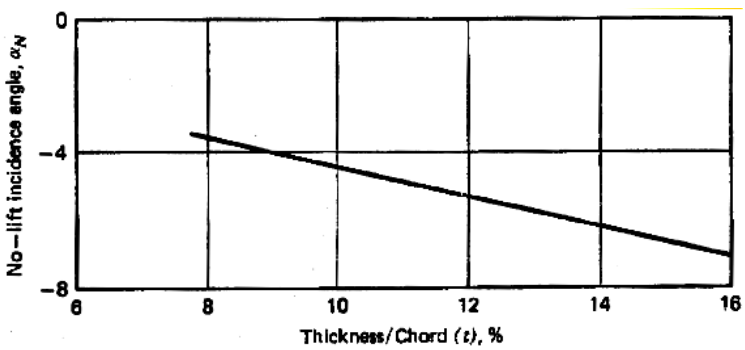

Figure 4.2 No-Lift Angle for Flat Undersurface Airfoils (ref. 1, p.159).

Firstly, only rotor is analyzed in the operating range to determine the maximum swirl that is to be removed by the straightener before the straightener design. Analysis is carried out only at the rotor blade root for different pitch angles (Fig. 4.3). It is clear from this figure that maximum swirl occurs at 0.2 flow coefficient and zero pitch angle.

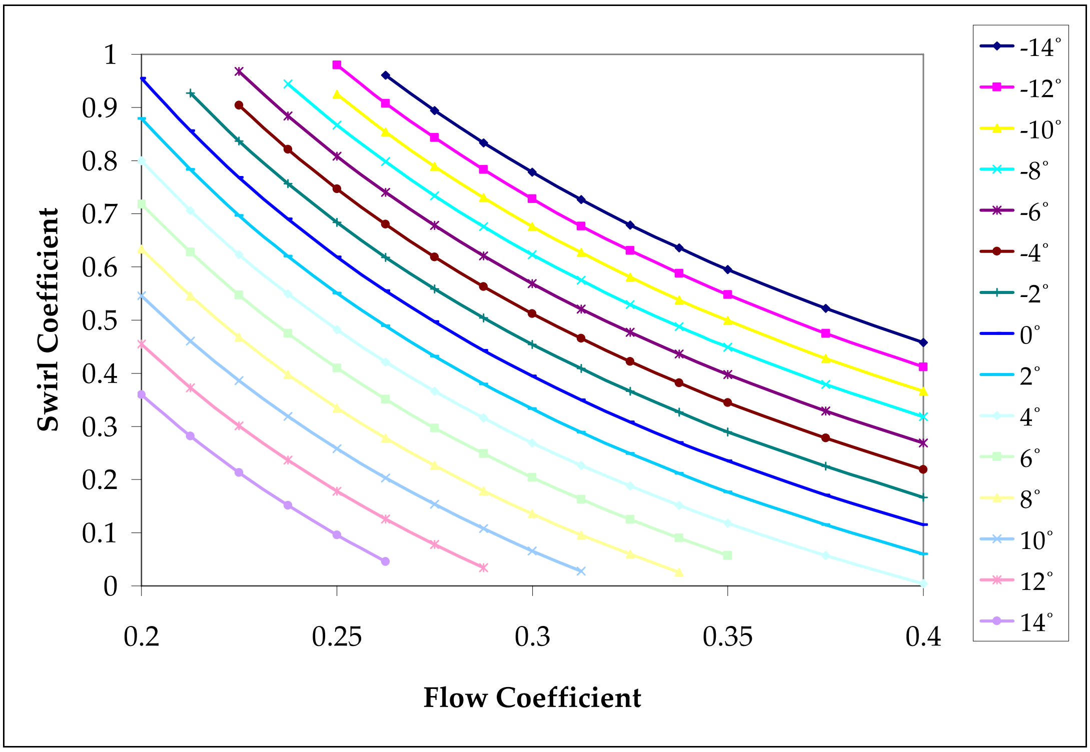

Figure 4.3 Swirl Coefficients at Rotor Blade Root for Different Flow Coefficients and Pitch Angles.

After that, analyses are performed from root to tip of the rotor at 0.2 flow coefficient and zero pitch angle and swirls along the rotor span are obtained (Table 4.1)

Table 4.1 Swirl Coefficients along the Rotor Span.

$x = r/R$	0.5	0.6	0.75	0.9	1.0
ε_s	0.955	0.830	0.709	0.600	0.535

Performance analysis of the fan according to the algorithm that given in Fig. 4.4 is made in the operating range that is between 0.2 and 0.4 flow coefficients. When the fan operates at maximum and minimum flow coefficients, blade pitch angle is changed between -14° and 12° relative to reference stagger angle ξ to obtain the required pressure rises given in Table 3.11. It is determined that it is necessary to give 10.79° and -13.37° pitch angle to the rotor blade respectively to obtain velocities of 79.7 m/s and 180 m/s at the AWT test section.

Analysis results at reference blade angle are given in Table 4.2, 4.3, and 4.4 in details.

Rotor and fan unit efficiencies for various blade settings are presented in Figs. 4.5 and 4.6 respectively.

Fan performance data, which consist of the fan characteristics curves, AWT loss characteristic curve, rotor stall line and different swirl coefficient lines, at various pitch setting are illustrated in Fig. 4.7. Fan performance data with efficiency contours is shown in Fig. 4.8. In both of figures, the fan characteristics curves cut AWT loss characteristics curve to give the operating point of the system.

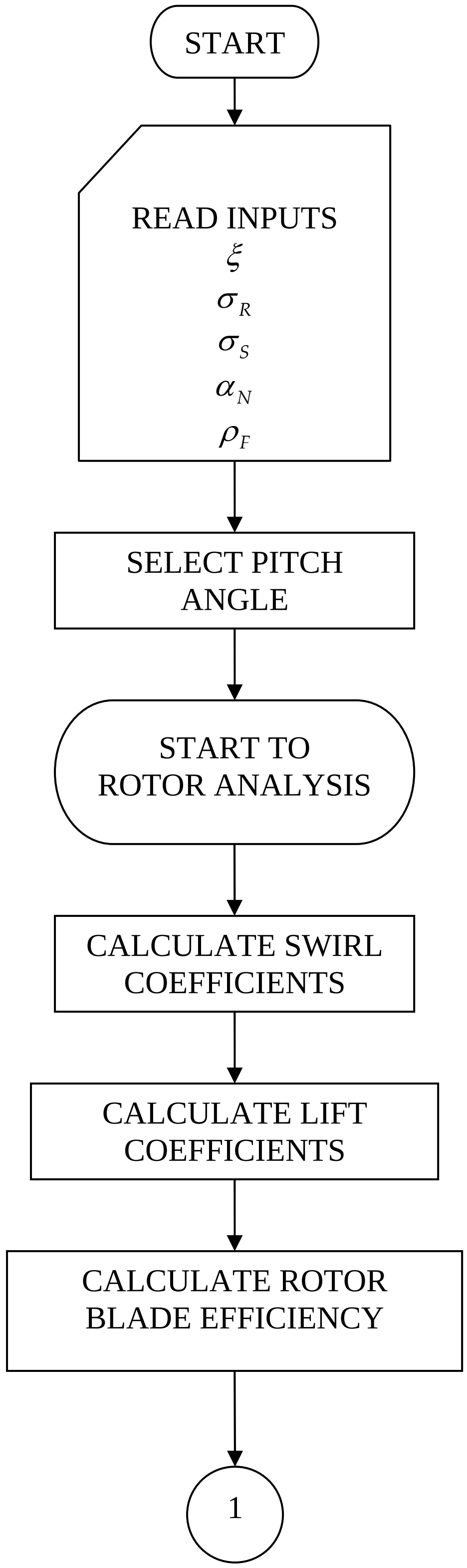
START
READ INPUTS
ξ
σ_R
σ_S
α_N
ρ_F
SELECT PITCH ANGLE
START TO ROTOR ANALYSIS
CALCULATE SWIRL COEFFICIENTS
CALCULATE LIFT COEFFICIENTS
CALCULATE ROTOR BLADE EFFICIENCY
1

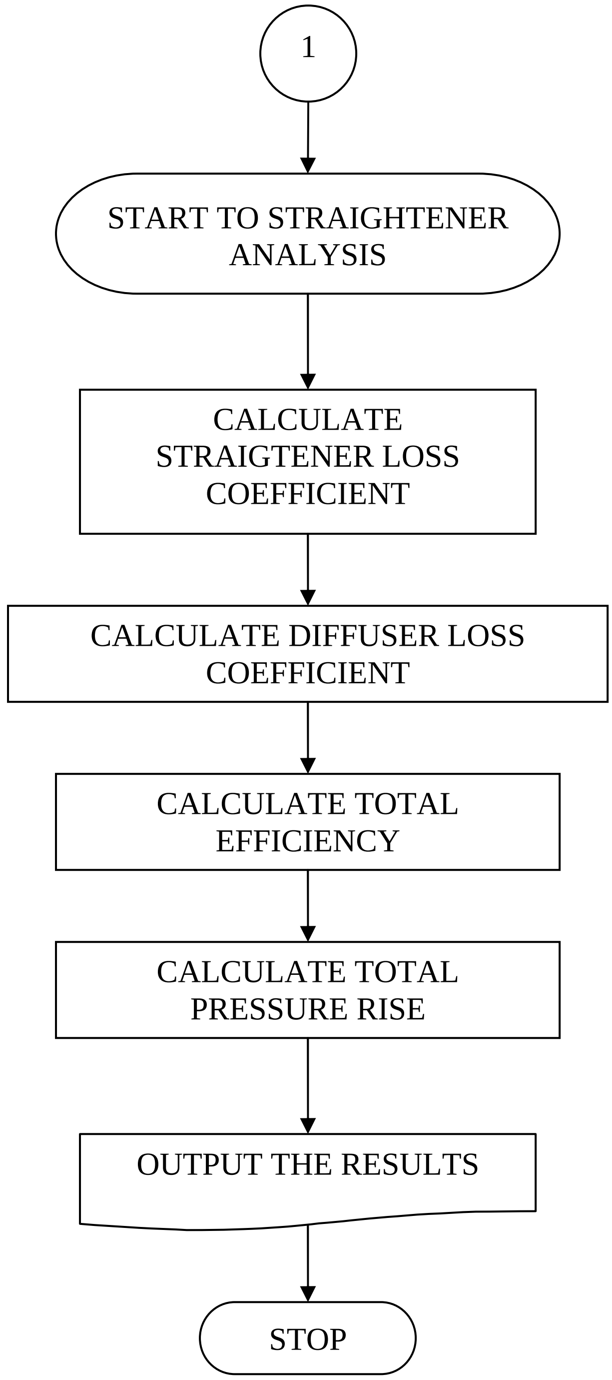

Figure 4.4 Rotor and Straightener Analysis Algorithm.

Table 4.2 Rotor Analysis at Reference Blade Setting Angle.

$\Lambda = V_a / \Omega \cdot R$	0.2	0.25	0.3	0.35	0.4
$\lambda = \Lambda / x_{MS}$	0.267	0.333	0.4	0.467	0.533
$\psi = \tan^{-1}\left(\dfrac{\sin\beta_N}{4/m\cdot\sigma + \cos\beta_N}\right)$	17.579	17.579	17.579	17.579	17.579
$\beta_N = \xi + \alpha_N$	60.539	60.539	60.539	60.539	60.539
$\varepsilon_s = 2\cdot\tan\psi\left[\dfrac{\cot\beta_N}{\lambda} - 1\right]$	0.709	0.44	0.261	0.133	0.037
$K_{th} = 2\cdot\dfrac{\varepsilon_s}{\lambda}$	5.314	2.641	1.306	0.571	0.141
$\beta_m = \tan^{-1}\left[\left(1 - \dfrac{1}{2}\cdot\varepsilon_s\cdot\lambda\right)/\lambda\right]$	73.591	70.215	67.118	64.282	61.688
$C_L\cdot\sigma = 2\cdot\varepsilon_s\cdot\cos\beta_m$	0.4	0.298	0.203	0.116	0.036
σ	0.311	0.311	0.311	0.311	0.311
C_L	1.287	0.958	0.653	0.372	0.114
C_{D_p} (from RAF 6E charact.)	0.015	0.01	0.009	0.009	0.009
$C_{D_S} = 0.015\cdot C_L^2$	0.025	0.014	0.006	0.002	0.0002
$\gamma = C_L / (C_{D_p} + C_{D_S})$	32.373	39.506	42.374	33.766	12.526
$\gamma\dfrac{k_R}{K_{th}} = \dfrac{\lambda}{\cos^2\beta_m}$	3.342	2.909	2.646	2.478	2.371
$\dfrac{k_R}{K_{th}}$	0.103	0.074	0.062	0.073	0.189
η_R	0.897	0.926	0.938	0.927	0.811

Table 4.3 Efficieny Loss Due to Straightener and Diffuser.

$\Lambda = V_a/\Omega \cdot R$	0.2	0.25	0.3	0.35	0.4
ε_s (from rotor analysis)	0.709	0.44	0.261	0.133	0.037
$\beta_{m_S} = \tan^{-1}(\varepsilon_s/2)$	19.509	12.411	7.44	3.814	1.073
$C_L \cdot \sigma = 2 \cdot \varepsilon_s \cdot \cos\beta_{m_S}$	1.336	0.86	0.518	0.266	0.075
σ (from design)	1.16	1.16	1.16	1.16	1.16
C_L	1.152	0.741	0.447	0.229	0.065
$\gamma \dfrac{k_S}{K_{th}} = \dfrac{\lambda}{\cos^2\beta_{mS}}$	0.3	0.349	0.407	0.469	0.534
C_{D_p}	0.016	0.016	0.016	0.016	0.016
$C_{D_S} = 0.018 \cdot C_L^2$	0.024	0.01	0.004	0.001	0
$\gamma = C_L/(C_{D_p} + C_{D_S})$	28.883	28.629	22.794	13.536	4.018
$\dfrac{k_S}{K_{th}}$	0.01	0.012	0.018	0.035	0.133
η_S	0.99	0.988	0.982	0.965	0.867
η_D	0.825	0.825	0.825	0.825	0.825
$k_D = (1-\eta_D)[x_b^2(2-x_b^2)]$	0.077	0.077	0.077	0.077	0.077
$\dfrac{k_D}{K_{th}}$	0.014	0.029	0.059	0.134	0.545

Table 4.4 Dimensional Data for Reference Blade Setting Angle ($\xi = 65.04^{\circ}$).

$\Lambda = V_a / \Omega \cdot R$	0.2	0.25	0.3	0.35	0.4
η_T	0.872	0.885	0.861	0.758	0.133
K_{th}	5.134	2.641	1.306	0.571	0.141
V_a	35.66	44.58	53.50	62.41	71.32
Q	559.3	699.2	839	978.8	1118.7
$\frac{1}{2} \cdot \rho \cdot V_a^2$	749.83	1171.61	1687.11	2296.35	2999.31
$\Delta p_T = K_{th} \cdot \eta_T \cdot \left(\frac{1}{2} \cdot \rho \cdot V_a^2 \right)$	3474.67	2738.65	1897.09	994.73	56.09

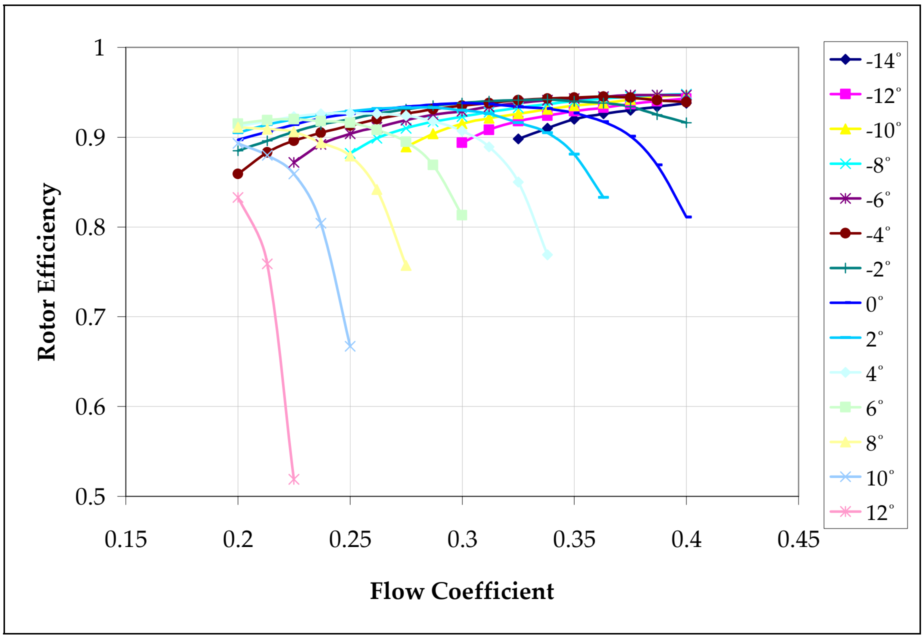

Figure 4.5 Rotor Efficiencies for Various Blade Settings.

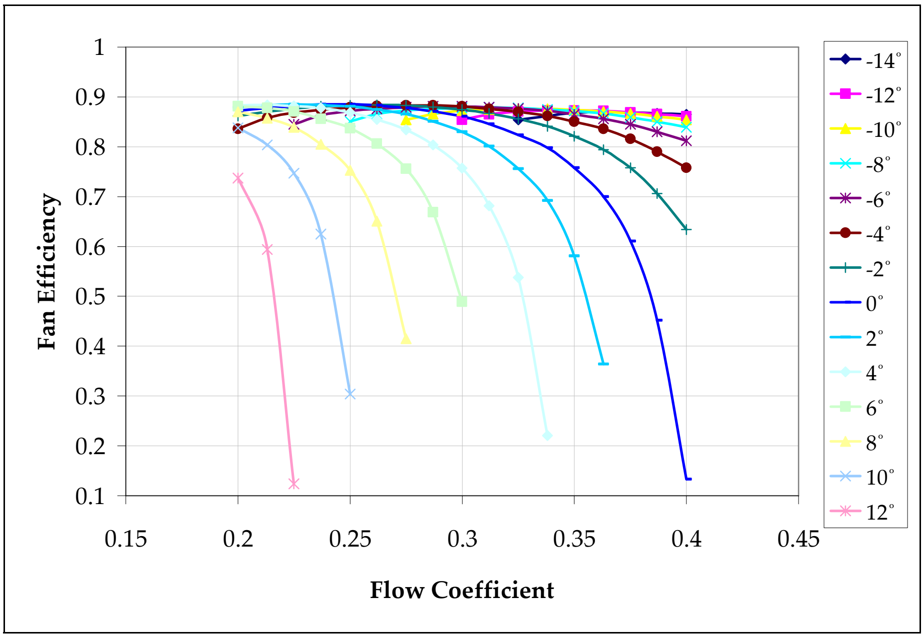

Figure 4.6 Fan Unit Efficiencies for Various Blade Settings.

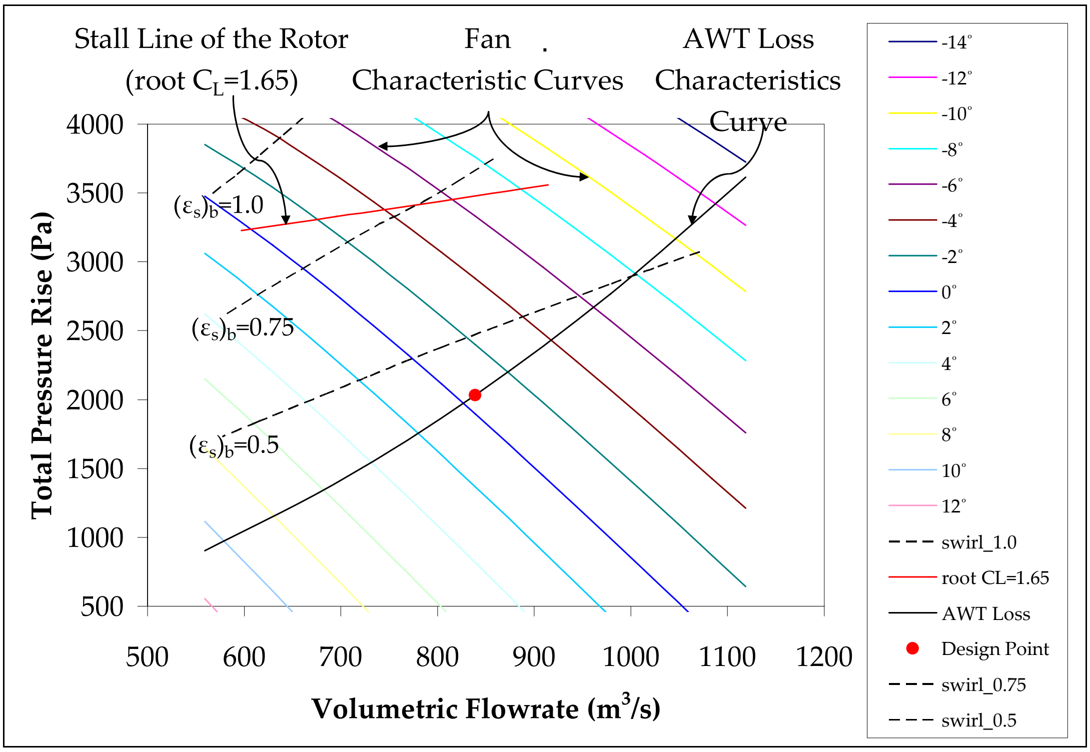

Figure 4.7 Fan Performance Chart.

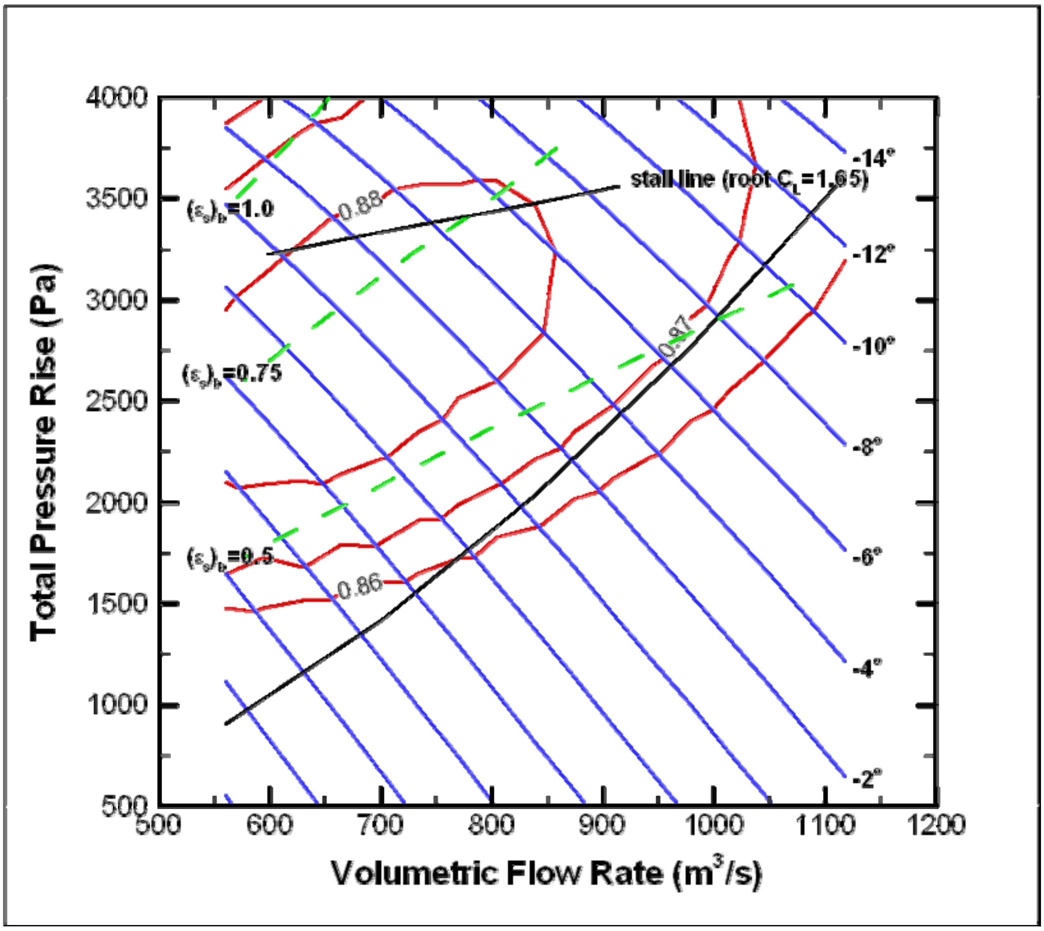

Figure 4.8 Fan Performance Chart with Efficiency Contours.

CHAPTER 5

CONCLUSION

A variable pitch axial flow fan is designed for Ankara Wind Tunnel (AWT) to increase the Mach number from 0.26 to 0.52. Thereafter the fan is analyzed over the operating range and performance characteristic curves are obtained. Based on loss characteristic of AWT, the existing fan aerodynamic efficiency is obtained as 74% and required power to reach a Mach number of 0.52 is found to be 4314.4 kW excluding model blockage. This value will be 4745.8 kW taking the 10% model blockage into account. According to the design and analysis results, rotor blade is placed by root angle of 38.33˚ to obtain 79.7 m/s. It is found that the necessary blade root angle for the velocity of 180 m/s (0.52 Mach) is 62.48˚.

Although two dimensional isolated airfoil data is used in the rotor blade design, secondary drag known as three dimensional losses is taken into account. This approach will increase the reliability of the results.

It is seen in the analysis that diffuser loss that is related with hub cone shape, increses when the velocity increases and it causes a reduction on the overall fan unit efficiency. It is concluded that the hub cone design is as important as the rotor and the straightener design.

Velocities lower than 79.7 m/s may be obtained by bringing down the rpm to half because flow coefficient remains constant. But at very low Reynolds numbers it may not be suitable to make tests in the wind tunnel because of low flow quality.

In both of fan design and analysis, it is assumed that velocity is uniform at the upstream of the fan. If large nonuniformities occur, there may be a big deviation on the fan unit efficiency.

It is advised to manufacture a scaled model of the fan and do some wind tunnel tests before the manufacture of full scale fan.

REFERENCES

[1] Wallis R. A., "Axial Flow Fans and Ducts", John Willey & Sons, New York, 1983.

[2] Wallis R. A., "Axial Flow Fans: Design and Practice", Academic Press, New York, 1961.

[3] Barlow J. B., Rae W. H. and Pope A., "Low Speed Wind Tunnel Testing", Willey, New York, 3rd edition, 1999.

[4] Barlow J., "Low Speed Wind Tunnel Testing",

[5] Pope A. and Harper J. J., "Low Speed Wind Tunnel Testing", Willey, New York, 1966.

[6] Eck B., "Fans: design and operation of centrifugal, axial-flow, and cross-flow fans", Pergamon Press, New York, 1973.

[7] Osborne W. C., "Fans", 1st edition, Pergamon Press, New York, 1966.

[8] Osborne W. C., "Fans: (in SI/metric units)", 2nd edition, Pergamon Press, New York, 1977.

[9] Eckert W. T., Mort K. W. and Pope J., "Aerodynamic Design Guidelines and Computer Program for Estimation of Subsonic Wind Tunnel Performance", NASA TN D-8243, 1976.

[10] Wolf T., "Computation of Power Requirements for Subsonic and Transonic Wind Tunnels", AIAA-1997-2223.

[11] Dress, D. A., "Computer Program for Calculating Flow Parameters and Power Requirements of Cryogenic Wind Tunnels", NASA TM-87609, 1989.

[12] Kahane¸A., "Investigation of Axial-Flow Fan and Compressor Rotors Designed for Three-Dimensional Flow", NACA Technical Note, No: 1652, 1948.

[13] Bogdonoff S. M. and Herrig L. J., "Performance of Axial-Flow Fan and Compressor Blades Designed for High Loadings", NACA Technical Note, No: 1201, 1947.

[14] Abrego A. I. and Bulaga R. W., "Performance Study of a Ducted Fan System", presented at the American Helicopter Society Aerodynamics, Acoustics, and Test and Evaluation Technical Specialist Meeting, San Francisco, January 23-25, 2002.

[15] Perl W. and Tucker M., "A General Representation for Axial-Flow Fans and Turbines", Report no: 814

[16] Winter K. G., "Comparative Tests of Thick and Thin Turning Vanes in the Royal Aircraft Establishment 4x3 –ft Wind Tunnel", R.A.E. Report Aero. 2217, 17th November 1947.

[17] Salter C., "Experiments on Thin Turning Vanes", N.P.L. Report Aero. 2469, 25th October 1946.

[18] Blake W. C.¸ "The Aerodynamics of a Wind Tunnel Fan", NACA Technical Note, No: 820, August 1941.

[19] Henry V. B., "A New Blade Element Method for Calculating the Performance of High and Intermediate Solidity Axial Flow Fans", NASA Contractor Report 3063, 1978.

[20] Fred E. W., "A Comparison of Propeller And Centrifugal Fans For Circulating The Air In A Wind Tunnel", NACA Technical Note, No: 281, March 1928